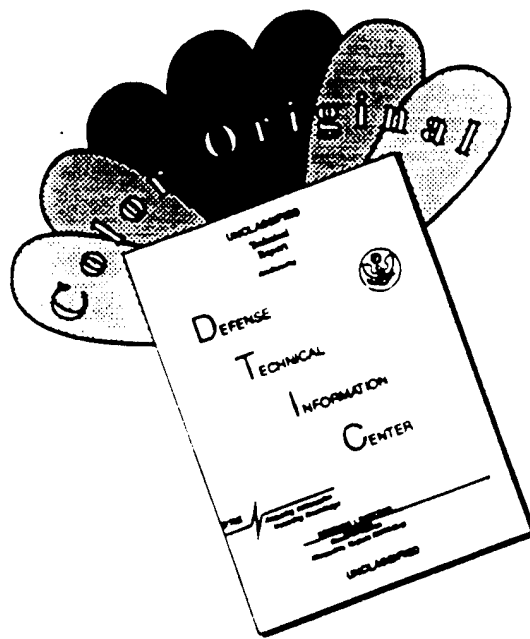


REPORT DOCUMENTATION PAGE			Form Approved OMB No. 0704-0188	
Public reporting burden for this collection of information is estimated to average 1 hour per response, including the time for reviewing instructions, searching existing data sources, gathering and maintaining the data needed, and completing and reviewing the collection of information. Send comments regarding this burden estimate or any other aspect of this collection of information, including suggestions for reducing this burden, to Washington Headquarters Services, Directorate for Information Operations and Reports, 1215 Jefferson Davis Highway, Suite 1204, Arlington, VA 22202-4302, and to the Office of Management and Budget, Paperwork Reduction Project (0704-0188), Washington, DC 20503.				
1. AGENCY USE ONLY (Leave blank)		2. REPORT DATE 10 Sep 95		3. REPORT TYPE AND DATES COVERED
4. TITLE AND SUBTITLE Meteorological Factors Responsible For Flooding In Central Texas During December, 1991			5. FUNDING NUMBERS	
6. AUTHOR(S) Rodney L. Clements				
7. PERFORMING ORGANIZATION NAME(S) AND ADDRESS(ES) AFIT Students Attending: Florida State University			8. PERFORMING ORGANIZATION REPORT NUMBER 95-099	
9. SPONSORING/MONITORING AGENCY NAME(S) AND ADDRESS(ES) DEPARTMENT OF THE AIR FORCE AFIT/CI 2950 P STREET, BLDG 125 WRIGHT-PATTERSON AFB OH 45433-7765			10. SPONSORING/MONITORING AGENCY REPORT NUMBER	
11. SUPPLEMENTARY NOTES				
12a. DISTRIBUTION/AVAILABILITY STATEMENT Approved for Public Release IAW AFR 190-1 Distribution Unlimited BRIAN D. GAUTHIER, MSgt, USAF Chief of Administration			<div data-bbox="1161 982 1523 1255" data-label="Image"> </div>	
13. ABSTRACT (Maximum 200 words) <p>"Original contains color plates: All DTIC reproductions will be in black and white"</p>				
14. SUBJECT TERMS			15. NUMBER OF PAGES 135	
			16. PRICE CODE	
17. SECURITY CLASSIFICATION OF REPORT		18. SECURITY CLASSIFICATION OF THIS PAGE		19. SECURITY CLASSIFICATION OF ABSTRACT
				20. LIMITATION OF ABSTRACT

19951017 162

DTIC QUALITY INSPECTED 8

DISCLAIMER NOTICE



THIS DOCUMENT IS BEST QUALITY AVAILABLE. THE COPY FURNISHED TO DTIC CONTAINED A SIGNIFICANT NUMBER OF COLOR PAGES WHICH DO NOT REPRODUCE LEGIBLY ON BLACK AND WHITE MICROFICHE.

THE FLORIDA STATE UNIVERSITY
COLLEGE OF ARTS AND SCIENCES

METEOROLOGICAL FACTORS RESPONSIBLE FOR FLOODING IN
CENTRAL TEXAS DURING DECEMBER, 1991

By

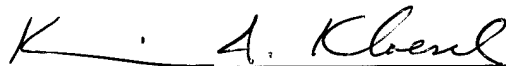
RODNEY L. CLEMENTS

Accession For		
NTIS CRA&I	<input checked="" type="checkbox"/>	
DTIC TAB	<input type="checkbox"/>	
Unannounced	<input type="checkbox"/>	
Justification		
By		
Distribution /		
Availability Codes		
Dist	Avail and/or Special	
A-1		

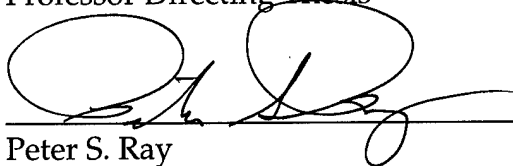
A Thesis submitted to the
Department of Meteorology
in partial fulfillment of the
requirements for the degree of
Master of Science

Degree Awarded:
Summer Semester, 1995

The members of the Committee approve the thesis of Rodney L. Clements
defended on July 11, 1995.



Kevin A. Kloesel
Professor Directing Thesis



Peter S. Ray
Committee Member



Paul H. Ruscher
Committee Member

ACKNOWLEDGMENTS

I would like to express my sincerest thanks to my major professor, Dr. Kevin A. Kloesel, for his support and guidance during my research. I would also like to thank my committee members, Dr. Peter S. Ray and Dr. Paul H. Ruscher, for their help and advice. I thank the United States Air Force for giving me this great opportunity to attend graduate school.

Thanks goes out to Chris Herbster for answering all my computer questions and John LoCastro of Synergy Design for his support. Lastly, special thanks goes out to my wife, Debra, for all her patience and keeping the faith through the past two years. She was the rock and anchor.

TABLE OF CONTENTS

List of Tables	vi
List of Figures	vii
Abstract	xii
1. Introduction	1
2. Data	8
3. Discussion of Meteorological Factors and Definitions	16
4. Case Study	33
12UTC 16 December 1991	35
00UTC 17 December 1991	40
12UTC 17 December 1991	43
00UTC 18 December 1991	51
12UTC 18 December 1991	55
00UTC 19 December 1991	63
12UTC 19 December 1991	66
00UTC 20 December 1991	76
12UTC 20 December 1991	83
00UTC 21 December 1991	102
12UTC 21 December 1991	108
Summary	119

5. Conclusions	129
References	132
Biographical Sketch	135

LIST OF TABLES

1	Ranking of annual per capita flood deaths per state during the period 1959-1991.	3
2	Upper air stations used for this study.	8
3	Rain gauge information.	13
4	Guide to interpretation of VIP colors.	15
5	Daily precipitation totals from the LCRA rain gauge sites.	34

LIST OF FIGURES

1	Monthly distribution of flooding events studied (Maddox et al. 1979).	5
2	The Highland Lakes Region and the Balcones Escarpment depicted by the arrows.	6
3	Location of upper air stations.	9
4	(a) Rain gauge locations in relation to the state of Texas. (b) Location of the rain gauges on a county map.	14
5	Typical overrunning case along a warm front (Moran and Morgan 1991).	20
6	Modified orographic map showing the location of the southeast coastal plain, the Balcones Escarpment, the Texas Hill Country, and the Gulf of Mexico.	21
7	Schematic representation of a vertically stable atmosphere with an oscillating air parcel motion (Emanuel 1984).	26
8	Schematic representation of a rotating fluid confined by two cylinders, with a radially oscillating tube of fluid (Emanuel 1984).	26
9	Cross section of an atmosphere representing relative positions of M surfaces (solid lines) and potential temperature surfaces (dashed lines). Parcel in an unstable displacement is shown (Emanuel 1984).	28
10	16 December 1991 12 UTC GEMPAK 850 mb diagram. Temperature in $^{\circ}\text{C}$ plotted upper left of station, dewpoint in $^{\circ}\text{C}$ plotted lower right of station, height in meters plotted lower left of station, and wind plotted with speed in knots.	36
11	16 December 1991 12 UTC upper air sounding profile for Brownsville, Texas. Temperature in $^{\circ}\text{C}$ is shown by the solid bold line and dewpoint in $^{\circ}\text{C}$ is shown by the dashed bold line. .	38
12	17 December 1991 0601 UTC water vapor satellite image.	39

13	16 December 1991 12 UTC upper air sounding profile for Corpus Christi, Texas. Temperature in $^{\circ}\text{C}$ is shown by the solid bold line and dewpoint in $^{\circ}\text{C}$ is shown by the dashed bold line. .	41
14	17 December 1991 12 UTC GEMPAK 850 mb diagram. Temperature in $^{\circ}\text{C}$ plotted upper left of station, dewpoint in $^{\circ}\text{C}$ plotted lower right of station, height in meters plotted lower left of station, and wind plotted with speed in knots.	42
15	17 December 1991 00 UTC upper air sounding profile for Brownsville, Texas. Temperature in $^{\circ}\text{C}$ is shown by the solid bold line and dewpoint in $^{\circ}\text{C}$ is shown by the dashed bold line. .	44
16	17 December 1991 00 UTC upper air sounding profile for Corpus Christi, Texas. Temperature in $^{\circ}\text{C}$ is shown by the solid bold line and dewpoint in $^{\circ}\text{C}$ is shown by the dashed bold line. .	45
17	17 December 1991 00 UTC upper air sounding profile for Corpus Christi, Texas. Temperature in $^{\circ}\text{C}$ is shown by the solid bold line and dewpoint in $^{\circ}\text{C}$ is shown by the dashed bold line. .	46
18	17 December 1991 12 UTC moisture convergence on a 295K isentropic surface.	47
19	17 December 1991 12 UTC moisture stability flux plotted for the isentropic layer 295:300K.	49
20	17 December 1991 12 UTC cross section analyses of equivalent potential temperature surfaces (dashed lines) and psuedo-angular momentum surfaces (solid) from Lubbock (LBB) to Corpus Christi (CRP), Texas. The hatched region depicts a region of potential instability.	50
21	17 December 1991 1631 UTC visible satellite image.	52
22	18 December 1991 00 UTC LFM 300 mb analysis.	53
23	18 December 1991 00 UTC LFM 500 mb analysis. The dashed line indicates the position of the weak short wave trough located west of the HLR.	54
24	18 December 1991 00 UTC LFM 850 mb analysis.	56
25	18 December 1991 12 UTC LFM 300 mb analysis.	57
26	18 December 1991 12 UTC LFM 500 mb analysis.	58
27	18 December 1991 12 UTC LFM 850 mb analysis.	60
28	18 December 1991 12 UTC daily surface weather map.	61

29	18 December 1991 12 UTC cross section analyses of equivalent potential temperature surfaces (dashed lines) and psuedo-angular momentum surfaces (solid) from Lubbock (LBB) to Corpus Christi (CRP), Texas. The hatched region depicts a region of potential instability and the cross hatched region depicts CSI.	62
30	19 December 1991 00 UTC LFM 300 mb analysis.	64
31	19 December 1991 00 UTC LFM 500 mb analysis.	65
32	19 December 1991 00 UTC LFM 850 mb analysis.	67
33	19 December 1991 12 UTC LFM 300 mb analysis.	68
34	19 December 1991 12 UTC LFM 500 mb analysis.	70
35	19 December 1991 12 UTC 700 mb vertical motion field. Negative values (dashed lines) indicate upward motion and positive values (solid lines) indicate downward motion.	71
36	19 December 1991 12 UTC LFM 850 mb analysis.	72
37	19 December 1991 12 UTC daily surface weather map.	74
38	19 December 1991 12 UTC cross section analyses of equivalent potential temperature surfaces (dashed lines) and psuedo-angular momentum surfaces (solid) from Lubbock (LBB) to Corpus Christi (CRP), Texas. The hatched region depicts a region of potential instability.	75
39	20 December 1991 00 UTC LFM 300 mb analysis.	77
40	20 December 1991 00 UTC LFM 500 mb analysis.	78
41	20 December 1991 00 UTC 700 mb vertical motion field. Negative values (dashed lines) indicate upward motion and positive values (solid lines) indicate downward motion.	80
42	20 December 1991 00 UTC LFM 850 mb analysis.	81
43	20 December 1991 00 UTC cross section analyses of equivalent potential temperature surfaces (dashed lines) and psuedo-angular momentum surfaces (solid) from Lubbock (LBB) to Corpus Christi (CRP), Texas. The hatched region depicts a region of potential instability and the cross hatched region depicts CSI.	82
44	20 December 1991 12 UTC LFM 300 mb analysis.	84
45	20 December 1991 12 UTC LFM 500 mb analysis.	85

46	20 December 1991 12 UTC 700 mb vertical motion field. Negative values (dashed lines) indicate upward motion and positive values (solid lines) indicate downward motion.	87
47	20 December 1991 12 UTC LFM 850 mb analysis.	88
48	20 December 1991 12 UTC re-analysis of daily surface weather map.	89
49	20 December 1991 00 UTC cross section analyses of equivalent potential temperature surfaces (dashed lines) and psuedo-angular momentum surfaces (solid) from Lubbock (LBB) to Corpus Christi (CRP), Texas. The hatched region depicts a region of potential instability and the cross hatched region depicts CSI.	91
50a	20 December 1991 1531 UTC visible satellite image.	92
50b	20 December 1991 1631 UTC visible satellite image.	93
50c	20 December 1991 1731 UTC visible satellite image.	94
50d	20 December 1991 1931 UTC visible satellite image.	95
51a	20 December 1991 22 UTC WSR57 weather radar image.	97
51b	20 December 1991 23 UTC WSR57 weather radar image.	98
51c	21 December 1991 00 UTC WSR57 weather radar image.	99
51d	21 December 1991 01 UTC WSR57 weather radar image.	100
51e	21 December 1991 02 UTC WSR57 weather radar image.	101
52	Isopleths of daily rainfall amounts at each LCRA rain gauge location on 20 December 1991. Rainfall amounts are shown in inches x 10 ⁻²	103
53	20 December 1991 composite map showing location of surface frontal features (solid lines), precipitation bands (hatched region), and location of Balcones Escarpment (dashed lines).	104
54	21 December 1991 00 UTC LFM 300 mb analysis.	105
55	21 December 1991 00 UTC LFM 500 mb analysis.	107
56	21 December 1991 00 UTC 700 mb vertical motion field. Negative values (dashed lines) indicate upward motion and positive values (solid lines) indicate downward motion.	109
57	21 December 1991 00 UTC LFM 850 mb analysis.	110
58	21 December 1991 12 UTC LFM 300 mb analysis.	111
59	21 December 1991 12 UTC LFM 500 mb analysis.	112

60	21 December 1991 12 UTC 700 mb vertical motion field. Negative values (dashed lines) indicate upward motion and positive values (solid lines) indicate downward motion.	114
61	21 December 1991 12 UTC LFM 850 mb analysis.	115
62	21 December 1991 12 UTC daily surface weather map.	116
63a	21 December 1991 0601 UTC water vapor satellite image.	117
63b	21 December 1991 1201 UTC water vapor satellite image.	118
64	Rainfall totals reported by the National Weather Service for the week 18 - 23 December 1991.	120
65	Location of the six HLR dams where (1) is the Buchanan Dam, (2) Inks Dam, (3) Wirtz Dam, (4) Max Starcke Dam, (5) Marshall Ford Dam, and (6) Tom Miller Dam.	121
66a	December 1991 Buchanan Dam water level information.	122
66b	December 1991 Inks Dam water level information.	123
66c	December 1991 Wirtz Dam water level information.	124
66d	December 1991 Max Starcke Dam water level information.	125
66e	December 1991 Marshall Ford Dam water level information. ...	126
66f	December 1991 Tom Miller Dam water level information.	127

ABSTRACT

Flooding occurred on 18 - 23 December 1991, in the Highland Lakes Region (HLR) of Central Texas. It will be shown that many meteorological factors were responsible for the flooding. These factors were "return-flow" of moisture from the Gulf of Mexico, "overrunning" of this moisture over a pre-existing shallow cold air mass, "orographic lifting" in the Texas Hill Country, "potential instability" (PI), and "conditional symmetric instability" (CSI). Furthermore, other observed phenomena such as elevated thunderstorms will be discussed. In addition, the tools used to analyze this event, including isentropic analysis techniques such as moisture stability flux will be reviewed.

CHAPTER 1

INTRODUCTION

Flooding occurs when the volume of water in a river or stream exceeds the capacity of the channel. Flooding also takes place along lake and coastal shorelines when higher than normal water levels inundate low-lying areas (Andrews 1993). Virtually any meteorological event that drops enormous volumes of water in heavy or widespread rainfalls has the potential to cause flooding. Floodstage is defined as the depth of water in the river when flooding is first observed. The excess above and beyond bankfull (top of the lowest riverbank) is floodwater. The nature of a flood is affected by the terrain into which the excess water flows. In flat areas, floods usually inundate wide areas, with slow-moving water. Flooding is exacerbated if the soil is saturated from earlier rain. Floodwaters on flat terrain can cause tremendous property and crop damage but usually cause little loss of human life. Small streams confined to narrow valleys or steep canyons in mountainous country have always been subject to sudden flooding when heavy rains fall in their watershed. A flood may be a storm surge driven

ashore by a hurricane or coastal storm; water descending from intense local storm clouds; slow accumulation from persistent, steady rain; or runoff from the rapid melting of deep snow cover. Floods can also be released by dam failures or arise upstream behind natural dams of debris or ice jams. Most great floods result from some combination of these causes (Ludlum 1991).

On the average, floods extract an annual toll of 200 lives and two billion dollars in property damage in the United States (Ludlum 1991). Dittman (1994) studied 33 years of flood data (1959 - 1991) and compiled statistics of annual per capita deaths from flooding for each of the 50 states and Puerto Rico (Table 1). He found that every state suffered a flood fatality except the state of Rhode Island. South Dakota is ranked number one with approximately 11 deaths annually, Puerto Rico is second with nearly five deaths, and third is Texas with three deaths per year.

A meteorological classification scheme was developed by Maddox and Chappell (1978) to group flooding events. The synoptic events were associated with significant large-scale weather systems and tropospheric wind fields that were quite strong. Frontal events were associated with quasi-stationary, generally west to east frontal zones embedded within weak large-scale patterns. Mesohigh events were associated with quasi-stationary, cool-air outflow boundaries that had been generated by prior thunderstorm

Table 1. Ranking of annual per capita flood deaths per state during the period 1959-1991.

Rank	State	Annual Per Capita Deaths	Number of Floods	Rank	State	Annual Per Capita Deaths	Number of Floods
1	South Dakota	10.75	245	26	Maryland	0.46	59
2	Puerto Rico	4.77	466	28	Mississippi	0.45	35
3	Texas	3.09	530	28	Utah	0.45	19
4	Colorado	2.42	203	30	Alaska	0.41	5
5	Montana	1.72	42	31	North Dakota	0.38	8
6	West Virginia	1.71	104	32	Iowa	0.35	33
7	Nevada	1.64	38	32	Ohio	0.35	120
8	New Mexico	1.47	58	34	California	0.32	235
9	Virginia	1.35	224	35	Minnesota	0.29	38
10	Arizona	1.22	95	36	North Carolina	0.25	46
11	Hawaii	1.15	33	36	Washington	0.25	31
12	Georgia	1.14	77	38	Maine	0.22	8
13	Wyoming	1.05	14	39	New Hampshire	0.21	6
14	Vermont	0.88	14	49	New Jersey	0.21	49
15	Kentucky	0.86	96	41	Indiana	0.17	29
16	Arkansas	0.81	56	42	Nebraska	0.16	8
16	Oklahoma	0.81	74	43	Delaware	0.12	12
18	Tennessee	0.79	110	44	Illinois	0.11	40
19	Oregon	0.64	49	44	New York	0.11	63
20	Connecticut	0.53	10	44	Wisconsin	0.11	16
20	Missouri	0.53	83	47	Florida	0.08	23
20	Pennsylvania	0.53	205	47	Michigan	0.08	24
23	Louisiana	0.48	60	49	Idaho	0.04	1
24	South Carolina	0.48	46	50	Massachusetts	0.01	2
25	Kansas	0.47	36	51	Rhode Island	0	0
26	Alabama	0.46	56				

activity. Western events were categorized as all flooding that occurred west of the 104° West longitudinal line regardless of meteorological conditions.

Using this scheme, Maddox et al. (1979) examined 151 intense, flood-producing precipitation events for the years 1973-77. The monthly distribution for all 151 events is shown in Figure 1. As would be expected, the most frequent flood-producing precipitation events occur from spring into the fall months, when favorable combinations of dynamic processes and thermodynamic conditions exist. July was clearly the predominant month of occurrence, accounting for almost 25% of the sample. Since heavy precipitation events are typically convective in nature, it is not surprising that about 86% of the entire sample took place during the warm season months (April - September). Winter time (December - February) flood-producing events accounted for only 4% of the total. Although statistically low, individual winter season flooding events can be significant. The focus of this study will be a winter-season flooding event which occurred in the Highland Lakes Region (HLR) of Texas (Figure 2).

The HLR incorporates the city of Austin, which has approximately a half million people in the metropolitan area. Also included in the HLR is a 600-mile chain of lakes created by six dams nestled in complex terrain on the Colorado river. The lake levels of Lakes Travis and Buchanan rise and fall at almost unbelievable rates throughout most "normal-rainfall" years because of

the demands of rice growers downstream in the Lower Colorado River Valley. The rice growers were farming before the six dams were built, and under law, have first call on what is considered the river's "normal flow" of water (Banks and Babcock 1988). Abnormally wet years give the area potential for significant flood damage of both property and lives.

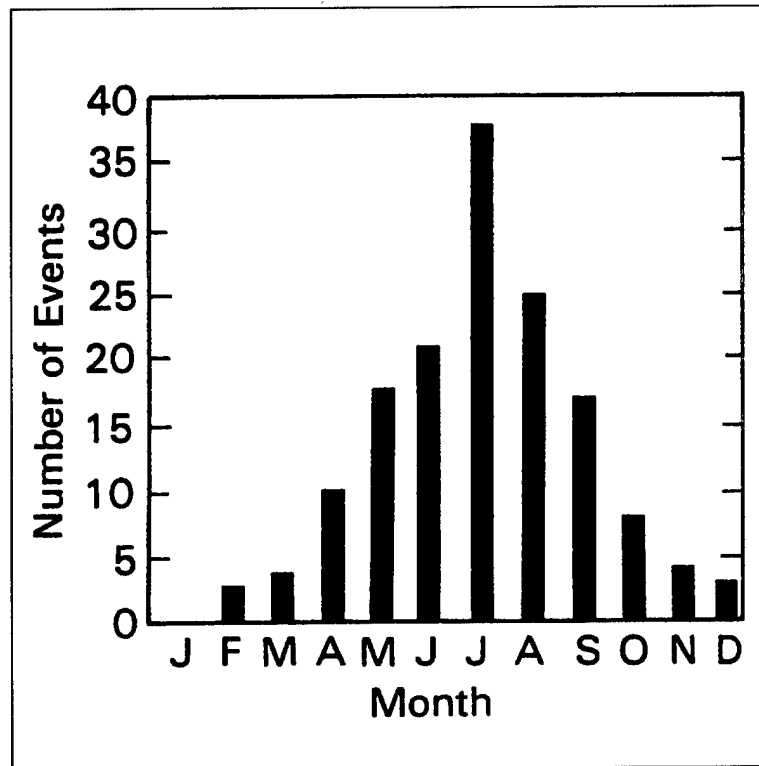


Figure 1. Monthly distribution of flooding events studied (Maddox et al. 1979).

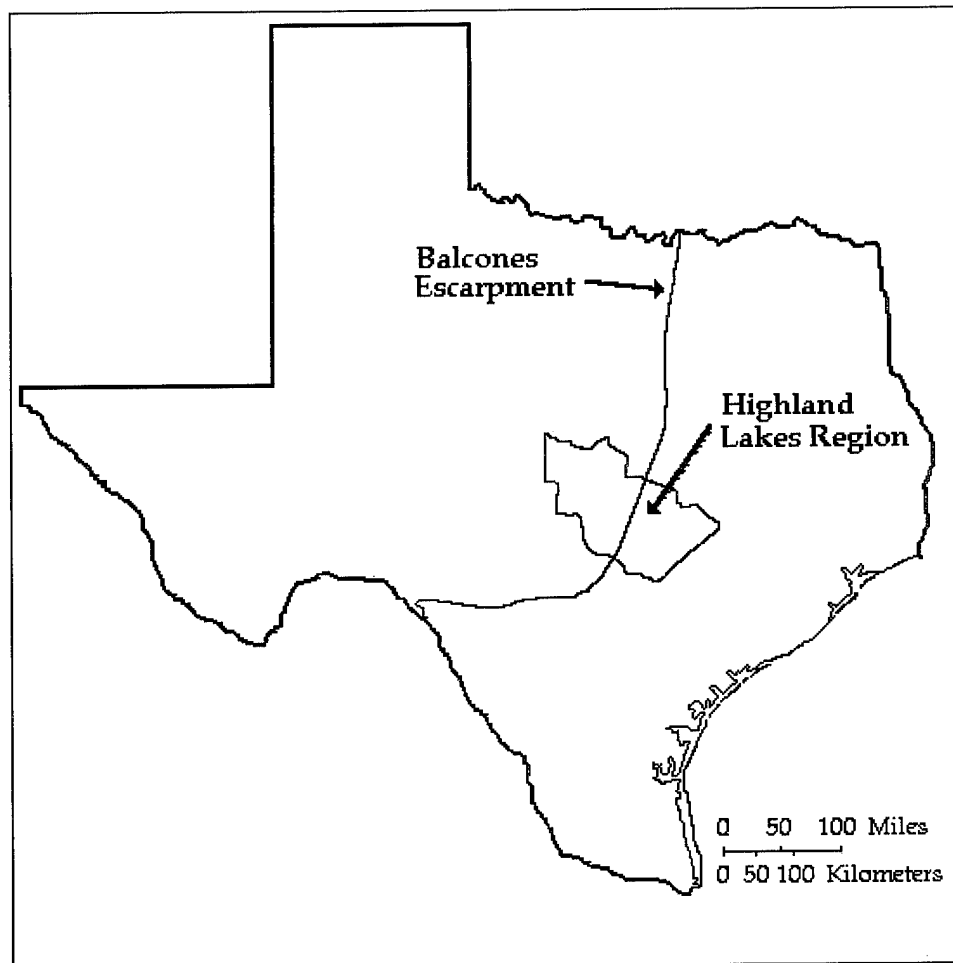


Figure 2. The Highland Lakes Region and the Balcones Escarpment depicted by the arrows.

During the period 17 December through 23 December 1991, the HLR received an overabundance of precipitation (some sites recorded in excess of 12 inches (Goodge 1991)). Travis County, where Austin is located, had a total of 265 single family homes which sustained flood damage. Roadways throughout the county sustained major damage. Estimates of damage to the

county totaled approximately five million dollars. After a disaster survey, eight counties along the Colorado River from HLR southward, were declared Federal disaster areas (Mahler 1995).

It is the purpose of this thesis to address analysis techniques which will allow agencies (both governmental and local) to better identify the meteorological conditions which can result in winter season flood events. Use of isobaric and isentropic analyses will be incorporated in this study. Improved analysis techniques will ensure that public awareness is heightened and will eliminate or potentially offset property damage.

This thesis will present a case study and examine many meteorological factors responsible for the flooding that occurred in the HLR. Chapter 2 will explain the data used for this thesis. Chapter 3 will give a discussion of meteorological factors and definitions which will be invoked to discuss the case study presented in Chapter 4. Chapter 5 will discuss conclusions.

CHAPTER 2

DATA

The data used for this study are conventional upper air soundings for 00 and 12 UTC from eleven stations (Table 2), (Figure 3).

Table 2. Upper air stations used for this study.

Three Letter I.D.	Station Name	State Where Located	Latitude	Longitude	Elevation in Feet
LZV	North Little Rock	Arkansas	34.83N	92.25E	172
AMA	Amarillo	Texas	35.23N	101.70E	1,094
SEP	Stephenville	Texas	32.21N	98.18E	399
GGG	Longview	Texas	32.34N	94.65E	124
MAF	Midland	Texas	31.95N	102.18E	873
CRP	Corpus Cristi	Texas	27.76N	97.50E	13
BRO	Brownsville	Texas	25.90N	97.43E	7
LCH	Lake Charles	Louisiana	30.11N	93.21E	5
OUN	Norman	Oklahoma	35.23N	97.46E	362
JAN	Jackson	Mississippi	32.32N	90.08E	101
ELP	El Paso	Texas	31.80N	106.40E	1,194

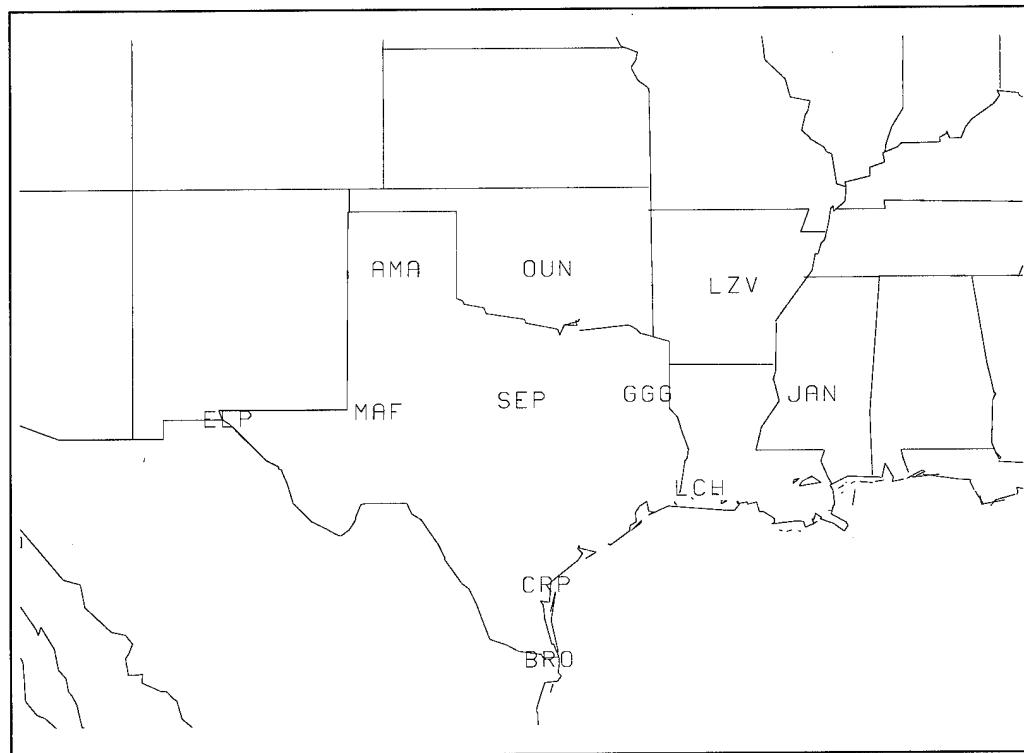


Figure 3. Location of upper air stations.

These data were archived by Forecast Systems Laboratory, Boulder, Colorado and National Climatic Data Center, Asheville, North Carolina. Raw data were extracted from the Radiosonde Data of North America 1946 - 1991 CD-ROM disk, and then decoded from the mandatory levels (TTAA), significant levels (TTBB), and the wind observations (PPBB). Parameters included were temperature, dewpoint, wind speed and direction for the mandatory and significant pressure levels. Graphical displays used were produced using

GEMPAK (General Meteorological Package) which was developed by the National Aeronautics and Space Administration at Goddard Space Flight Center, MD (desJardins et al. 1991). Within GEMPAK, parameters such as equivalent potential temperature, geostrophic momentum, etc., were calculated and analyzed.

Using GEMPAK, gridded data sets were created from the 00 and 12 UTC decoded raw upper air data. Fields of temperature and dewpoint in degrees Celsius, u- and v-wind components, height, and pressure values for mandatory levels were created. The domain was bound from 20.5 degrees North latitude, 115 degrees West longitude at the southwest corner to 42.5 degrees North latitude, 83 degrees West longitude in the northeast corner, with grid spacing in the x and y directions every two degrees.

Isentropic grids were created in a similar manner. The 00 and 12 UTC decoded raw upper air data were used. Fields of temperature and dewpoint in degrees Celsius, pressure, mixing ratio, the Montgomery stream function, and u- and v-wind components were created. The gridded data fields were produced at 5K intervals beginning at 295K and extending to 330K.

It is important to note that graphical displays generated from GEMPAK using gridded data and isentropic gridded data sets may not show the entire domain of the grid, but a subset of that grid. These displays are dependent on geographical area, defined by the user. The smaller the defined area, the

smaller the grid displayed. Using Austin as the geographical area, this reduced the size of the grid domain displayed to 21 degrees North latitude, 115 degrees West longitude in the southwest corner and 37 degrees North latitude, 85 degrees West longitude in the northeast corner.

In addition to the upper air data from CD-ROM, supplemental data like daily surface weather maps from the Climate Analysis Center, Washington, D.C. and upper air DIFAX charts for the 850 mb, 700 mb, 500 mb, and 300 mb levels were utilized. Notice in Figure 3 that data from Del Rio, Texas (DRT), a National Weather Service radiosonde site, are missing from the CD-ROM. In addition, DRT appears only intermittently on the upper air analysis products. As a sensitivity study, the mandatory level data for DRT from the DIFAX charts were manually included with the data extracted from CD-ROM. There were no perceptible differences in the gridded data sets that were created. It was not possible to incorporate significant level data, therefore it was not possible to assess whether the significant level data would have made a difference in the gridded data sets.

Precipitation data from thirty-three HLR Lower Colorado River Authority (LCRA) rain gauge stations were also used for this study. Although data from all thirty-three rain gauge sites were reported, only twenty-seven were plotted for clarity given the resolution of the diagram used (Table 3), (Figure 4). Cook and Newton are shown as one (C44), Turner and Sulteimier are shown as one

(D33), Robbins, Lawson, Moursund, Camp Peniel, and Monroe are shown as one (D77). These data were obtained from the LCRA located in Austin, Texas.

Infrared, visible, and water vapor satellite imagery were obtained from the Texas A&M University geostationary satellite image archive. Visible and water vapor satellite imagery will be shown in Chapter 4 as supporting evidence for the case study. Lastly, the radar images which will be depicted in Chapter 4, were obtained from the WSR57 weather radar at the Austin Municipal Airport National Weather Service Office. Table 4 is provided as a guide to interpret the Video Integrator and Processor (VIP) colors.

Table 3. Rain gauge information.

Station Identifier	Rain Gauge Name	Latitude	Longitude
B11	Bastrop	30.06N	97.19E
B22	Brady	31.00N	99.16E
B33	Columbus	29.42N	96.32E
B44	Junction	30.30N	99.44E
B55	La Grange	29.54N	96.53E
B66	Mason	30.39N	99.06E
B77	Menard	30.55N	99.47E
B88	Mullin	31.31N	98.44E
B99	Onion Creek	30.10N	97.41E
B00	Red Bluff	31.13N	98.33E
C11	San Saba	31.12N	98.43E
C22	Walnut Creek	30.16N	97.39E
C33	Winchell	31.28N	99.09E
C44	Cook	30.40N	98.33E
C44	Newton	30.40N	98.33E
C55	Sullivan Knob	31.00N	98.24E
C66	Schulz	30.49N	98.33E
C77	Braddocks	30.31N	97.56E
C88	Riley	30.40N	98.12E
C99	Dean	30.58N	98.45E
C00	Yates	30.57N	98.32E
D11	Jordan	30.50N	98.21E
D22	Oliver	31.09N	98.28E
D33	Turner	30.42N	98.18E
D33	Sulteimier	30.42N	98.18E
D44	Wirtz Dam	30.33N	98.22E
D55	Phillips	30.16N	98.14E
D66	Mathiews	30.26N	98.20E
D77	Robbins	30.23N	98.05E
D77	Lawson	30.23N	98.05E
D77	Moursund	30.23N	98.05E
D77	Camp Peniel	30.23N	98.05E
D77	Monroe	30.23N	98.05E

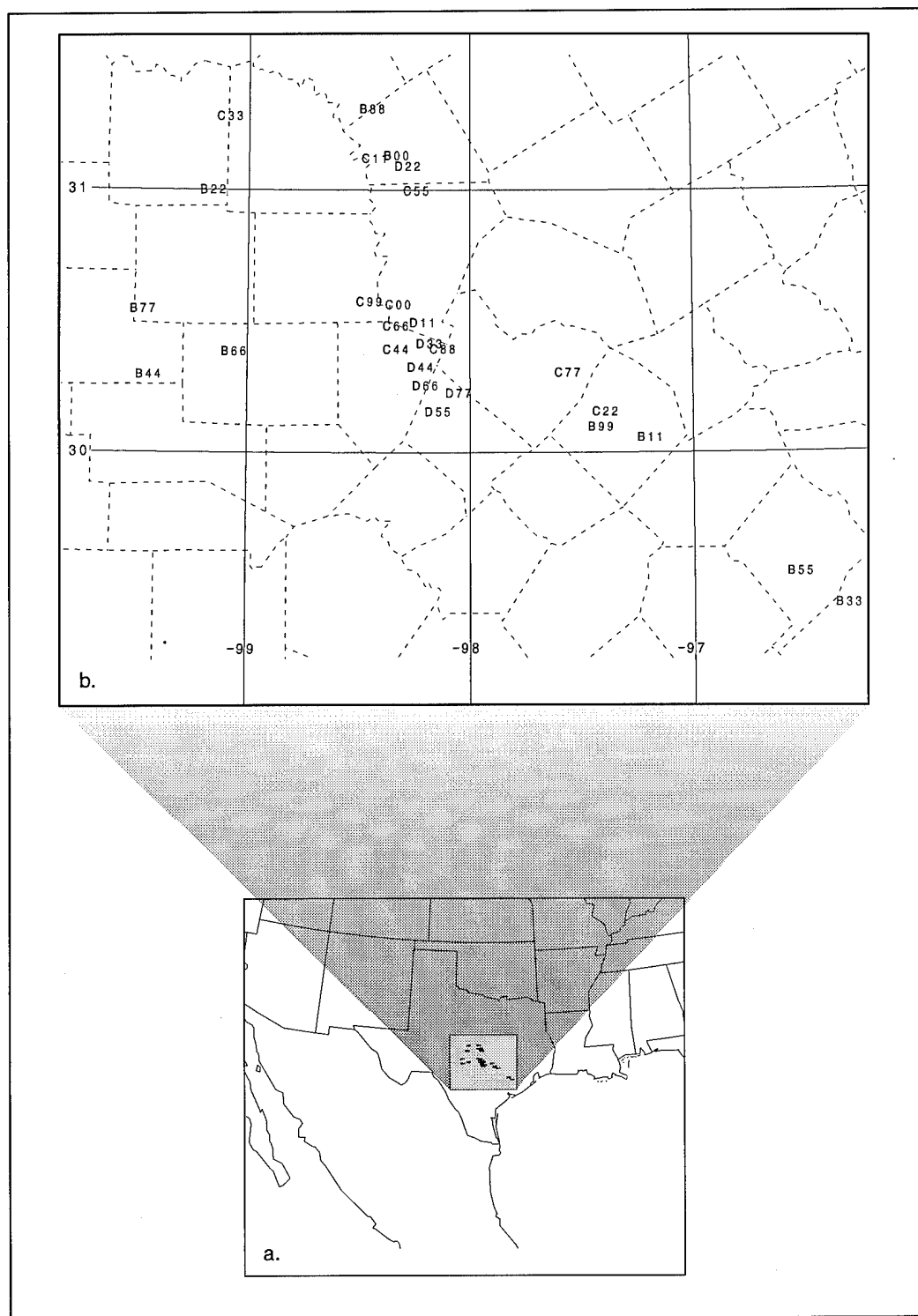


Figure 4. (a) Rain gauge locations in relation to the state of Texas. (b) Location of the rain gauges on a county map.

Table 4. Guide to interpretation of VIP colors.

Color Shade	VIP Level	Rainfall Rate	Precipitation Is Termed
Light Green	1	<.1 in. per hr.	Light
Dark Green	2	.1 to .5 in. per hr.	Moderate
Yellow	3	.5 to 1.0 in. per hr.	Heavy
Orange	4	1.0 to 2.0 in. per hr.	Very Heavy
Red	5	2.0 to 5.0 in. per hr.	Intense
Dark Red	6	>5.0 in. per hr.	Extreme

CHAPTER 3

DISCUSSION OF METEOROLOGICAL FACTORS AND DEFINITIONS

In Chapter 4 it will be shown that a multitude of meteorological factors were responsible for the flooding that occurred in the HLR in December, 1991. These factors were "return-flow" of moisture from the Gulf of Mexico, "overrunning" of this moisture over a pre-existing shallow cold air mass, "orographic lifting" in the Texas Hill Country, "potential instability" (PI), and "conditional symmetric instability" (CSI). A discussion of each factor is appropriate before continuing. Furthermore, other observed phenomena such as elevated thunderstorms will be discussed. In addition, the tools used to analyze this event, including isentropic analysis techniques such as moisture stability flux will be reviewed.

Return Flow. In order to identify the various processes involved in a "return-flow" event, a discussion of air mass classification must be addressed. For this thesis, the air mass classification scheme used will be that proposed by Merrill (1992) specifically for return flow events. Four source regions are defined in this scheme. Maritime tropical (mT) and continental Tropical (cT),

which are standard types, as well as maritime midlatitude (mM) and continental midlatitude (cM). The mM designation is added to accommodate return flow, and cM is suggested as a more accurate designator for polar air of Pacific origin as it modifies across and east of the Rocky Mountains. Mean winter surface temperatures for the four different air masses are $\geq 25^{\circ}\text{C}$ for mT, 25 to 30°C for cT, 15 to 24°C for mM, and 10 to 20°C for cM. Mean dewpoint temperatures for these air masses during the winter are 21°C for mT, -8 to 10°C for cT, 12 to 20°C for mM, and -15 to 5°C for cM.

Return flow can be characterized by two cycles. The first phase of the cycle is defined as the movement of cold, dry air from the continent to the Gulf of Mexico and is called the *offshore-flow phase*. The second phase is defined as the movement of modified post-cold frontal moist air from the Gulf of Mexico to the continent and is called the *return-flow phase* (Crisp and Lewis 1992).

The invasion of the cold air mass constituting the first phase of the return-flow cycle in many return flow events is the cM air mass. The offshore-flow phase is initiated when the wind first exhibits an offshore component along the Texas-Louisiana coast, typically associated with cold frontal passage. This phase subsequently ends when the surface wind first exhibits an onshore component, typically in response to the eastward movement of the surface high pressure associated with the post-frontal cold

air mass. The cold shallow dome of air associated with the cM air mass begins to modify once over the Gulf of Mexico.

The processes that characterize the modification of the boundary layer in a cold-air outbreak over the Gulf can be summarized as follows. The shallow boundary layer that has been formed over the continent is rapidly heated from below by the Gulf water. Turbulence is produced by both convective and mechanical mixing. In a layer near the water surface, this turbulence overcomes the stable stratification and forms a mixed marine boundary layer that is characterized by a homogeneous distribution of temperature (θ) and moisture (q) properties in all directions. With the sustained production of turbulence and continued heat input, this mixed layer erodes the stable layer aloft, entraining air from above that has different properties from the mixed layer (different temperature, humidity, and passive scalar concentrations). The depth and properties of the mixed layer will continuously change with time, until the mixed-layer potential temperature approaches the sea surface temperature (Liu et al. 1992). During the modification process with the marine surface, the cold dry air dome (associated with the cM air mass) begins to take on the characteristics of the moist warm air in the surface layer, and becomes a mM type air mass.

Once the high pressure associated with the cM air mass begins to move eastward, the return-flow phase begins. The return-flow phase is initiated

when the wind first exhibits an onshore component along the south Texas coast, and this phase ends when the wind subsequently exhibits an offshore component (Crisp and Lewis 1992). West of the center of the surface high, the cM air that was modified over the Gulf is now returned to the continent as a mM air mass. This moisture is then advected with the anticyclonic circulation around the high and provides a source of moisture to south Texas and eventually the entire south-central and southeastern United States.

Overrunning. The *Glossary of Meteorology* (Huschke 1959) defines overrunning as a condition existing when an air mass is in motion aloft above another air mass of greater density at the surface. This term is usually applied in the case of warm air ascending the surface of a warm front or quasi-stationary front. Rising motion above the frontal zone is associated quasi-geostrophically with warm advection. This type of rising motion is often referred to as *overrunning*, since the "warm" air mass "overruns" the "cool" air mass. A schematic of this process is shown in Figure 5. Precipitation associated with overrunning is usually stratiform and light, owing to the high static stability in the frontal zone (Bluestein 1992b).

Orographic Lifting. The *Glossary of Meteorology* (Huschke 1959) defines orographic lifting as the lifting of an air current caused by its passage up and over mountains. Similarly, Reinking and Boatman (1986), defined upslope as being named under the presumption that advection over the generally rising

terrain induces lifting, cloudiness, and precipitation. Both "orographic" lifting and "upslope" are synonymous with one another (Bluestein 1992a).

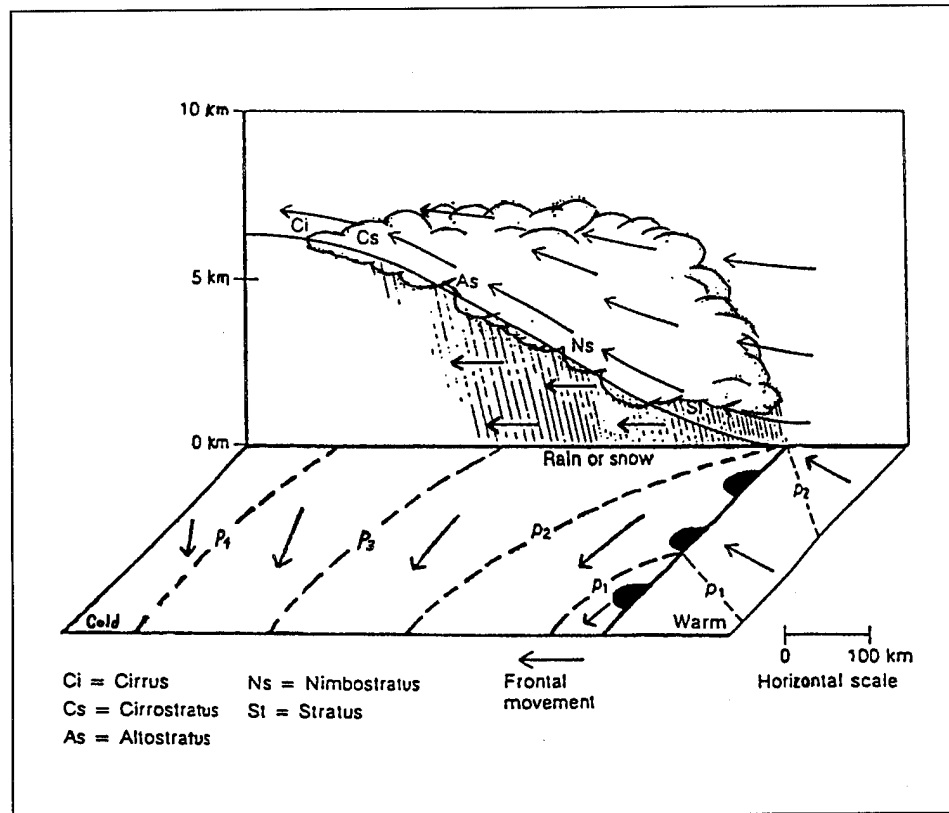


Figure 5. Typical overrunning case along a warm front (Moran and Morgan 1991).

Physically, the HLR is nearly split in half by the Balcones Escarpment (Figure 6). The Balcones Escarpment is oriented south southwest to north northeast across Central Texas and extends to approximately 400 feet in height over the HLR. East of the Balcones Escarpment the terrain is fairly flat

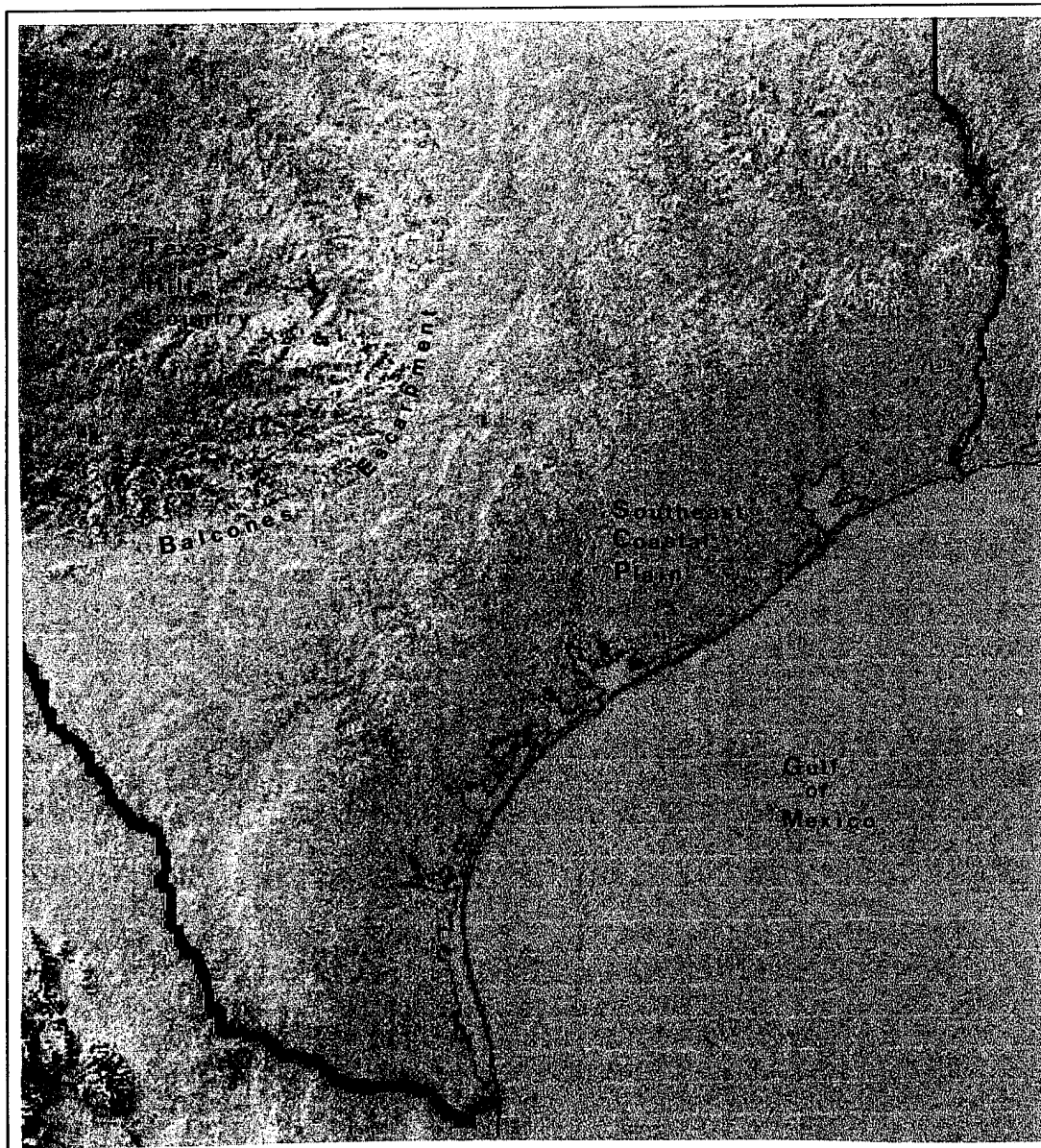


Figure 6. Modified orographic map showing the location of the southeast coastal plain, the Balcones Escarpment, the Texas Hill Country, and the Gulf of Mexico.

(approximately 100 to 200 feet) and is part of the Gulf Coastal Plains. West of the Balcones Escarpment the terrain is known as the Texas Hill Country, and elevations in this region extend up to approximately 1800 feet. This terrain is complex with many streams, green valleys, tablelands, and lakes. The Balcones Escarpment is important in that once a return-flow event sets up, orographic lifting conditions become favorable because prevailing winds advect warm moist air from the southeast coastal plains of Texas at sea level to elevations of several hundred feet on the eastside of the Balcones Escarpment.

Potential Instability (PI). Theory shows that layers within which the equivalent potential temperature decreases with height may become unstable when lifted sufficiently. The potential instability is defined analogously to the ordinary static stability, but in terms of equivalent potential temperature,

$$\begin{array}{ll} \partial\theta_e / \partial z & > 0 \text{ potential stability} \\ & < 0 \text{ potential instability} \end{array}$$

A potentially unstable atmosphere becomes absolutely unstable when saturation occurs in the layer. Usually saturation is achieved by lifting of the layer, hence the designation "convective instability." However, saturation may be achieved also by evaporation of rain that falls through the layer (Djuric 1994) and by overrunning over a pre-existing frontal boundary.

Conditional Symmetric Instability (CSI). Emanuel (1983) pointed out that inertial, symmetric and convective instabilities are very closely related in a dynamical sense. In the simplest terms, each of these instabilities may be thought of as resulting from an unstable distribution of body forces acting on a fluid. In the case of convection, the responsible body forces are gravitational, while the body forces are centrifugal in the case of inertial instability. The two differ principally in direction, with gravity acting vertically and centrifugal forces acting radially. Symmetric instability represents motion from a combination of these forces; thus, the motion is "slantwise."

How then, can we determine if a parcel has "slantwise" motion? Consider a base state in which a steady, purely meridional flow is in geostrophic balance. In this case, the potential temperature is a function only of x and z , so the thermal wind can be written

$$f(\partial v_g / \partial z) = ((g/\theta_{v0})(\partial \theta_v / \partial x)), \quad (1)$$

where the subscript g denotes the geostrophically and hydrostatically balanced base state.

Suppose a tubular parcel of fluid, extending infinitely in the y direction, is displaced in the $x - z$ plane. The displacement is assumed to proceed slowly so that the fields of v_g and θ_v are undisturbed. The parcel equations are then

$$dv_p/dt = -fu_p, \quad (2)$$

$$du_p/dt = f(v_p - v_g), \quad (3)$$

$$dw_p/dt = (g/\theta_{vo})(\theta_{vp} - \theta_v), \quad (4)$$

where the subscript p refers to the parcel. It can be shown using (2) that a pseudoangular momentum, M , defined as

$$M = v + fx \quad (5)$$

is conserved following the parcel, if the vertical shear is unidirectional. Eq. (3) can be written

$$du_p/dt = f(M_p - M_g). \quad (6)$$

If, after the displacement, the left-hand sides of (4) and (6) have the same sign as the displacement, the parcel will continue accelerating so the displacement is unstable. In particular, slanted displacements may be unstable if the slope of M_g -surfaces are less than those of θ -surfaces. If the environment is saturated, as it will be in this case study, equivalent potential

temperature (θ_e) should be substituted for θ to account for release of latent heat (Wolfsberg et al. 1986).

Typically, potential (or equivalent) temperature surfaces are oriented horizontally. Consider only the common parcel theory dealing with vertical motions in a stable atmosphere. Within this environment, displacement of a parcel either upward or downward will result in a corresponding potential temperature deficit or excess relative to the ambient conditions (assuming no perturbation of the environment by the parcel). Since the parcel density is greater for upward motion (or less for downward motion) than the environment, a buoyancy or reduced gravitational body force is imposed, accelerating the parcel back to the original position before displacement. This effect is demonstrated in Figure 7 for an upwardly displaced parcel, showing the stable oscillatory motion that would exist (Emanuel 1984).

Ideally, momentum surfaces are oriented vertically. Take as an example a revolving fluid confined between two cylindrical walls, as in Figure 8. Consider a tube of fluid circling the center of rotation with a given value of angular momentum per unit mass, M , as defined in the figure. If the parcel (tube) is displaced in the outward radial direction, the conservation of angular momentum, M , provides less angular velocity for the tube than that required to balance the local pressure gradient force, which is again assumed to remain unperturbed by the displacement. This creates a net acceleration of the tube

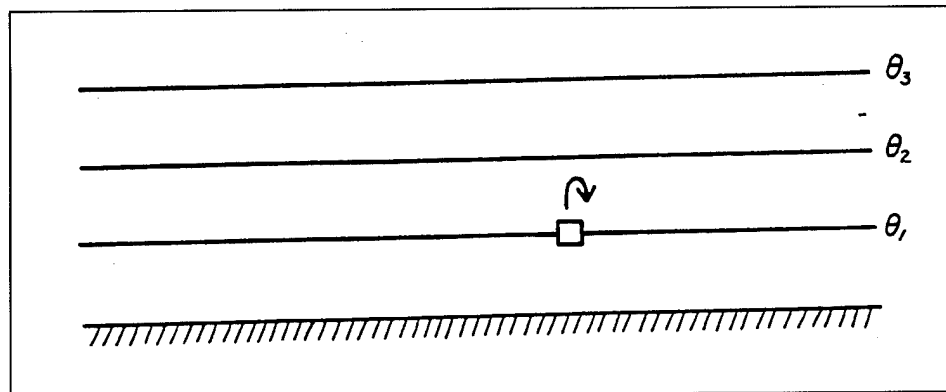


Figure 7. Schematic representation of a vertically stable atmosphere with an oscillating air parcel motion (Emanuel 1984).

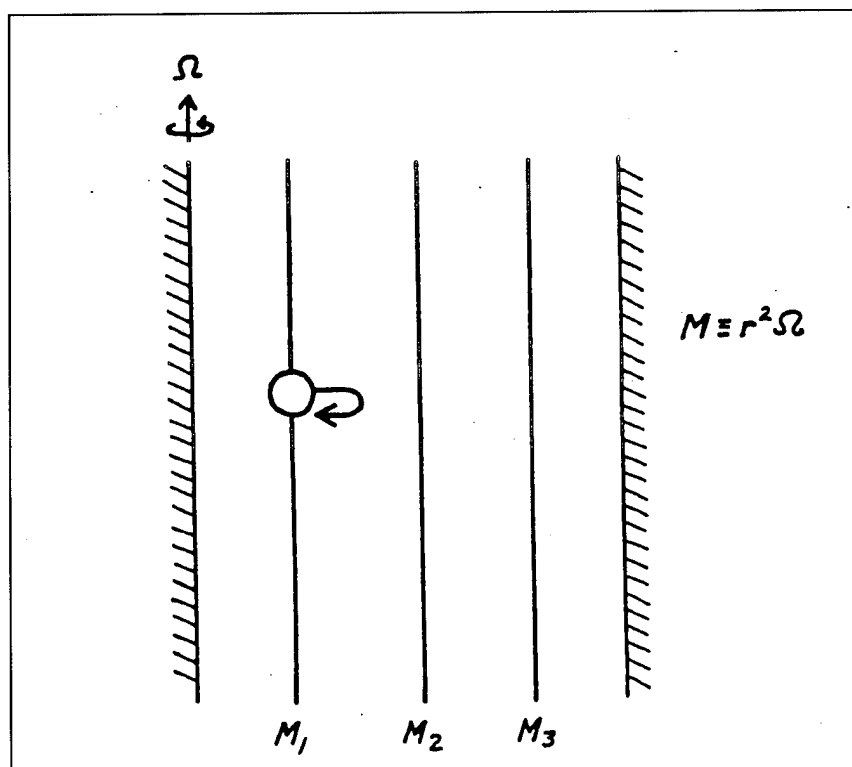


Figure 8. Schematic representation of a rotating fluid confined by two cylinders, with a radially oscillating tube of fluid (Emanuel 1984).

back toward the ambient initial M surface, thus describing a stable system. In this case the acting body force is the centrifugal "force," rather than gravity (Emanuel 1984).

CSI is observed in a region where the slope of the momentum surface is more horizontal than that of the equivalent potential temperature surface. An illustration is shown in Figure 9. From the pseudoangular momentum equation (5), v is the y component of velocity, with the y direction directed into the figure, and x is the zonal displacement relative to the coordinate system. When considering a parcel displacement in this environment, it is necessary to analyze both the effect of buoyancy and geostrophic momentum conservation simultaneously. If a parcel, A, is displaced in either the vertical or horizontal direction, the stable processes described above are qualitatively applicable. However, if a parcel, B, is displaced within the shaded area, an unstable acceleration arises. As the parcel is forced back toward both its original potential temperature surface and its angular momentum surface, its net acceleration is in the direction between both surfaces or "slantwise" (Emanuel 1984).

Elevated Thunderstorms. Colman (1990) defined elevated thunderstorms as those occurring above frontal surfaces. A strong frontal inversion is required because the sharper the thermodynamic contrast across the frontal inversion, the more nearly complete the decoupling between the two layers.

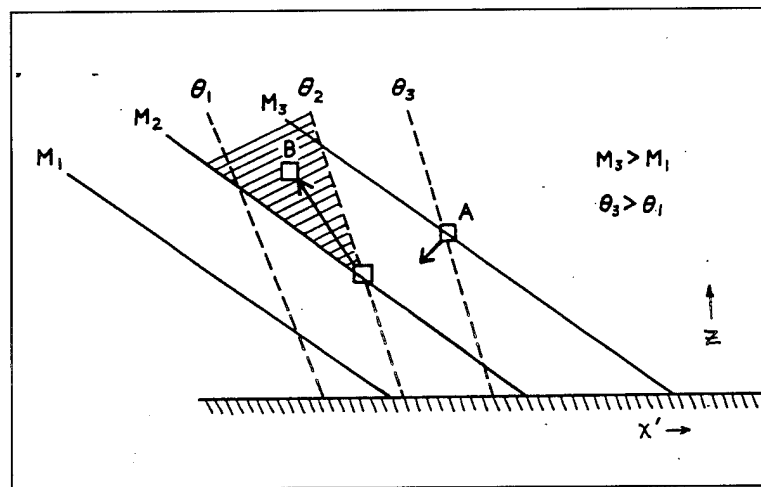


Figure 9. Cross section of an atmosphere representing relative positions of M surfaces (solid lines) and potential temperature surfaces (dashed lines). Parcel in an unstable displacement is shown (Emanuel 1984).

The decoupling would act to decrease the drag on the overriding air, approximating a free-slip interface, and could allow for a more efficient convective overturning. The apparent cessation of elevated thunderstorms upon dissolution of the underlying frontal inversion (often through downward mixing) suggests that the frontal surface plays an active role in the maintenance of these storms. Such storms are isolated from surface diabatic effects, which are often considered fundamental to the development of thunderstorms. Nearly all winter-season thunderstorms over the United States east of the Rockies, but outside of the Florida Peninsula, are of the elevated type. The term "elevated thunderstorms" is intended to replace the more commonly used "overrunning" terminology. The preference for "elevated" over "overrunning" is based on the finding that forcing for these storms does not typically come from convectively unstable air ascending a sloped surface (implied by overrunning), but that they are simply elevated above a frontal inversion. Moore and Lambert (1993) indicate that elevated thunderstorms can also form heavy precipitation bands and are typically associated with regions of observed CSI.

By using the 850 mb and 500 mb analysis maps as tools, one can attempt to forecast where elevated thunderstorms will occur. There is an apparent relationship between the location of elevated thunderstorms and the associated wind maximums at these levels. Colman (1990) indicated that

elevated thunderstorms were frequently located downwind from the 850 mb maximum-wind region and on the cyclonic shear side of this wind maximum. At 500 mb, the pattern differs in that the thunderstorms tend to be located downwind and on the anticyclonic shear side of the wind maximum. This configuration provides a mechanism for the winds to veer with height. Assuming geostrophic balance, mid-tropospheric warm advection is thus indicated in an environment conducive to elevated thunderstorms. The wind speed generally increases with height between these levels producing strong shear and inducing a strong baroclinic environment.

Isentropic Analysis. Using isentropic coordinates offers several advantages in the detection of atmospheric processes over the conventional isobaric analyses. The main advantage comes from the absence of vertical motion under adiabatic conditions. In this way, the air parcels stay on the same "horizontal" (x, y) coordinate surface. Therefore, the considerations about air trajectories and advection of various quantities are simplified. The trajectories on θ surfaces give a better depiction of air motion than isobaric trajectories (Djuric 1994). Isentropic flow presents a more accurate representation of the three-dimensional air motion than isobaric surfaces and preserves the quasi-horizontal behavior of the three-dimensional flow (Carlson 1991). One can estimate if vertical motion is occurring quickly from the advection pattern on the isentropic analysis. By noting the strength of the winds, their

orientation across the isobars, and the strength of the isobaric gradient one can immediately deduce vertical motions.

The ability to track the three-dimensional motion of moisture is probably one of the greatest advantages of isentropic analysis. Unsaturated air parcels not only conserve their potential temperature, but also their mixing ratio (or specific humidity) value while moving along an isentropic surface. Many a forecaster probably has seen patches of moisture "pop up" on 850 mb or 700 mb charts, especially during warm air advection (overrunning) situations. Undoubtedly this moisture is coming up from below the 850/700 mb surfaces - a process one cannot see using a constant pressure perspective. Isentropic uplifting typically represents not only vertical motion but moisture advection as well (Moore 1993).

Moisture Stability Flux (MSF). MSF is a parameter devised by Ralph Petersen of the Development Division of National Meteorological Center (NMC). It is defined as:

$$MSF = -\nabla \bullet [(\bar{q}\Delta P) \mathbf{V}] = \underbrace{-\mathbf{V} \bullet \nabla(\bar{q}\Delta P)}_{\mathbf{A}} - \underbrace{(\bar{q}\Delta P)\nabla \bullet \mathbf{V}}_{\mathbf{B}} \quad (7)$$

where \bar{q} is the average mixing ratio in the layer from θ to $\theta + \Delta\theta$, ΔP is the pressure distance in millibars between the two isentropic surfaces (a measure of the static stability) and \mathbf{V} is the wind vector. Term **A** is the advection of

moisture and static stability. Term **B** is the convergence field acting on the moisture/static stability field. MSF values > 0 indicate that the layer is becoming more moist and less statically stable due to advection and/or convergence. MSF can be useful in the prestorm environment to evaluate the large scale support for deep convection (Moore 1993).

Each of the factors discussed above played an important role in some phase of the HLR flooding event. They didn't come together simultaneously. The return-flow started the sequence of events. Overrunning, MSF, and potential instability were factors present during the 18th and 19th of December 1991, but were not enough to trigger the heavy precipitation. It wasn't until the 20th that CSI and possibly orographic lifting generated elevated thunderstorms, resulting in heavy precipitation. These elevated cells produced heavy precipitation over the same complex terrain which had experienced nearly three days of steady rain associated with the return-flow event.

CHAPTER 4

CASE STUDY

During the week 17 - 23 December 1991, the HLR received abundant amounts of precipitation. Initially, the precipitation started out as light rain, with December 17th accumulations averaging less than one quarter inch. December 18th averages tripled to just under three quarters of an inch as the rain continued to fall. During the three days, December 19 - 21, meteorological conditions combined to generate widespread heavy rainfall. Average three day totals during this period were just over six inches. Flooding was definite by this time, as soil absorption could not keep up with the volume of liquid that was falling.

Table 5 shows the daily precipitation totals at each of the thirty-three LCRA rain gauge locations located in the HLR. Note the anomaly on Monday, 23 December 1991, at Sulteimier (D33). No significant precipitation was recorded at any of the other 32 locations, therefore, it is likely that these totals are accumulations from the weekend (December 23rd was a Monday). This rain

Table 5. Daily precipitation totals from the LCRA rain gauge sites.

Station	Name	17	18	19	20	21	22	23
B11	Bastrop	0.12	1.22	1.22	1.52	4.53	1.85	0.01
B22	Brady	0.09	0.41	0.95	3.92	0.45	0.22	0
B33	Columbus	0.13	1.33	0.49	0.02	3.43	0.73	0
B44	Junction	0.05	0.34	0.5	1.87	0.68	0.12	0
B55	La Grange	0.05	1.17	0.63	0.03	2.98	0.56	0
B66	Mason	0.17	0.4	1.76	4.13	1.03	0.08	0
B77	Menard	0.7	0.23	0.96	3.24	0.6	0.22	0
B88	Mullin	0.02	0.49	1.15	4.91	0.27	0.21	0
B99	Onion Creek	0.23	1.29	0.91	4	2.77	1.63	0
B00	Red Bluff	0.12	0.43	1.16	5.74	0.78	0.1	0
C11	San Saba	0.13	0.54	1.13	5.61	0.82	0.43	0
C22	Walnut Creek	0.29	1.26	0.85	4.1	2.55	1.44	0.01
C33	Winchell	0	0.41	0.91	2.95	0.1	0.15	0
C44	Cook	0.16	0.84	1.48	3	1.76	0.16	0
C44	Newton	0.12	0.72	0.64	3.88	1.76	0.16	0
C55	Sullivan Knob	0.04	0.64	0.76	5.52	1.56	0.16	0
C66	Schulz	0.12	0.64	1.08	4.04	1.8	0.2	0
C77	Braddocks	0.12	0.24	0.36	2.28	1.48	0.84	0
C88	Riley	0.12	0.56	0.8	2.04	2.4	0.92	0
C99	Dean	0.08	0.56	1.36	5.36	1.28	0.12	0
C00	Yates	0.08	0.68	1.28	5.44	1.76	0.16	0
D11	Jordan	0.08	0.56	0.52	2.92	2.24	0.32	0
D22	Oliver	0.04	0.56	0.6	3.92	0	0.2	0
D33	Turner	0.36	0.84	0.48	0.44	0.16	0	0.2
D33	Sulteimier	0.44	1	1.28	2.56	0	0	2.84
D44	Wirtz Dam	0.2	0.64	1.04	1.72	3.08	0.8	0
D55	Phillips	0.32	1	1	2.56	3.8	0.64	0
D66	Mathiews	0.32	0.84	1.64	2.56	2.84	0.04	0.04
D77	Robbins	0.2	0	0.36	0.68	0.96	0.72	0
D77	Lawson	0.28	1.16	2.2	3.68	2.76	0.88	0
D77	Moursund	0.36	0.96	1.72	2.68	4.04	0.44	0
D77	Camp Peniel	0.6	1.12	1.6	3.88	3.52	0.64	0
D77	Monroe	0.32	0.92	1.48	3.56	2	1	0

gauge site is manned by a cooperative observer, and in this instance he may have been absent over the weekend.

This case study will be presented in a chronological format beginning on 12 UTC 16 December 1991. Although precipitation first began on the 17th, it is important to document the evolution of the "return-flow" event that served as a mechanism for providing moisture into the HLR. The study will then proceed in twelve hour increments. Both synoptic scale and mesoscale processes will be discussed, and both isobaric and isentropic analyses will be used to analyze this event. In order to assess the stability of the atmosphere over the HLR and the potential for dynamical lifting, vertical cross section analyses will be used, constructed from Lubbock (LBB) to CRP. These data will be presented in 24 hour intervals, except during the period of most severe flooding when a 12 hour increment will be used. These cross sections (LBB - CRP) were constructed perpendicular to the mean wind in order to evaluate both PI and CSI. In order to accomplish the stability analysis, pseudo-angular momentum and equivalent potential temperature surfaces were constructed.

12 UTC 16 December 1991

Figure 10 is an 850 mb analysis that shows evidence of each phase of the return flow event which first provided moisture to the HLR. The winds at LCH are indicative of the off-shore phase. CRP is in a transitional phase where the winds are parallel to the coast, but becoming more onshore. BRO

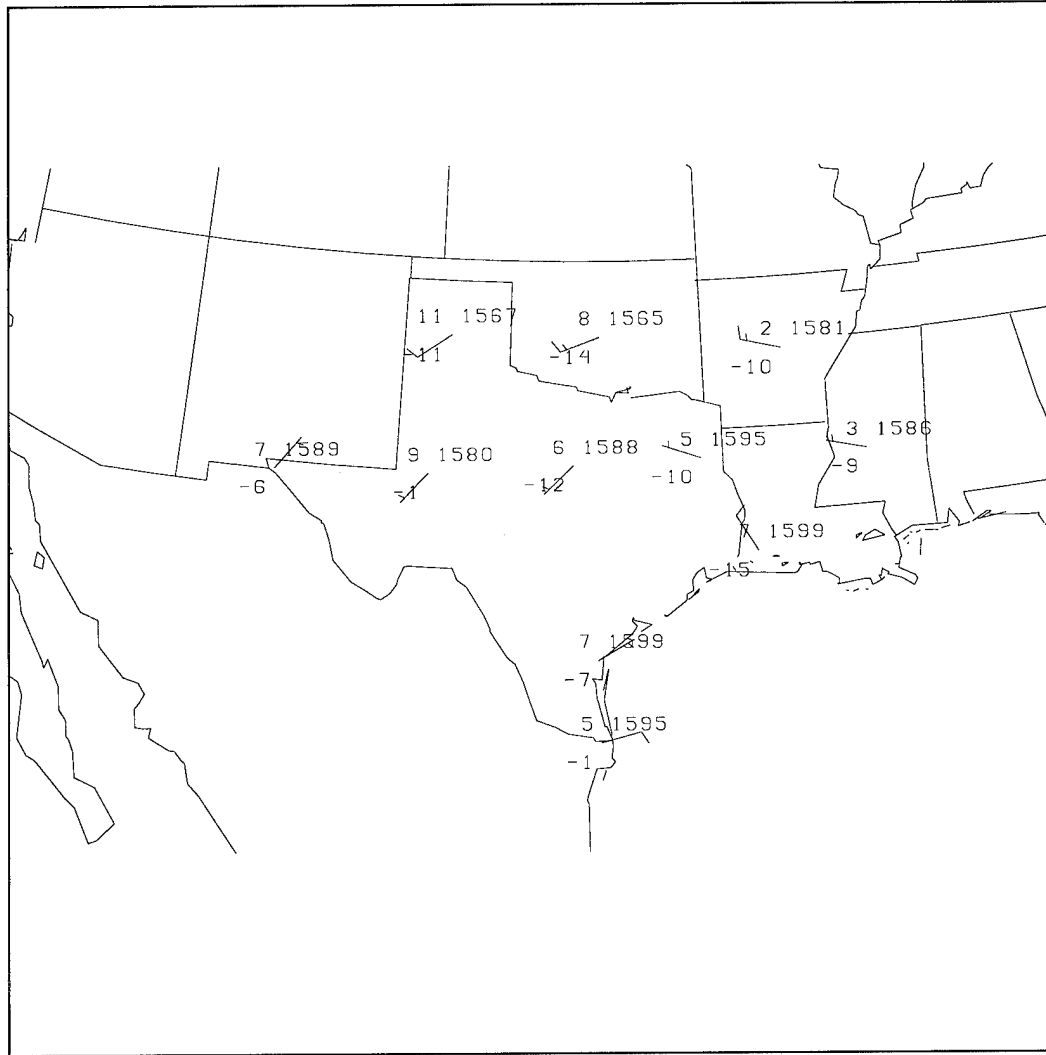


Figure 10. 16 December 1991 12 UTC GEMPAK 850 mb diagram. Temperature in °C plotted upper left of station, dewpoint in °C plotted lower right of station, height in meters plotted lower left of station, and wind plotted with speed in knots.

definitely is under the influence of onshore flow. Dewpoints at 850 mb are dry for LCH (-15°C), characteristic of the cM air mass moving southeastward across the central Gulf states. Where onshore flow is occurring, conditions are more moist (BRO dewpoint -1°C), exhibiting the characteristics of the mM air mass discussed earlier. At CRP, where the flow is perpendicular to the coast, the dewpoint is -7°C ; certainly drier than BRO, but more moist than LCH. Notice also that moisture of Pacific origin appears to be present in west Texas where the dewpoint at MAF is -1°C and the flow is weak southwesterly.

Radiosonde sounding data can also be used to analyze the characteristics of this return-flow event. The BRO sounding (Figure 11) indicates the beginning of the onshore phase of the return-flow event. One can see that above a pre-existing shallow surface cold air mass, the winds are directed onshore, and nearly saturated conditions are evident from 1000 to 850 mb. Also note that upper level westerly winds are advecting nearly saturated conditions aloft, possibly the same Pacific moisture plume seen at 850 mb at MAF. One also notes two distinct frontal inversions; one located just above the surface and another one just above 850 mb, indicative of flow from two separate source regions. Figure 12 shows a water vapor image from six hours prior to the sounding observation. It is apparent from this image, that Pacific moisture is being advected into north Texas by the upper level westerlies. It also

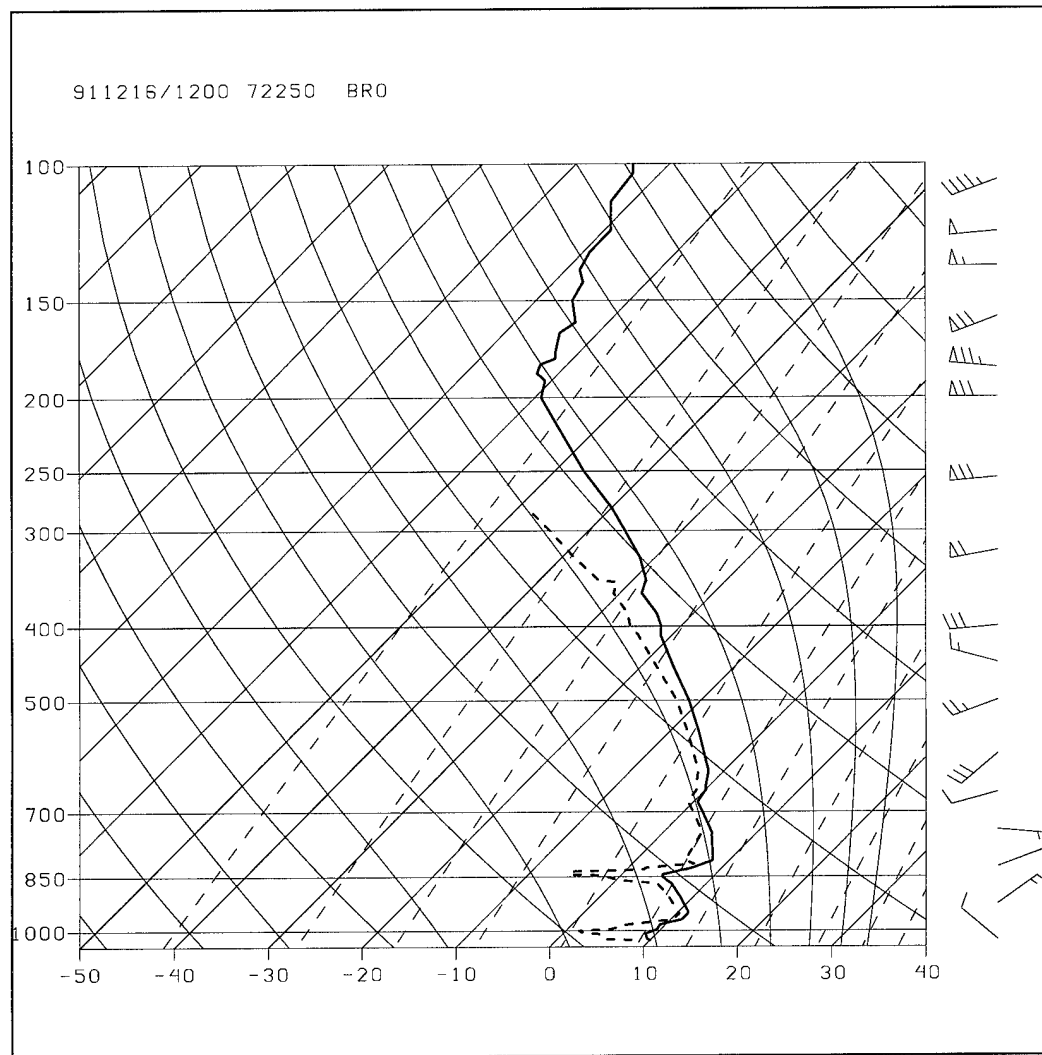


Figure 11. 16 December 1991 12 UTC upper air sounding profile for Brownsville, Texas. Temperature in °C is shown by the solid bold line and dewpoint in °C is shown by the dashed bold line.

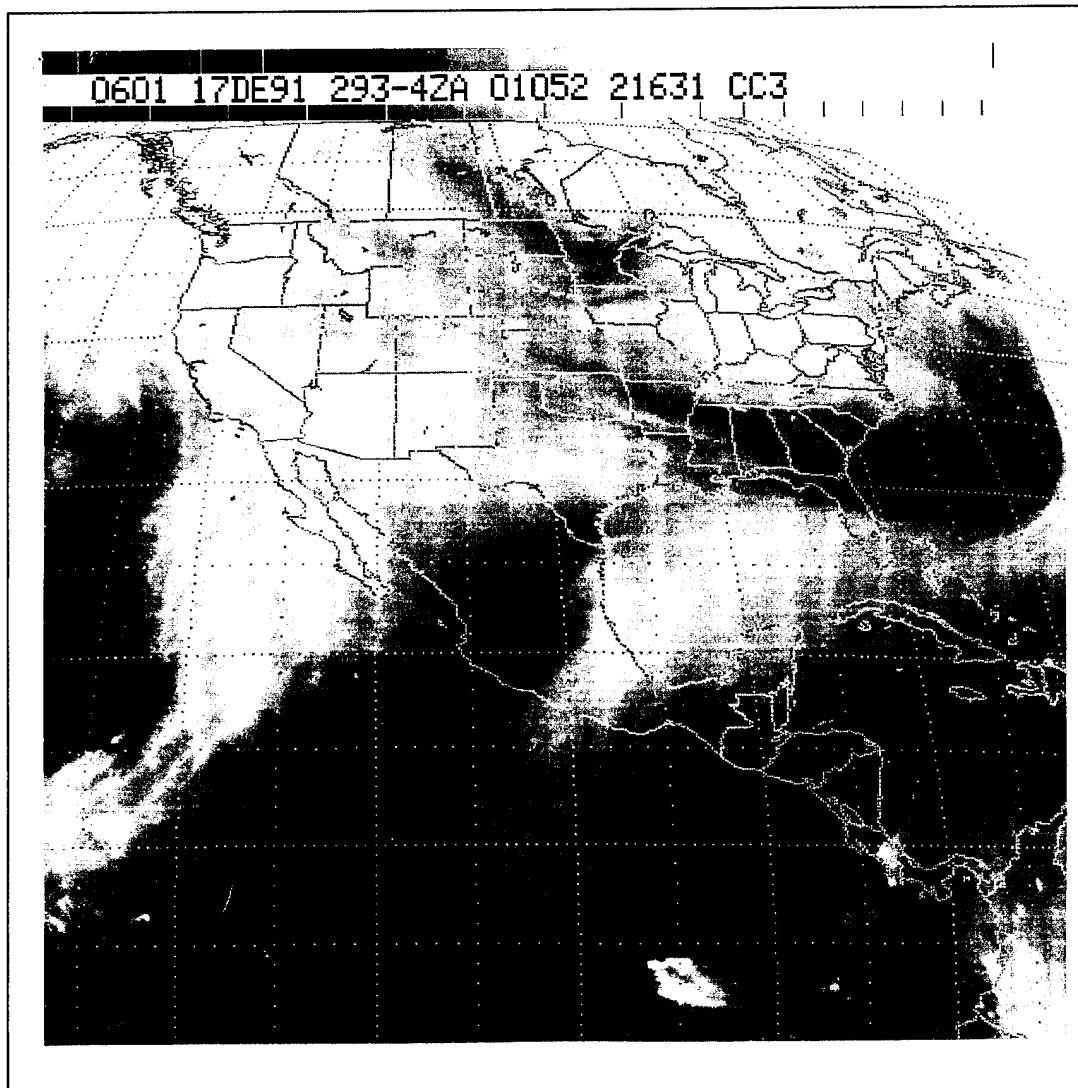


Figure 12. 17 December 1991 0601 UTC water vapor satellite image.

appears that the Gulf moisture being advected into south Texas is being augmented by a second Pacific moist plume originating south of Mexico.

Although the CRP 850 mb data showed less evidence of the start of phase two of the return-flow event, a very shallow, near saturated layer near 900 mb exhibits onshore return-flow characteristics (Figure 13).

It appears that 850 mb data, used by itself, was insufficient to capture the 3D structure of the return-flow event. However, by using isentropic analysis, one can get a more accurate representation of the three-dimensional air motion. The isentropic viewpoint preserves the quasi-horizontal behavior of the three-dimensional flow (Carlson 1991). Using isentropic techniques for December 17th, one will see where the moisture converges and the region where static stability has decreased.

00 UTC 17 December 1991

By this time, the onshore phase is evident over a much deeper layer at BRO and CRP. In fact, LCH also exhibits the "return-flow" at this time. Figure 14 shows an 850 mb analysis where all three Gulf coastal stations exhibit onshore flow. The dewpoints at BRO and CRP are 8 - 11°C higher than 12 hours prior. Notice that although the winds at LCH are southerly, the dewpoint has not changed, indicating that the phase two cycle has just recently begun at LCH. Notice that the Pacific moisture evident at MAF at 12 UTC has now reached SEP. The convergence of the three moist plumes, two of Pacific origin, one of

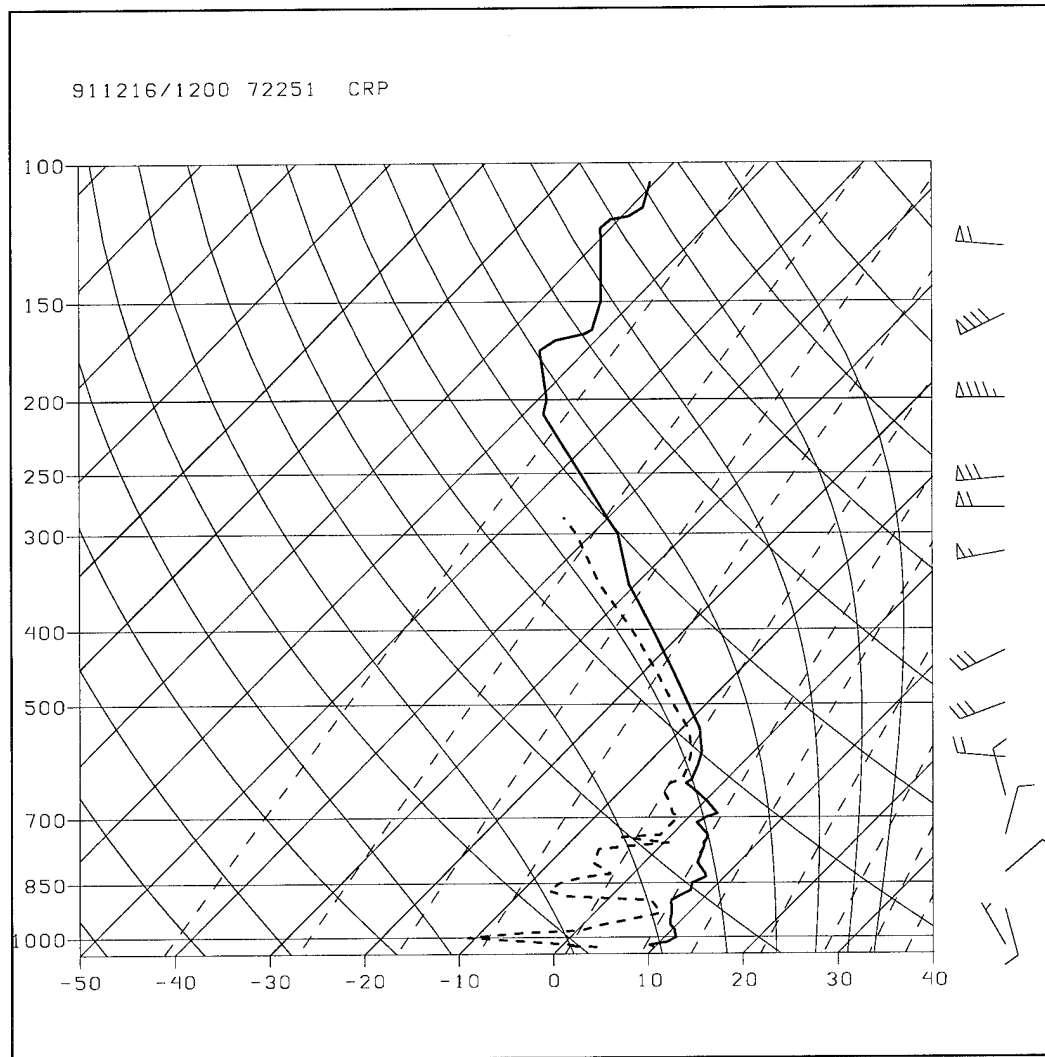


Figure 13. 16 December 1991 12 UTC upper air sounding profile for Corpus Christi, Texas. Temperature in °C is shown by the solid bold line and dewpoint in °C is shown by the dashed bold line.

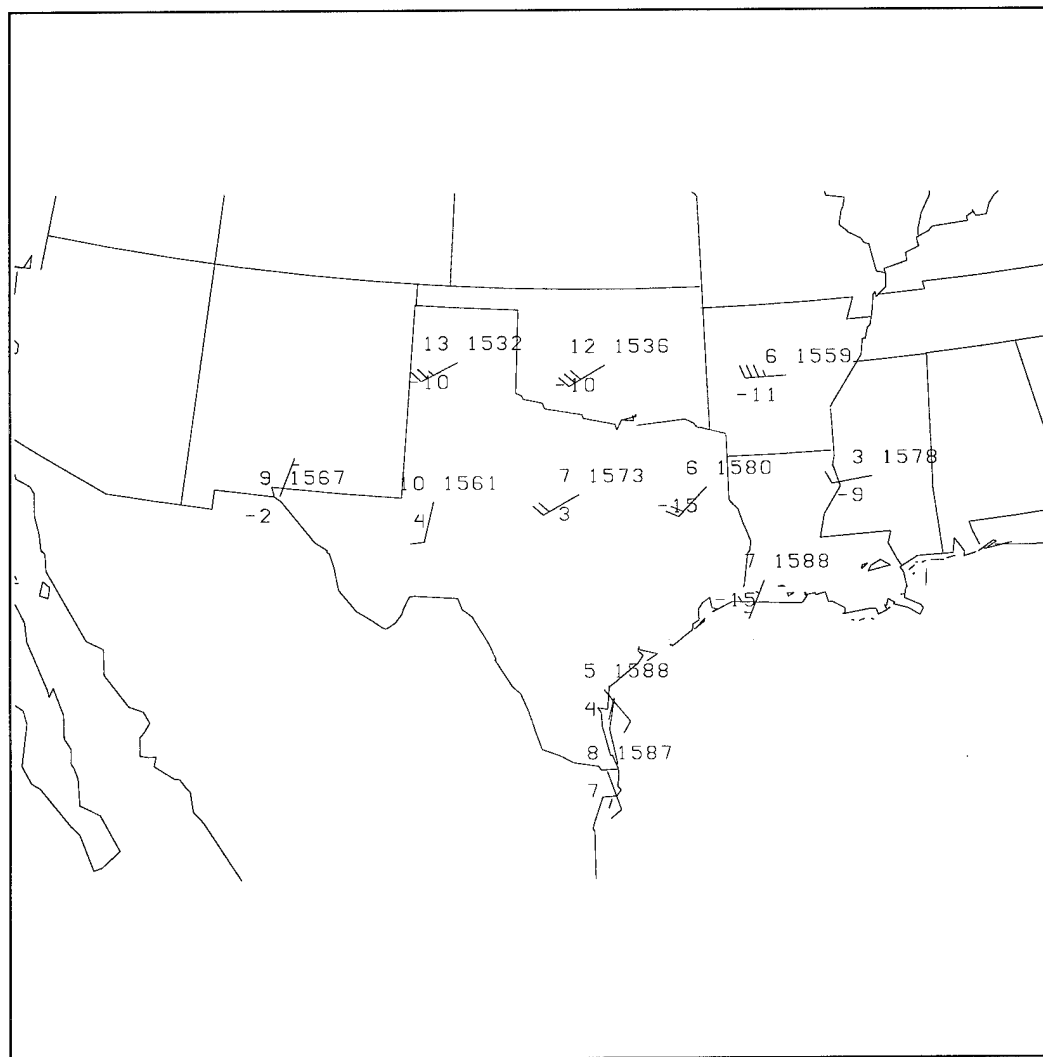


Figure 14. 17 December 1991 00 UTC GEMPAK 850 mb diagram. Temperature in °C plotted upper left of station, dewpoint in °C plotted lower right of station, height in meters plotted lower left of station, and wind plotted with speed in knots.

Gulf origin, over the HLR served as a precursor to the flooding which would take place over the next several days.

Figure 15 and 16 are the SkewT - ln p diagrams for BRO and CRP respectively. Although a very shallow surface cold air mass continues to be in place over south Texas, a deep layer of Gulf air is overrunning this shallow cold air dome. The CRP sounding (Figure 16) looks very similar to the BRO sounding from 12 hours previous. This progression of similar thermodynamic conditions northward along the Texas coast is evidence of a classical return-flow event. Note that the moisture from 750 - 400 mb is probably of Pacific origin and is flowing over the top of the layer of Gulf return-flow.

12 UTC 17 December 1991

The CRP sounding, shown in Figure 17, continues to show strong indications of both Pacific and Gulf moisture extending from the surface to approximately 625 mb. Gulf moisture continues to surge northward overrunning shallow cold air, and Pacific moisture is still overrunning the Gulf air. In order to assess the magnitude of the influx of these two moisture sources into south Texas, an isentropic analysis of moisture convergence on the 295K surface was constructed (Figure 18). The 295K surface was selected because it was representative of the temperature characteristics of the return-flow mM air mass. Negative values (dashed) indicate moisture convergence and positive values (solid) indicate moisture divergence regions. One plume extends

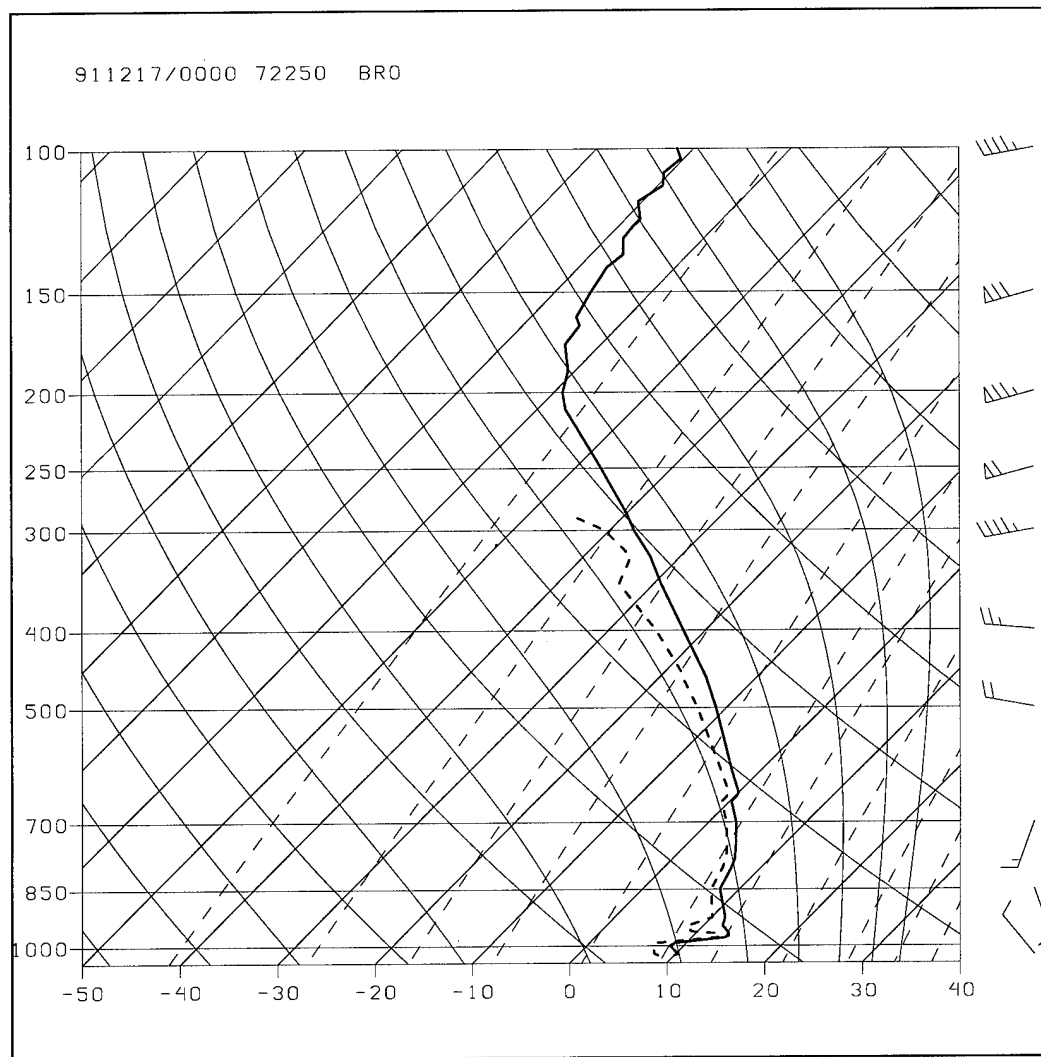


Figure 15. 17 December 1991 00 UTC upper air sounding profile for Brownsville, Texas. Temperature in °C is shown by the solid bold line and dewpoint in °C is shown by the dashed bold line.

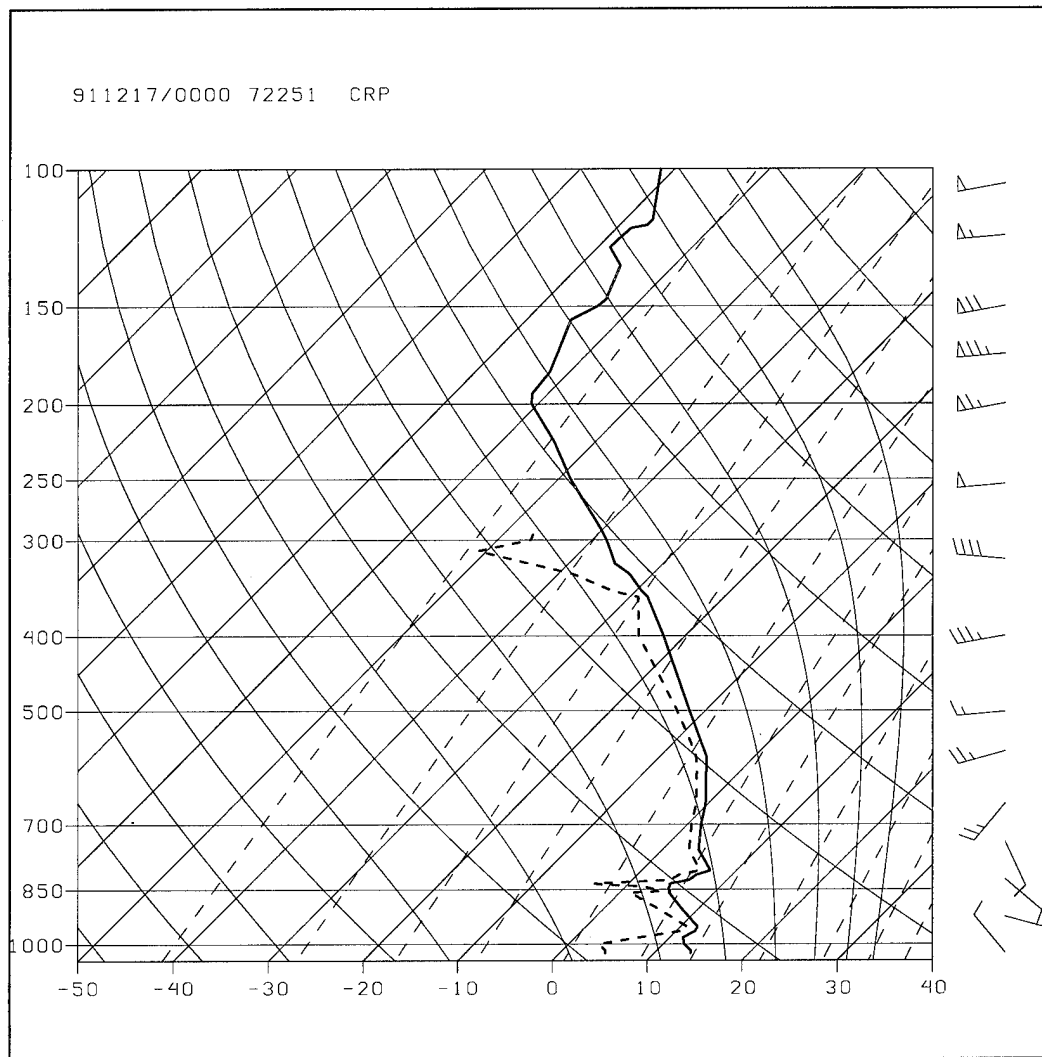


Figure 16. 17 December 1991 00 UTC upper air sounding profile for Corpus Christ, Texas. Temperature in °C is shown by the solid bold line and dewpoint in °C is shown by the dashed bold line.

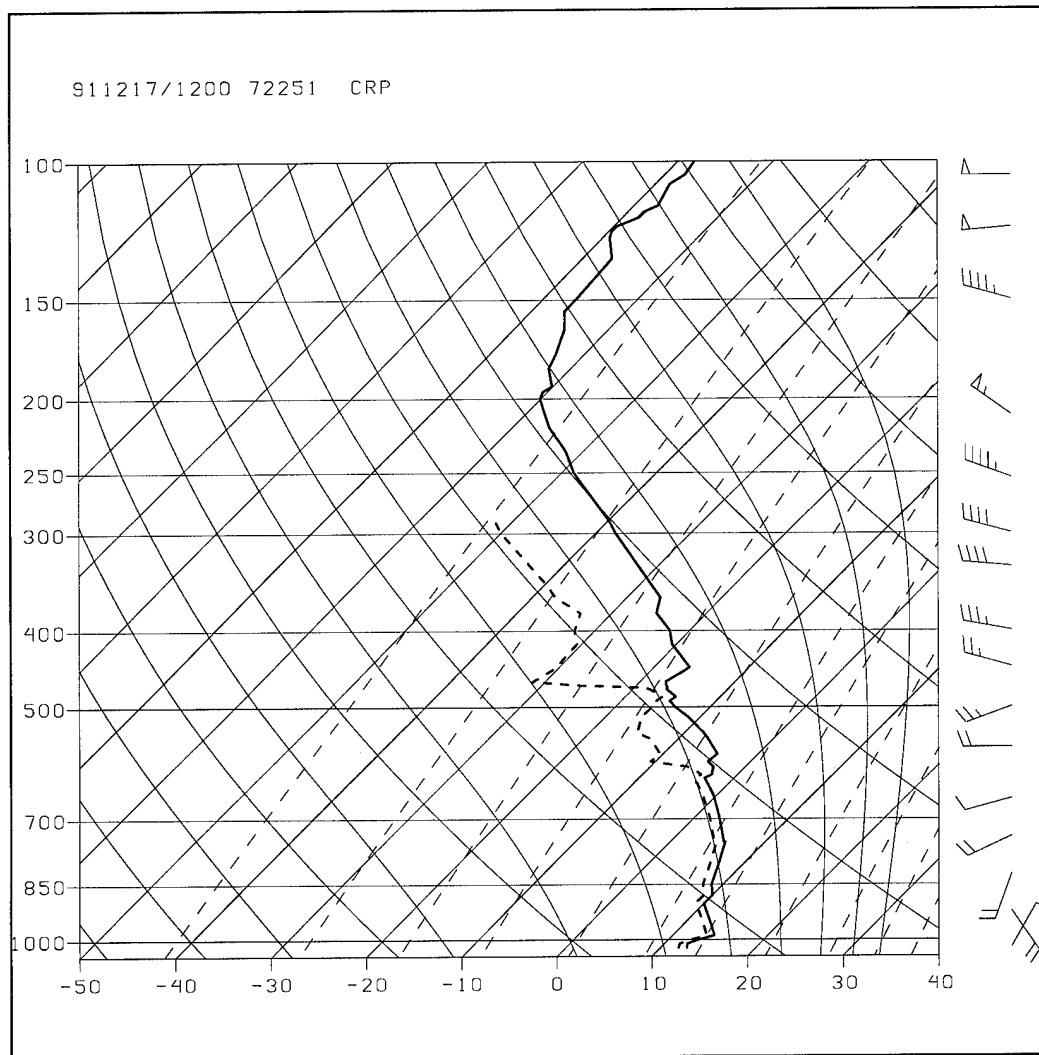


Figure 17. 17 December 1991 12 UTC upper air sounding profile for Corpus Christi, Texas. Temperature in °C is shown by the solid bold line and dewpoint in °C is shown by the dashed bold line.

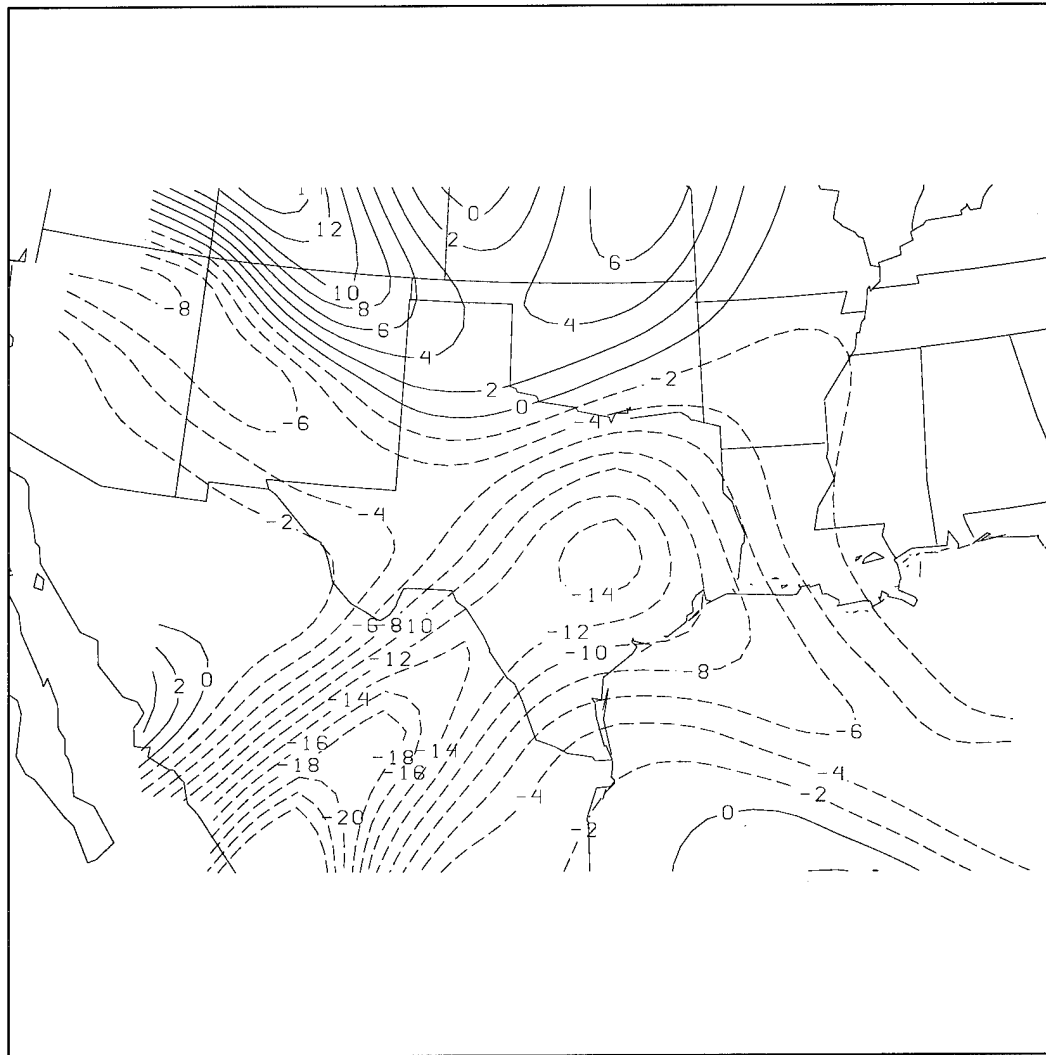


Figure 18. 17 December 1991 12 UTC moisture convergence on a 295K isentropic surface.

across Mexico and into southwest Texas. The other extends from the Gulf and is the return-flow mM air mass. These two axes converge across central Texas and the HLR.

In addition to the advection of moisture, one can also assess the advection of stability. The combined advection of moisture and static stability can be summarized as MSF (Chapter 3). An MSF diagram was plotted for the 295 - 300K layer and is shown in Figure 19. Rationale for choosing this layer was identical to that of Figure 18. Areas of moisture convergence and decreased static stability are indicated by positive values (solid lines). Moisture divergence and statically stable regions are indicated by negative values (dashed lines). The strongest convergence lies over south central Texas at the intersection of the previously analyzed dual moist tongues. Notice that this intersection is just south of the Balcones Escarpment. Any influx of this moisture northward into the complex terrain of central Texas would result in certain lifting of these deep, nearly saturated plumes.

Figure 20 shows a gridded cross section analysis constructed from Lubbock (LBB) to CRP. Pseudo-angular momentum surfaces are shown in solid lines and equivalent potential temperature surfaces are shown in dashed lines. A region of PI is shown by the hatched shading. This region is at the intersection of the moist plumes, and the PI appears to be created by the influx of low level warm air from both the Pacific and the Gulf.

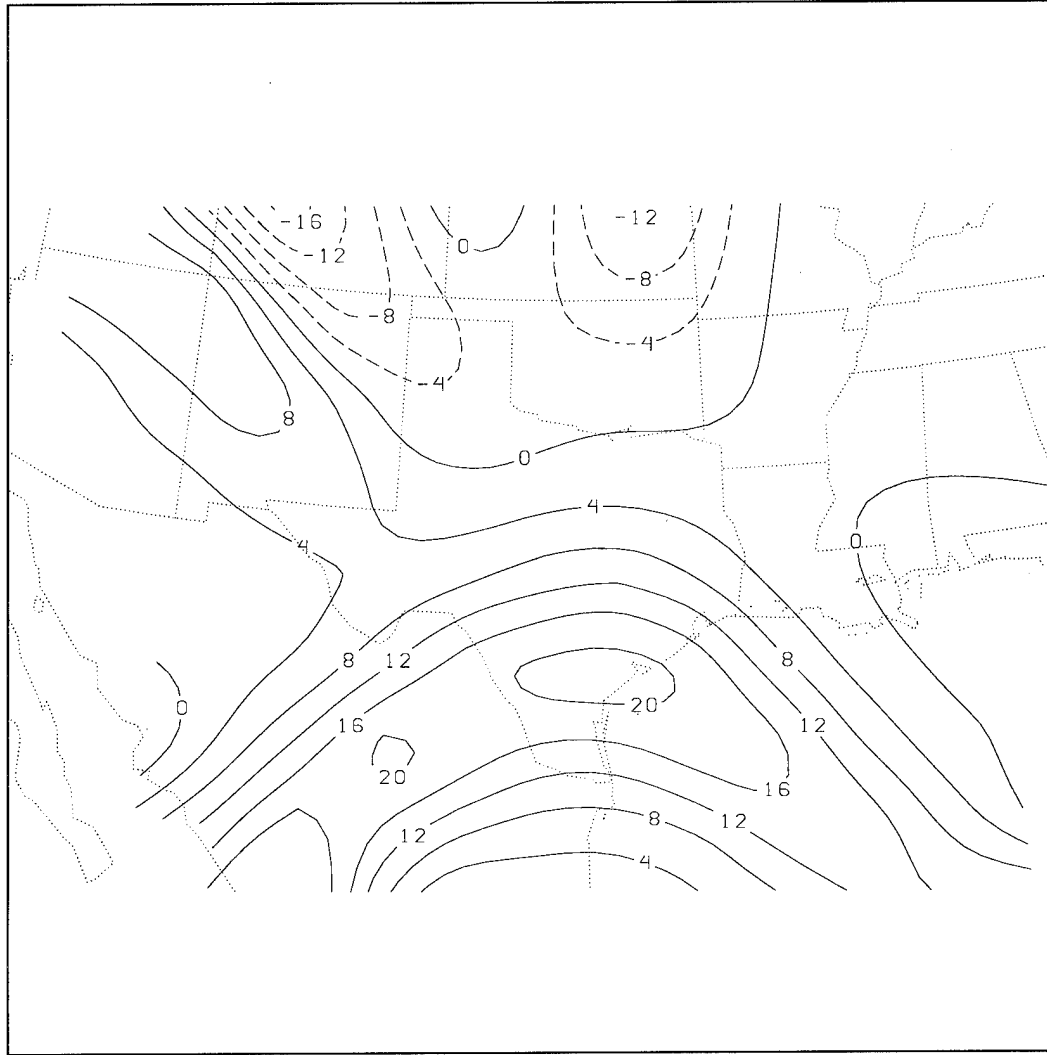


Figure 19. 17 December 1991 12 UTC moisture stability flux plotted for the isentropic layer 295:300K.

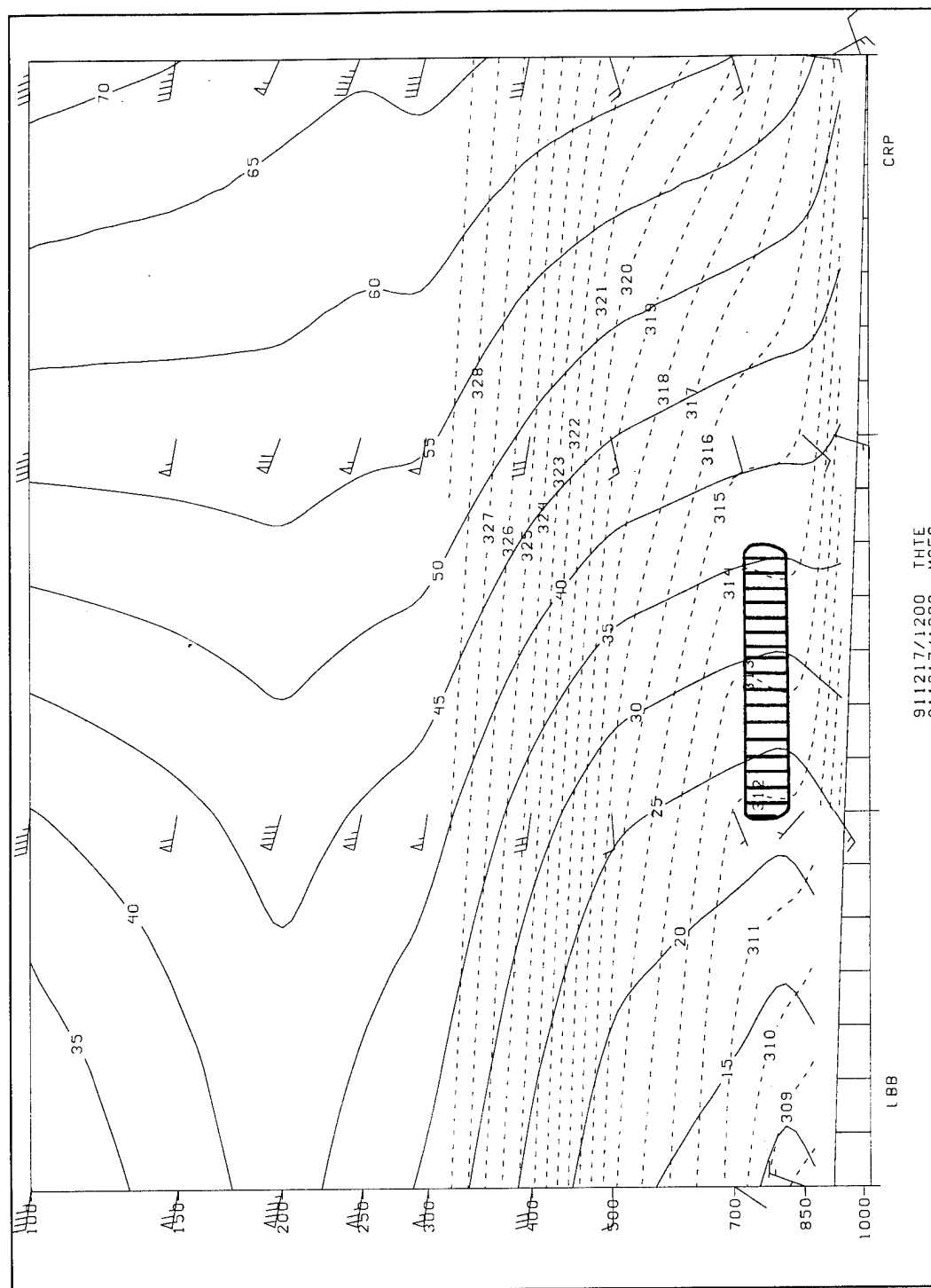


Figure 20. 17 December 1991 12 UTC cross section analyses of equivalent potential temperature surfaces (dashed lines) and psuedo-angular momentum surfaces (solid) from Lubbock (LBB) to Corpus Christi (CRP), Texas. The hatched region depicts a region of potential instability.

Figure 21 shows a visible satellite image during this time indicating solid stratified cloudiness from the southeast Texas coastal area into the HLR. The cloud cover field matches nearly identically with the MSF field depicted in Figure 19. It was during this time period that light precipitation began to fall in the HLR. Precipitation amounts were light, with most accumulations less than one quarter of an inch. There were two reports greater than one half inch. Menard (B77) reported .70 and Camp Peniel (D77) reported .60 inches of rain.

00 UTC 18 December 1991

After the onset of the return-flow, an approaching synoptic scale cyclone from the west began to influence the HLR. The strong dynamical forcing associated with this system began to act on the existing saturated conditions, providing the necessary conditions for heavy precipitation. Figure 22 shows the 300 mb analysis. A 110 knot wind speed maximum located over the central Gulf of Alaska was moving down the west side of a long wave trough. This trough was oriented on a north-south axis and extended from the northern Gulf of Alaska to the east central Pacific. Nearly zonal flow extended from southern New Mexico, into central Texas, and then into the northern Gulf of Mexico.

Figure 23 shows the 500 mb analysis. The long wave trough off the Pacific coast evident at 300 mb, is also apparent. A closed low was located in the central Gulf of Alaska. The long wave trough extended from this low

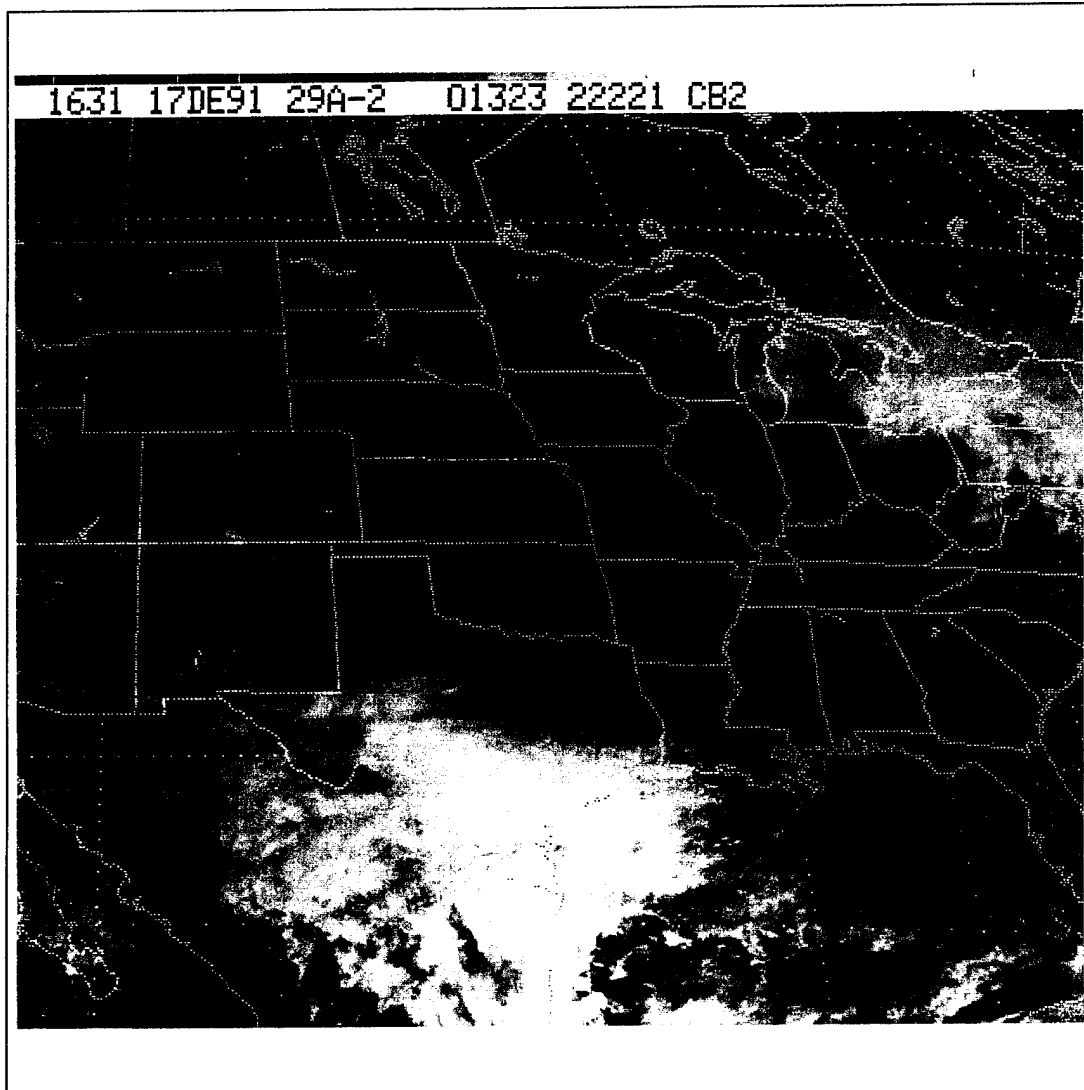


Figure 21. 17 December 1991 1631 UTC visible satellite image.

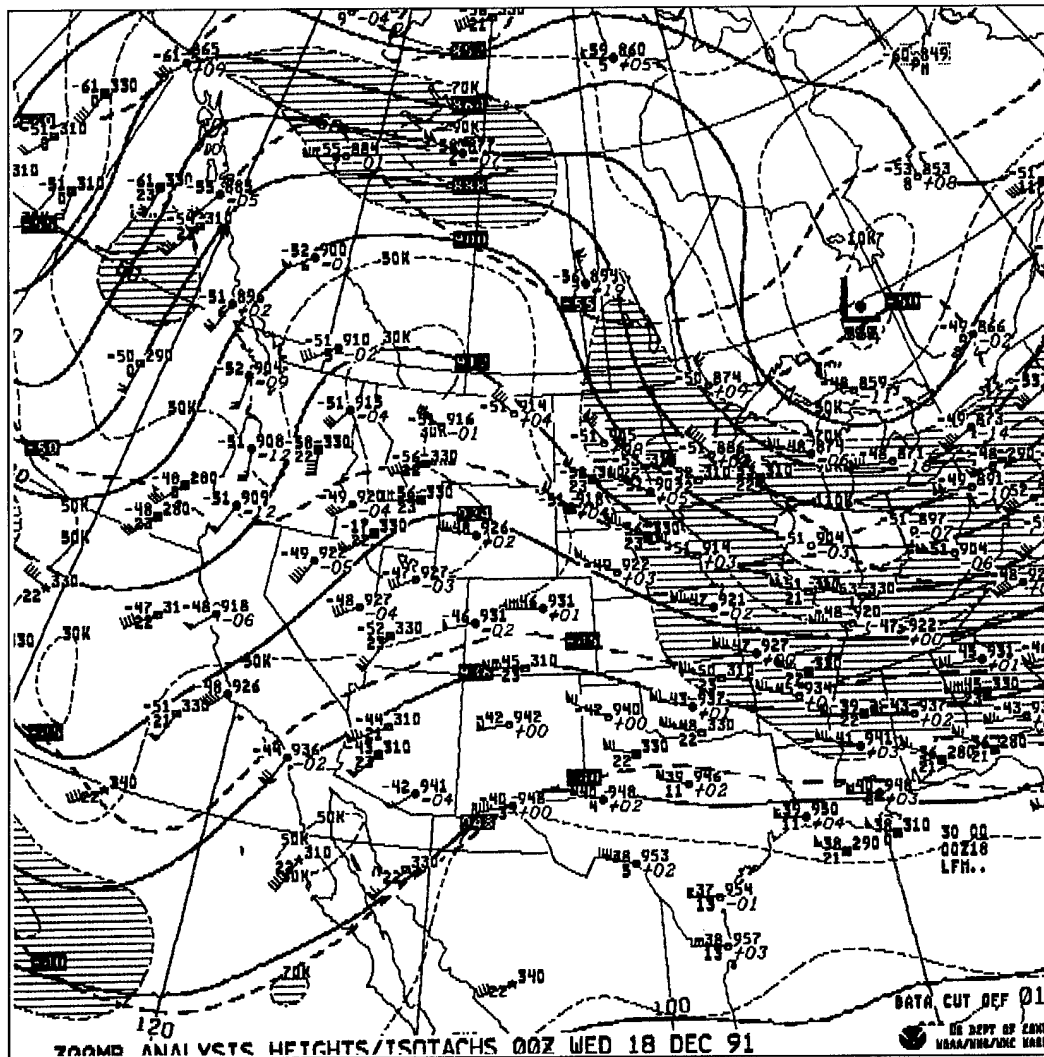


Figure 22. 18 December 1991 00 UTC LFM 300 mb analysis.

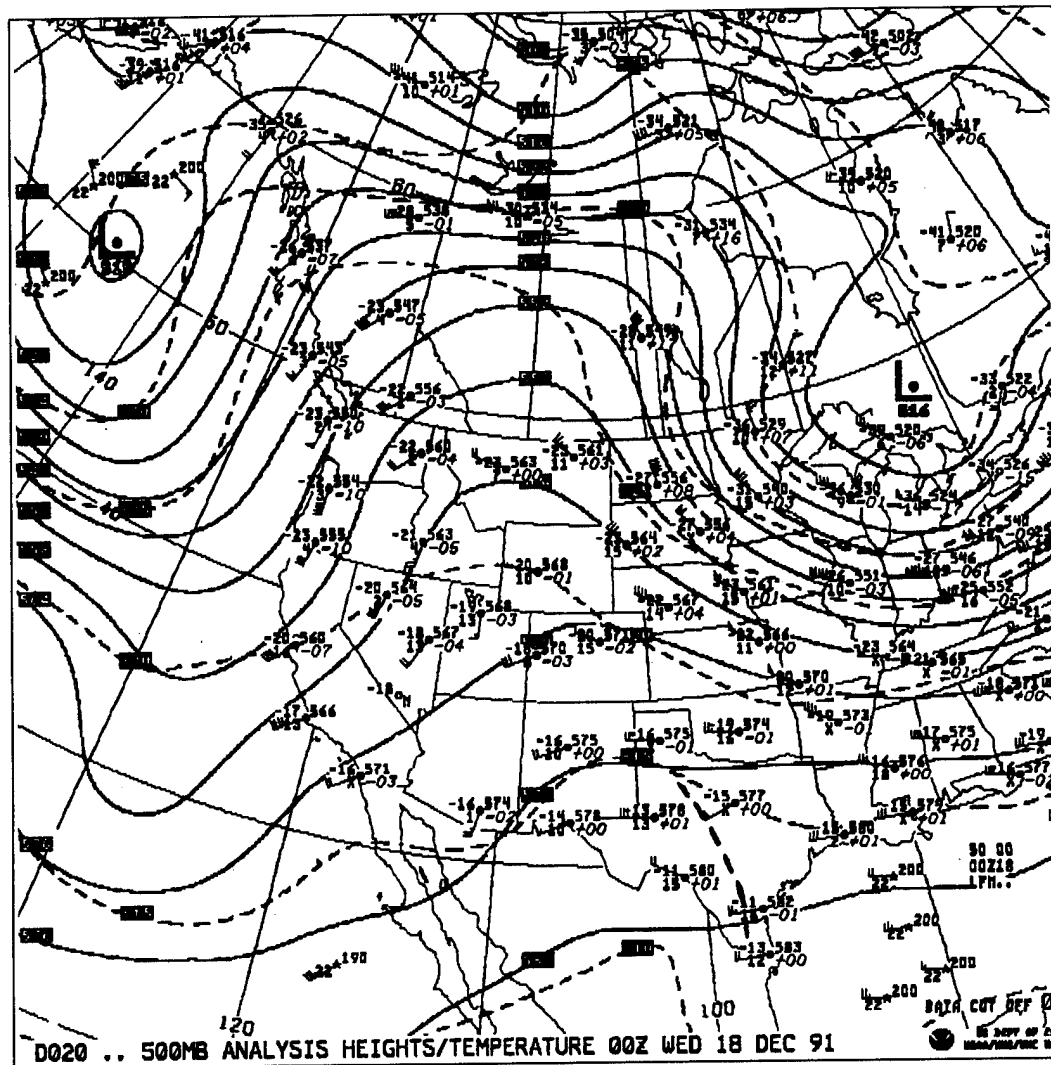


Figure 23. 18 December 1991 00 UTC LFM 500 mb analysis. The dashed line indicates the position of the weak short wave trough located west of the HLR.

southward to the east central Pacific. The location of this trough was slightly east of the 300 mb trough. In addition, there was a weak short wave trough located west of the HLR (bold dashed line on Figure 23). This trough extended on a line northwest to southeast from just west of SEP to just west of CRP. The existence of this short wave would also support the enhanced cloudiness and light precipitation observed at this time.

At 850 mb (Figure 24), the long wave trough depicted at 300 mb and 500 mb was evident. One notes the anticyclonic curvature and confluent nature of the flow over the HLR, a configuration which would also support the observed conditions.

12 UTC 18 December 1991

The 110 knot wind speed maximum continued to move down the west side of the 300 mb long wave trough located off the northern California coast (Figure 25). An eastward propagation of the trough was evident. Continued zonal flow was also observed through central Texas with speeds of 45 - 50 knots.

Figure 26 shows the 500 mb analysis. The closed low that was evident twelve hours earlier is no longer apparent, although the open long wave trough is still present and is located east of the 300 mb long wave. Weak anticyclonic curvature is evident through central Texas and wind speeds in this region are between 30 and 40 knots.

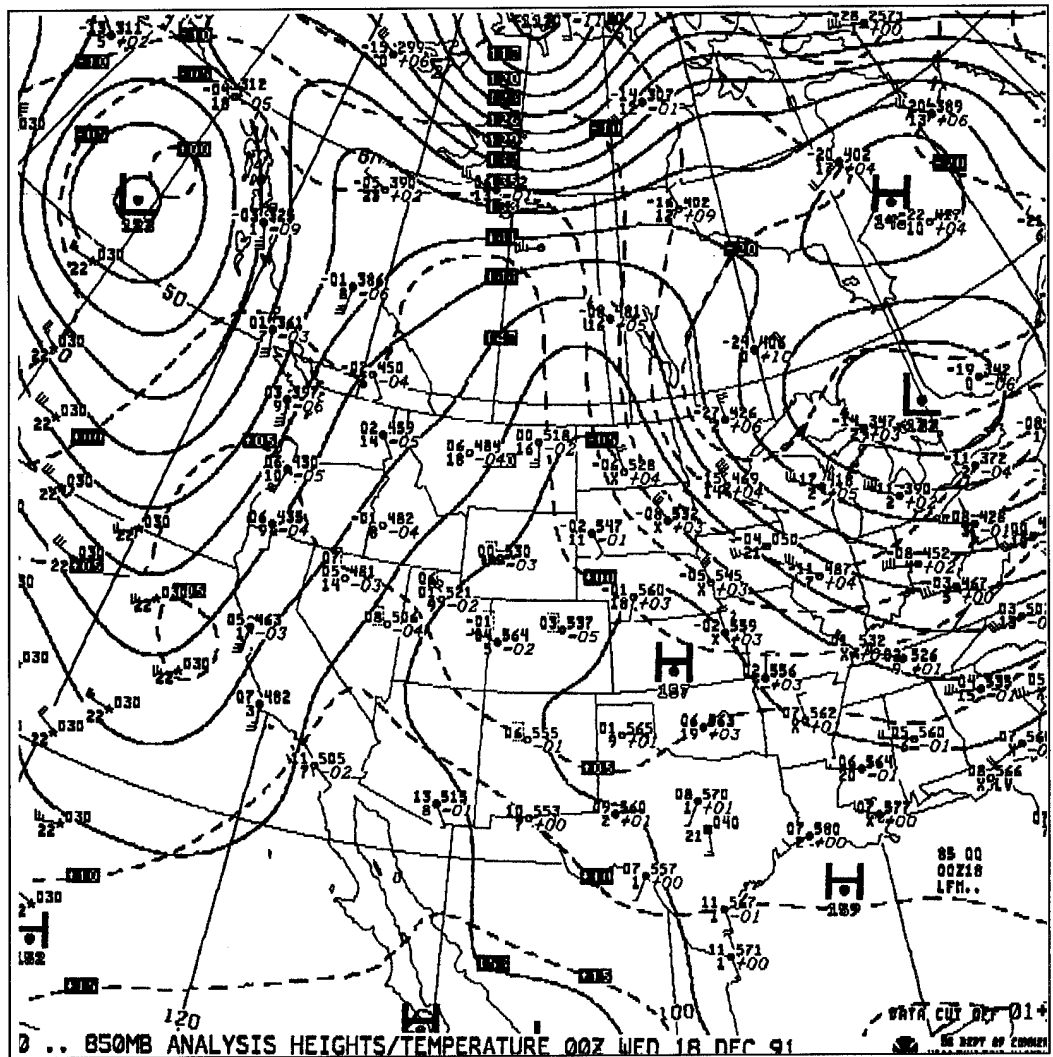


Figure 24. 18 December 1991 00 UTC LFM 850 mb analysis.

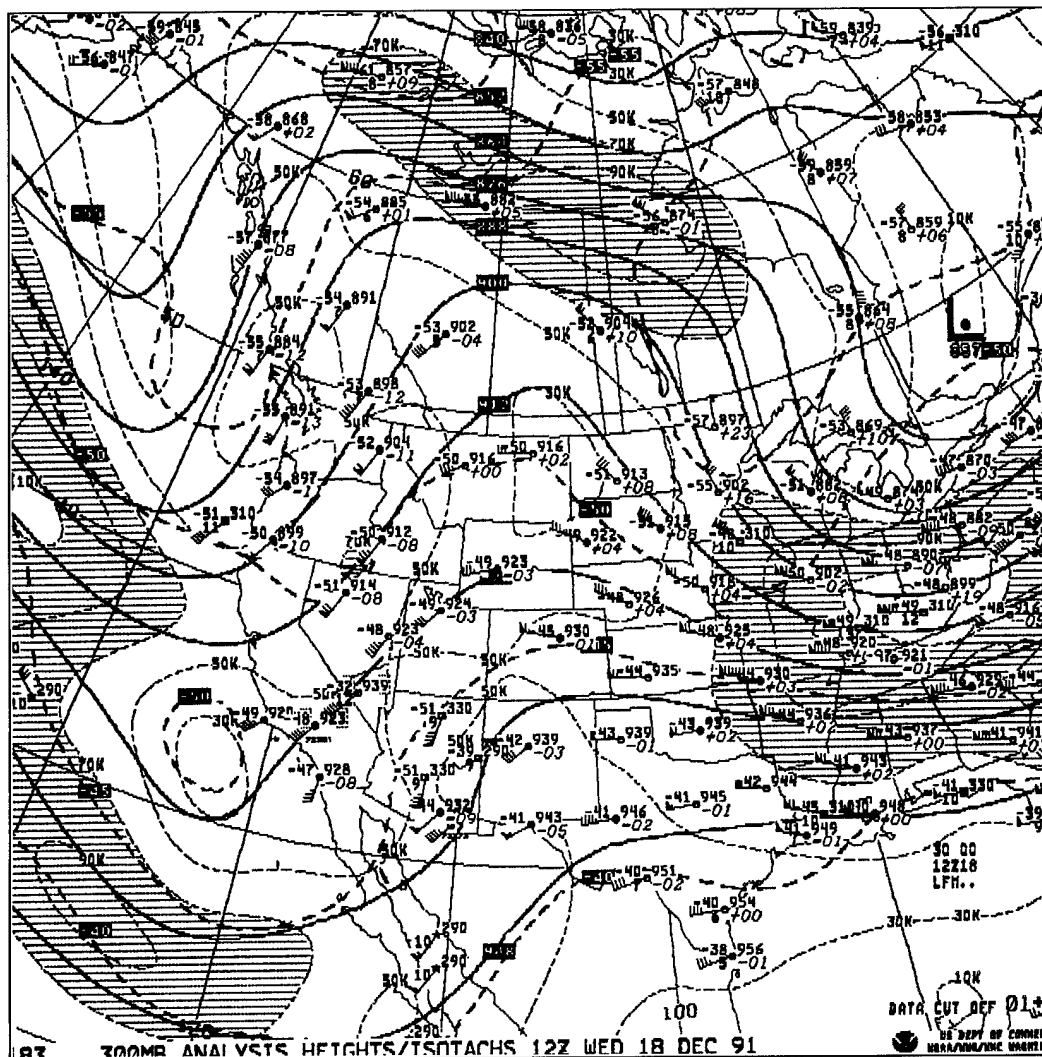


Figure 25. 18 December 1991 12 UTC LFM 300 mb analysis.

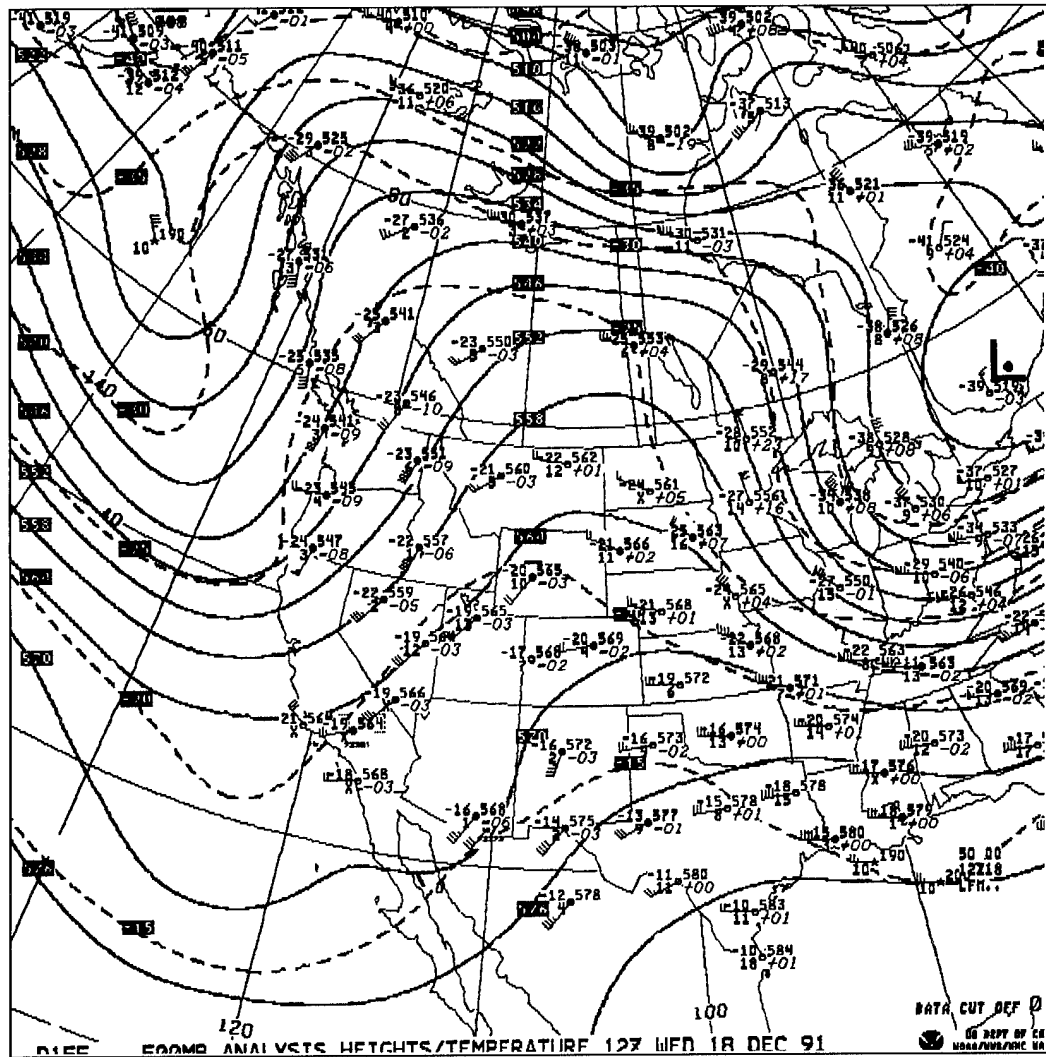


Figure 26. 18 December 1991 12 UTC LFM 500 mb analysis.

Figure 27 shows the 850 mb long wave trough aligned with the same orientation as the 300 mb and 500 mb long wave troughs. A closed low has formed in the base of the long wave trough and is located over northwestern Mexico. Strong ridging continues to persist along the Texas - Louisiana border. The low level Gulf moisture plume now extends northward to the Texas - Oklahoma border.

Surface features are shown in Figure 28. An inverted trough is analyzed over the southeast coast of Texas. Light rain and drizzle extends from southeastern Texas into north central Texas. Although the surface wind field shows a northeasterly component, Pacific and Gulf moisture continue to overrun the top of the shallow cold air dome.

Analysis of the vertical structure of the atmosphere across this region shows the persistence of PI and a developing region of CSI through central Texas associated with the overrunning moisture (Figure 29). This warm moist overrunning air shows up as a wedge of high equivalent potential temperature air, generating a vertical profile of equivalent potential temperature which results in PI. The depth of this layer has increased as the return-flow process continues. The surface stationary front also appears on this diagram. One notices the strong stability indicated from the tight packing of the equivalent potential temperature surfaces between 850 - 700 mb.

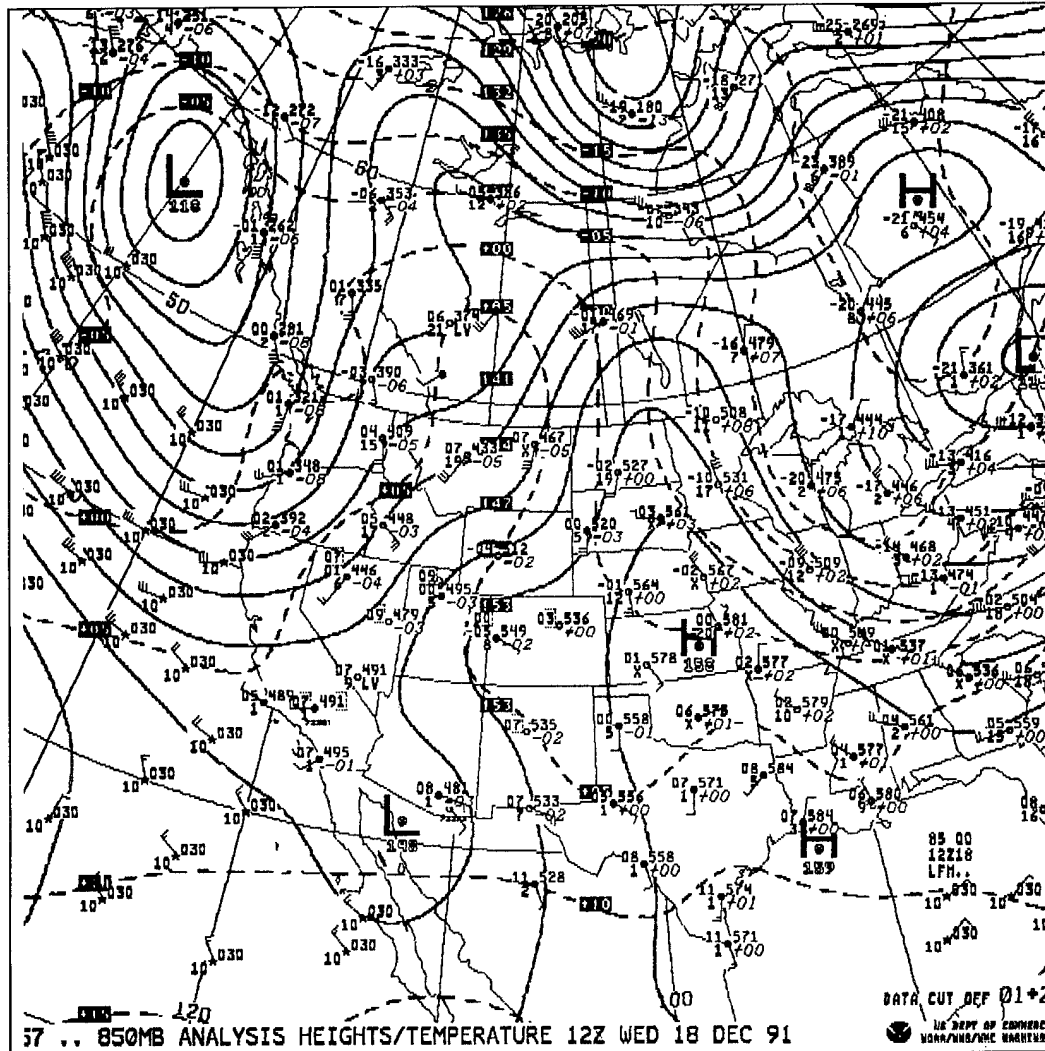


Figure 27. 18 December 1991 12 UTC LFM 850 mb analysis.

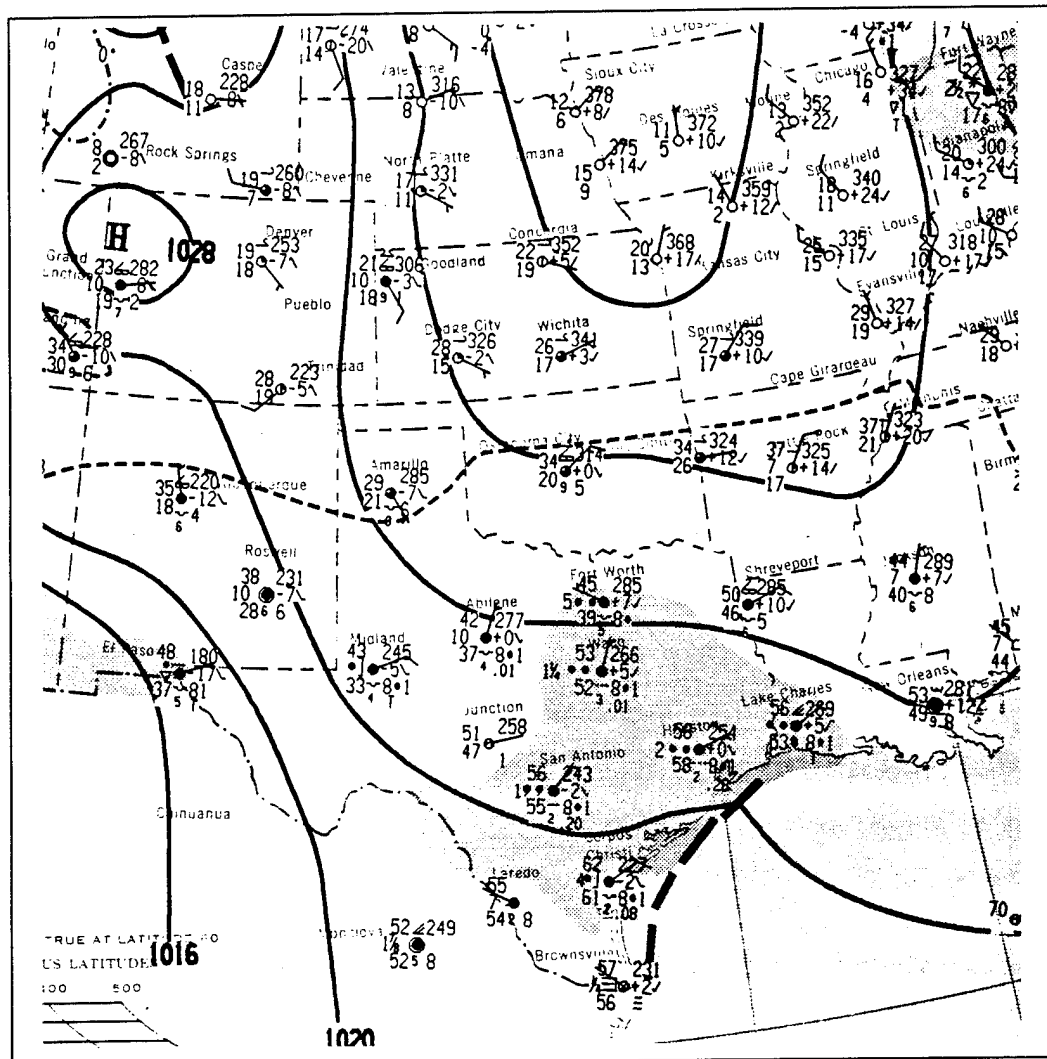


Figure 28. 18 December 1991 12 UTC daily surface weather map.

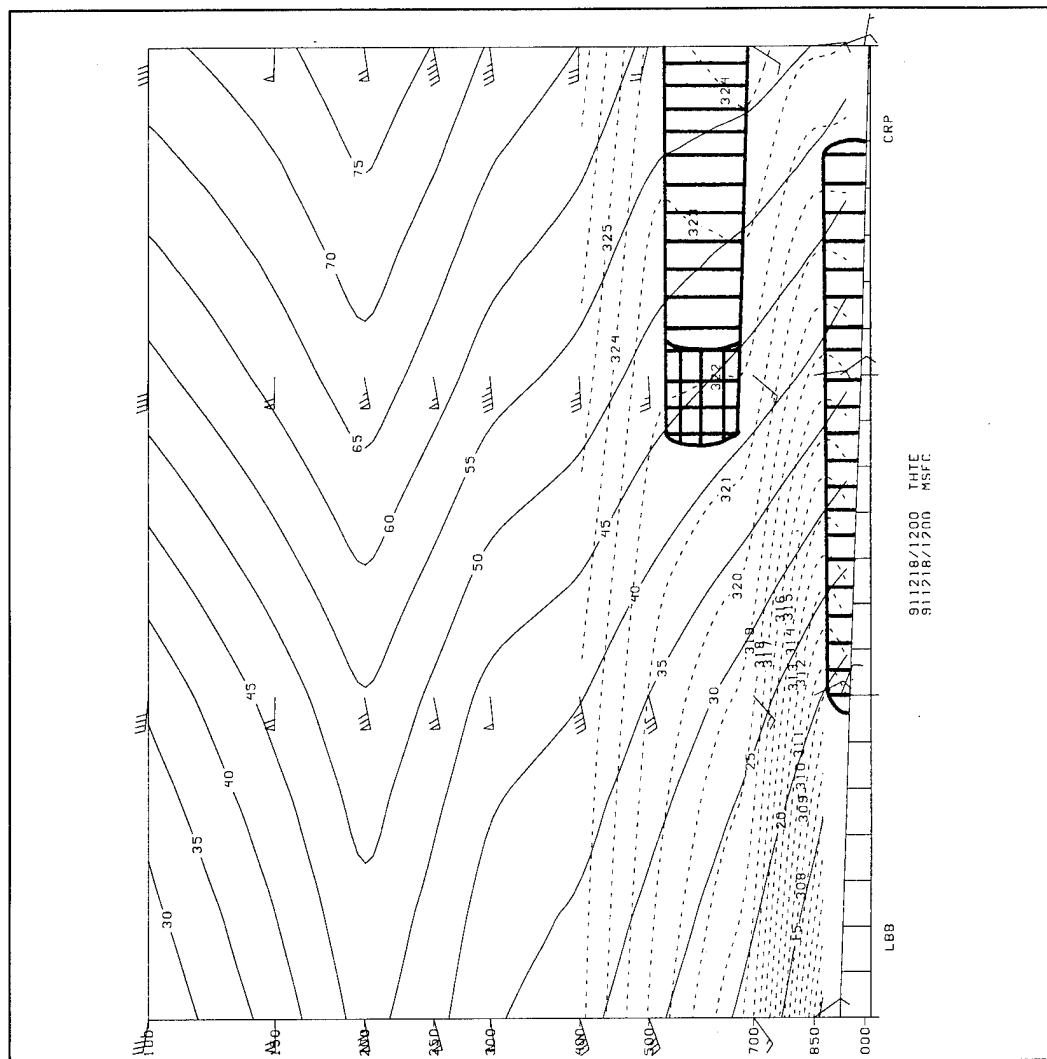


Figure 29. 18 December 1991 12 UTC cross section analyses of equivalent potential temperature surfaces (dashed lines) and pseudo-angular momentum surfaces (solid) from Lubbock (LBB) to Corpus Christi (CRP), Texas. The hatched region depicts a region of potential instability and the cross hatched region depicts CSI.

Precipitation amounts on this day increased three-fold from the previous day. Daily precipitation averages were near three quarters of an inch. There were multiple reports greater than one inch with a maximum of 1.33 inches being reported at Columbus (B33). The increase in precipitation was probably due to the significant deepening of the moist layer, thus increasing the PI, CSI, and making more moisture available to precipitate out.

00 UTC 19 December 1991

Figure 30 shows the 300 mb analysis. The long wave trough axis has continued to move slowly eastward. The long wave trough extends from the south-central Alaska coastal region to central Baja. A 110 - 120 speed maximum continues to move down the west side of this trough and is located off the north central California coast. A secondary speed maximum (90 knots) is also apparent in the base of the trough off the Mexican coast. Weak anticyclonic curvature and wind speeds of 40 - 55 knots are located over central Texas.

Figure 31 shows the 500 mb analysis. The long wave trough continues to mirror the 300 mb long wave trough. Ridging is evident from southern Texas into the northern Plains. There is a low center located in southern Alaska. Wind speeds of 20 - 25 knots and anticyclonic curvature are apparent over the HLR, and the moisture amounts have also increased over north central Texas. The 500 mb flow pattern also appears to be diffluent over the HLR which

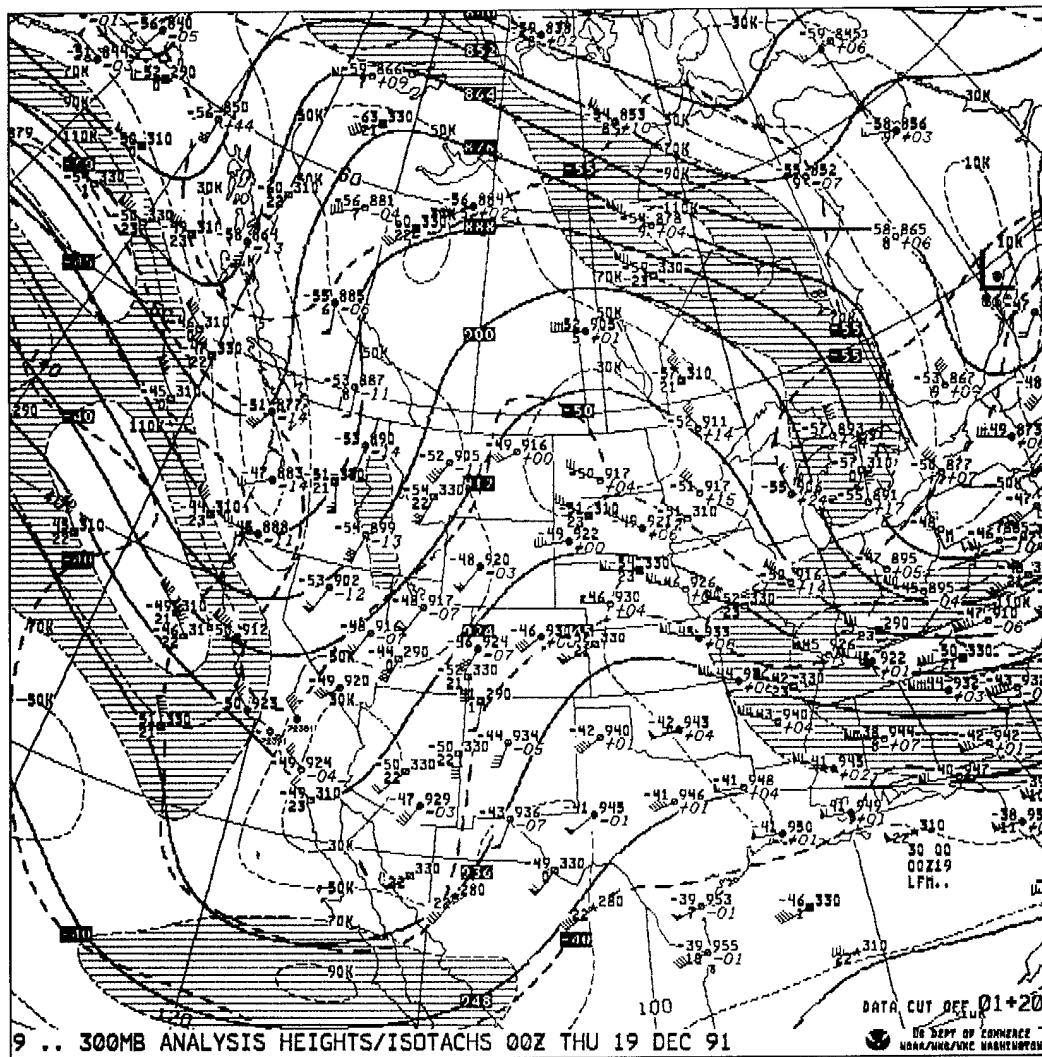


Figure 30. 19 December 1991 00 UTC LFM 300 mb analysis.

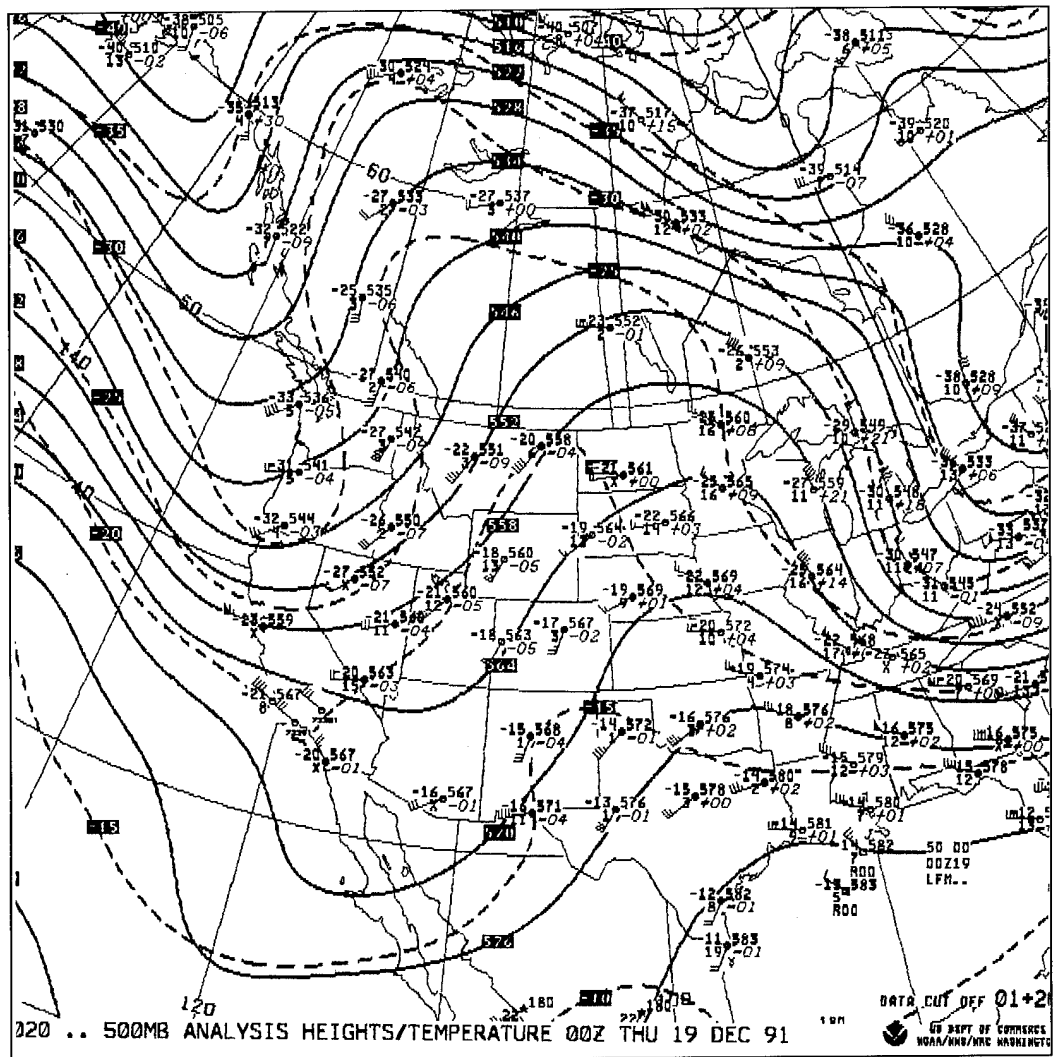


Figure 31. 19 December 1991 00 UTC LFM 500 mb analysis.

would provide the support for lifting the already saturated layer of PI evident the last two days. Maddox et al. (1979) discussed that although weak 500 mb meso- α scale troughs usually act to help intensify frontal overrunning and initiate convection, the actual location of heaviest rainfalls is often just west of the large-scale ridge position. The ridge axis continues to be right over or just to the east of the HLR.

Figure 32 is the 850 mb analysis. The long wave trough continues to be apparent and is located east of the trough axis at 300 mb and 500 mb. A closed high is evident over central Arkansas. Texas continues to remain in strong southerly flow. Gulf moisture continues to be advected northward and now extends to the Oklahoma - Kansas border. Cyclonic circulation is observed in the HLR, with the approach of the trough to the west. This cyclonic flow at low levels, indicating a convergent wind field, along with the diffluence at 500 mb documented above, provides for a very focused region of ascent over the HLR.

12 UTC 19 December 1991

Figure 33 shows the 300 mb analysis. The long wave trough continues to move eastward into the western U.S. The axis of the trough extends from northwestern British Columbia to the base of the trough in central Baja. A 130 knot wind speed maximum continues moving down the west side of this trough and is nearing the base of the trough axis. A 85 knot wind speed

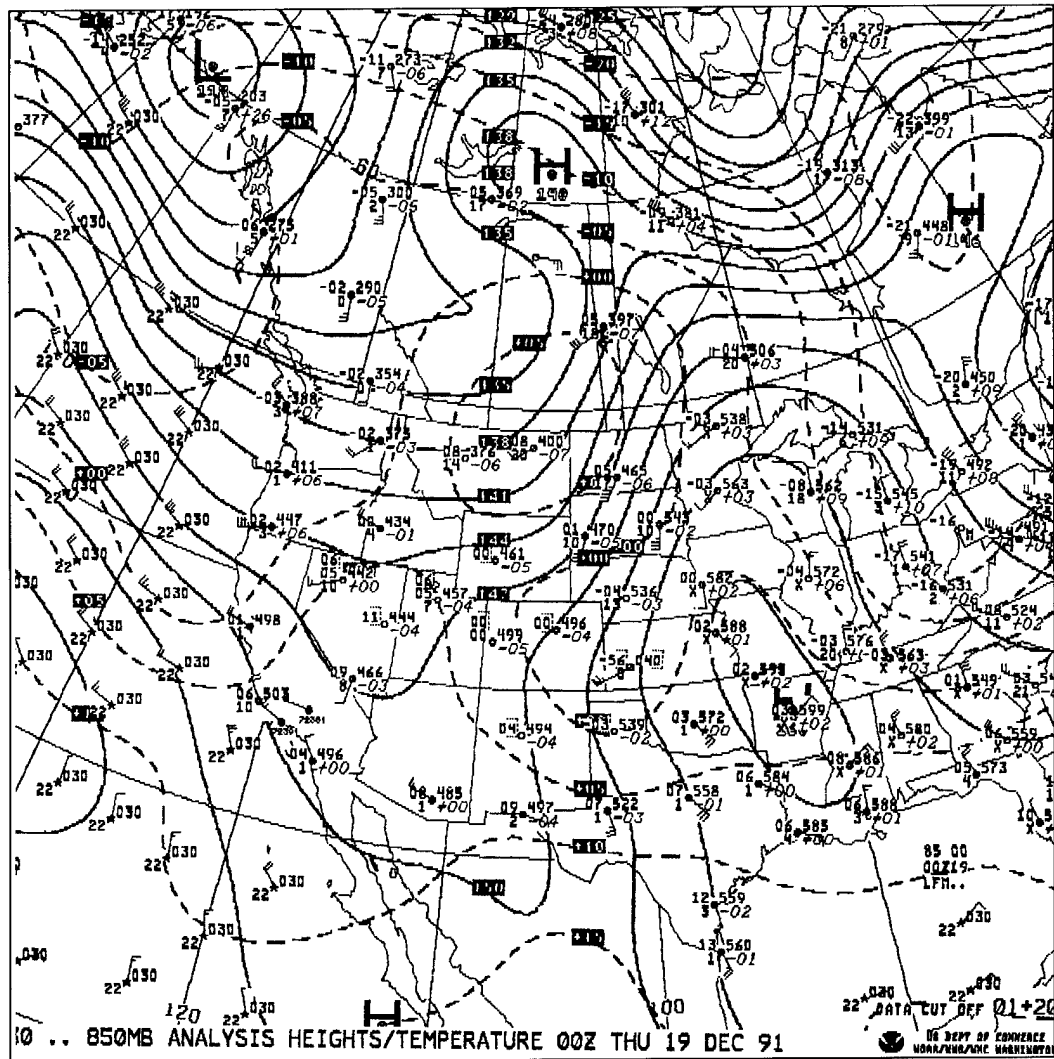


Figure 32. 19 December 1991 00 UTC LFM 850 mb analysis.

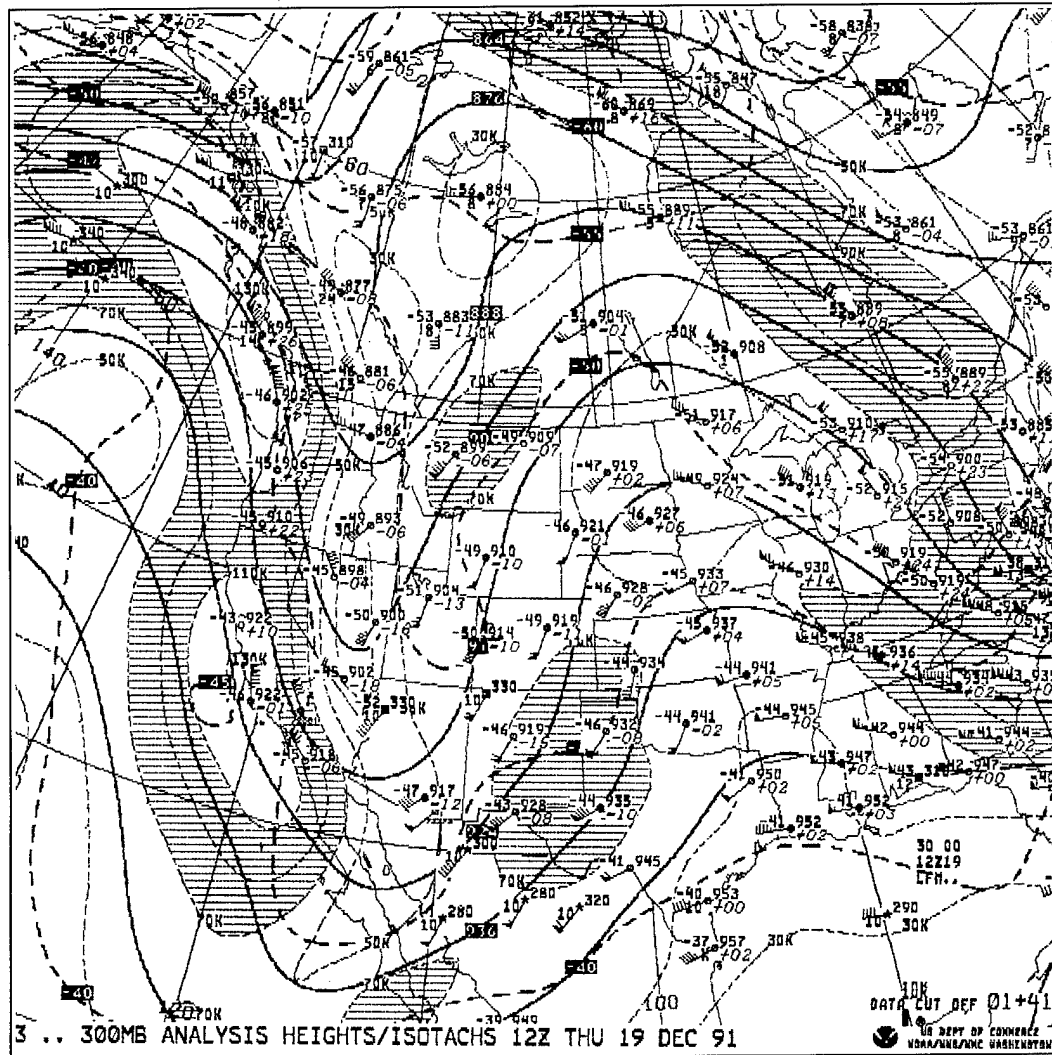


Figure 33. 19 December 1991 12 UTC LFM 300 mb analysis.

maximum is over west Texas which places the right entrance region across the HLR and enhances upward motion.

Figure 34 shows the 500 mb analysis. The long wave trough remains just east of the 300 mb long wave trough. The area of diffluence between the cyclonic curvature northwest of the HLR and anticyclonic curvature southeast of the region continues to enhance upward motion across the HLR, thus increasing precipitation possibilities in a region which has already experienced two days of steady light precipitation.

Figure 35 shows the 700 mb vertical motion field. Negative values indicate upward vertical motion and positive values indicate downward vertical motion. One upward vertical motion region extends across Mexico and into southwest Texas probably associated with the 300 mb jet. Another one extends from the Gulf into southeast Texas. The axes of these two regions converge in south central Texas continuing to enhance precipitation in the region.

Figure 36 shows the 850 mb analysis. The low that was located near the southern border of Arizona, moved northward to southern Nevada. The position of the long wave trough now extends from north central Saskatchewan into the low in southern Nevada. Strong southerly flow continues to persist from the Gulf Coast into the Upper Great Plains. The flow

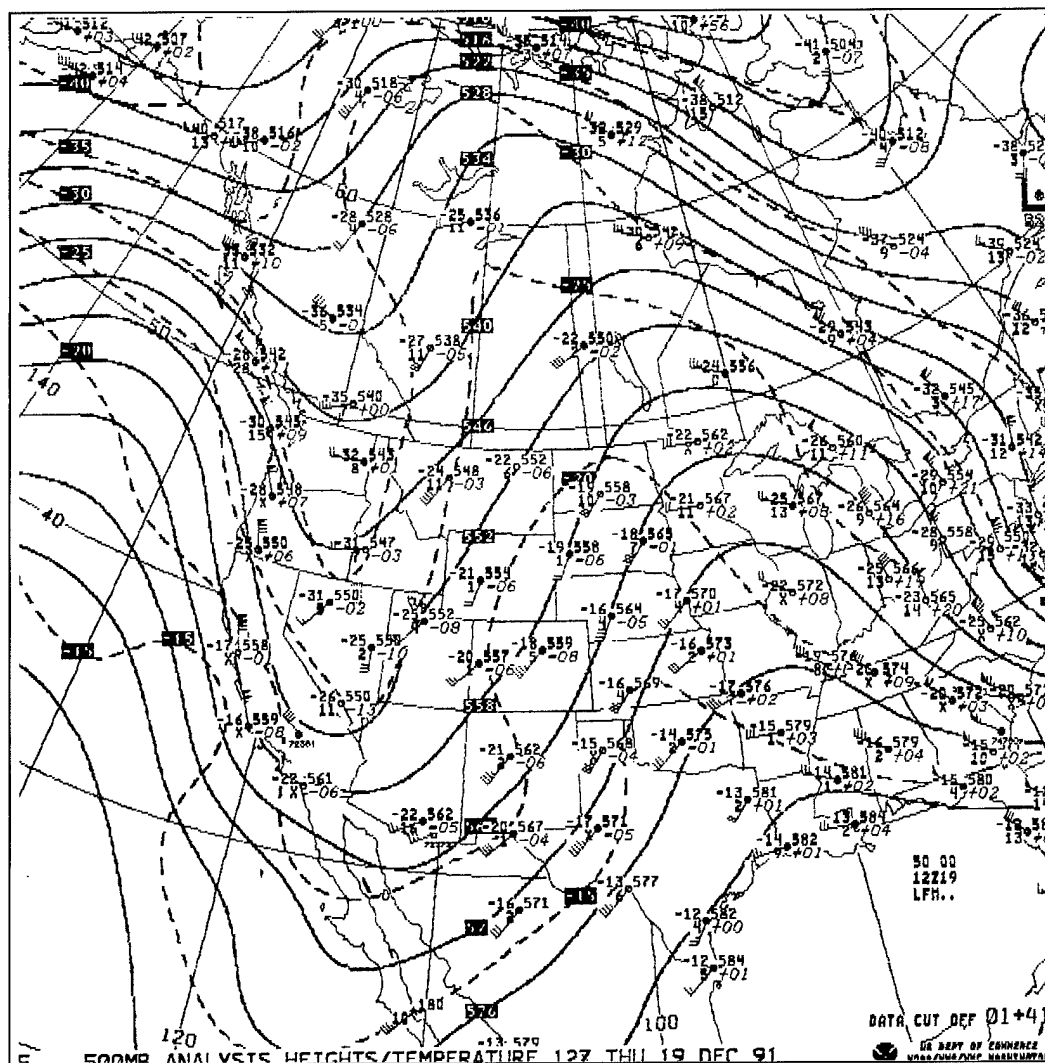


Figure 34. 19 December 1991 12 UTC LFM 500 mb analysis.

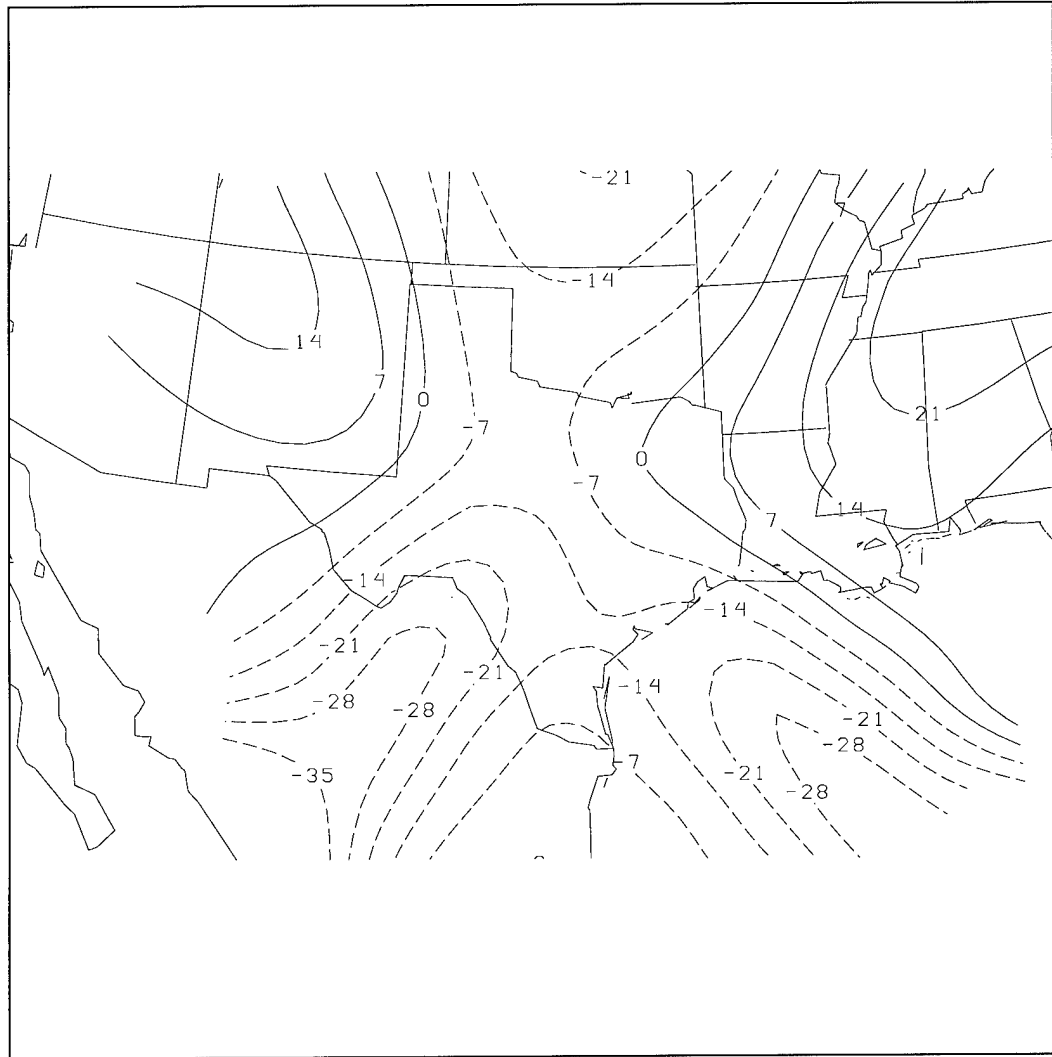


Figure 35. 19 December 1991 12 UTC 700 mb vertical motion field. Negative values (dashed lines) indicate upward motion and positive values (solid lines) indicate downward motion.

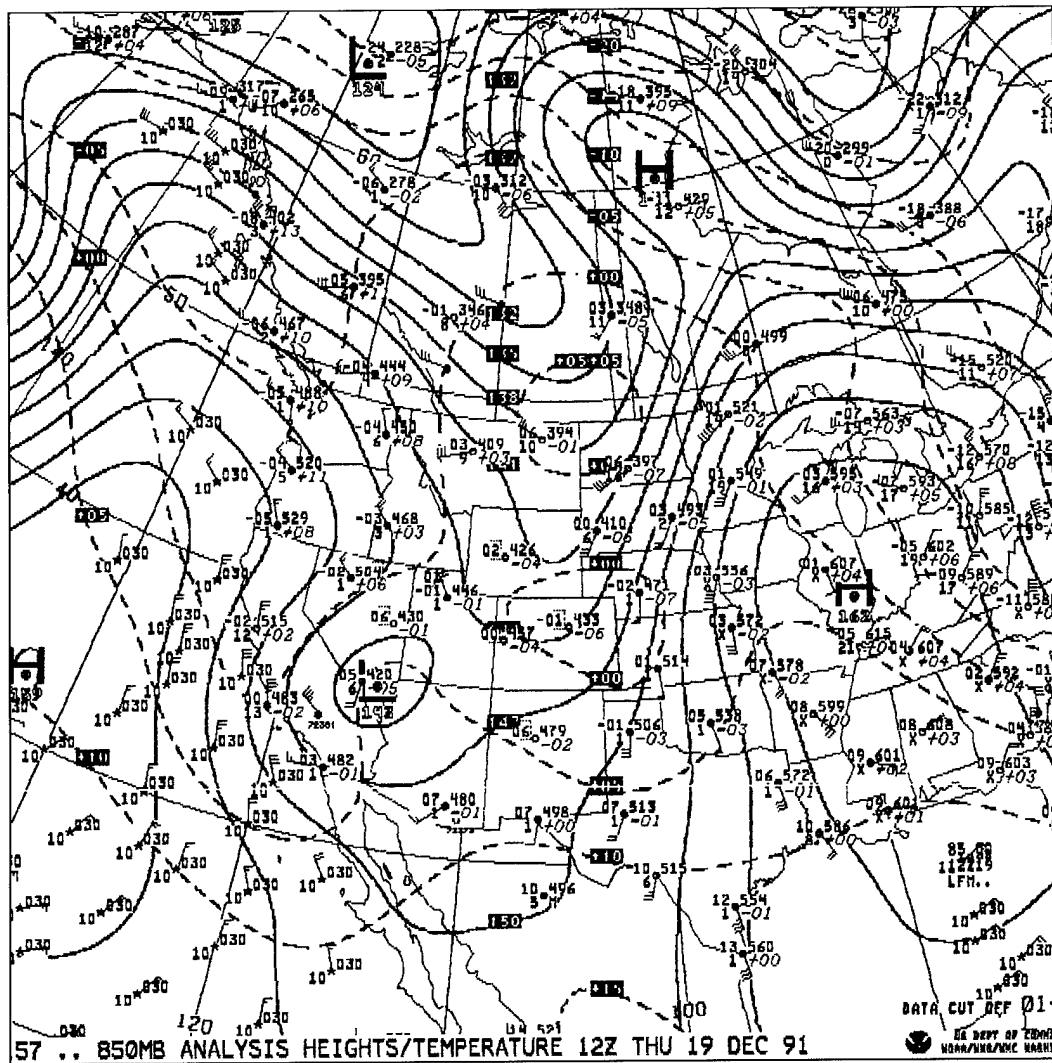


Figure 36. 19 December 1991 12 UTC LFM 850 mb analysis.

in southwest Texas is slightly convergent which also contributes to the upward motion detected in this region.

Figure 37 shows the surface analysis. Warm frontogenesis is occurring from ELP into south central Texas and south of Houston. Light rain and drizzle continue to be reported along and north of the warm frontogenesis boundary. Southeasterly flow is now apparent in the HLR. This warm, moist flow at the surface is now perpendicular to the Balcones Escarpment enhancing the potential for orographic lifting. The overrunning of these warm moist parcels over the shallow surface cold air entrenched over the Texas Hill Country is enhancing the ascent over the HLR.

Figure 38 shows an extensive area of PI (hatched region) across the entire state. The substantial increase in PI can be attributed to the multiple processes addressed above. The strong frontal gradient and surface cold air are still evident as well.

As the Gulf and Pacific processes continue to focus ascent in the HLR, rain totals continue to increase. The average amount for this day was in excess of one inch. There were multiple stations that reported larger amounts. The largest amount reported was 2.20 inches in Lawson (D77).

The persistence of the influx of Gulf moisture over the past several days has now inundated the HLR with steady precipitation. Total precipitation amounts for the past three days averaged near two inches. A combination of

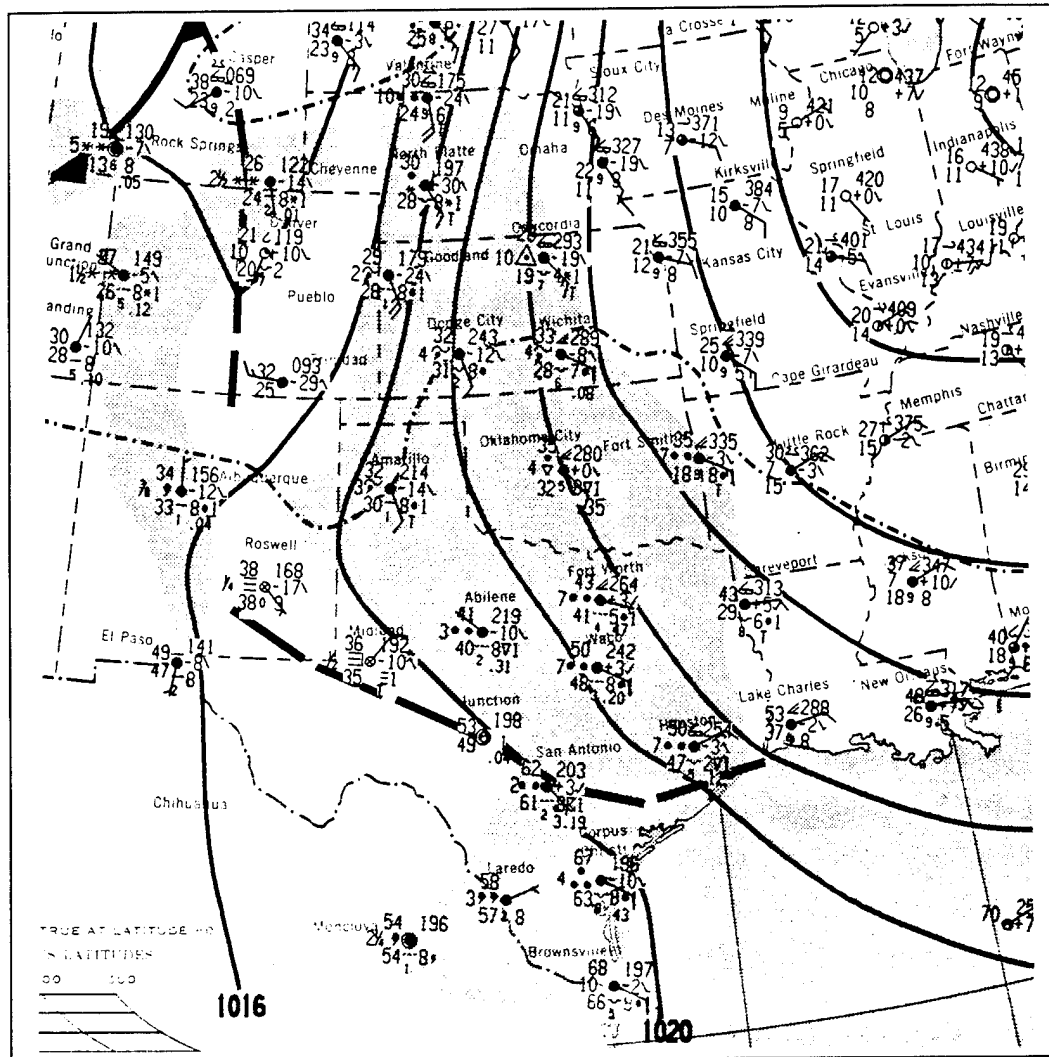


Figure 37. 19 December 1991 12 UTC daily surface weather map.

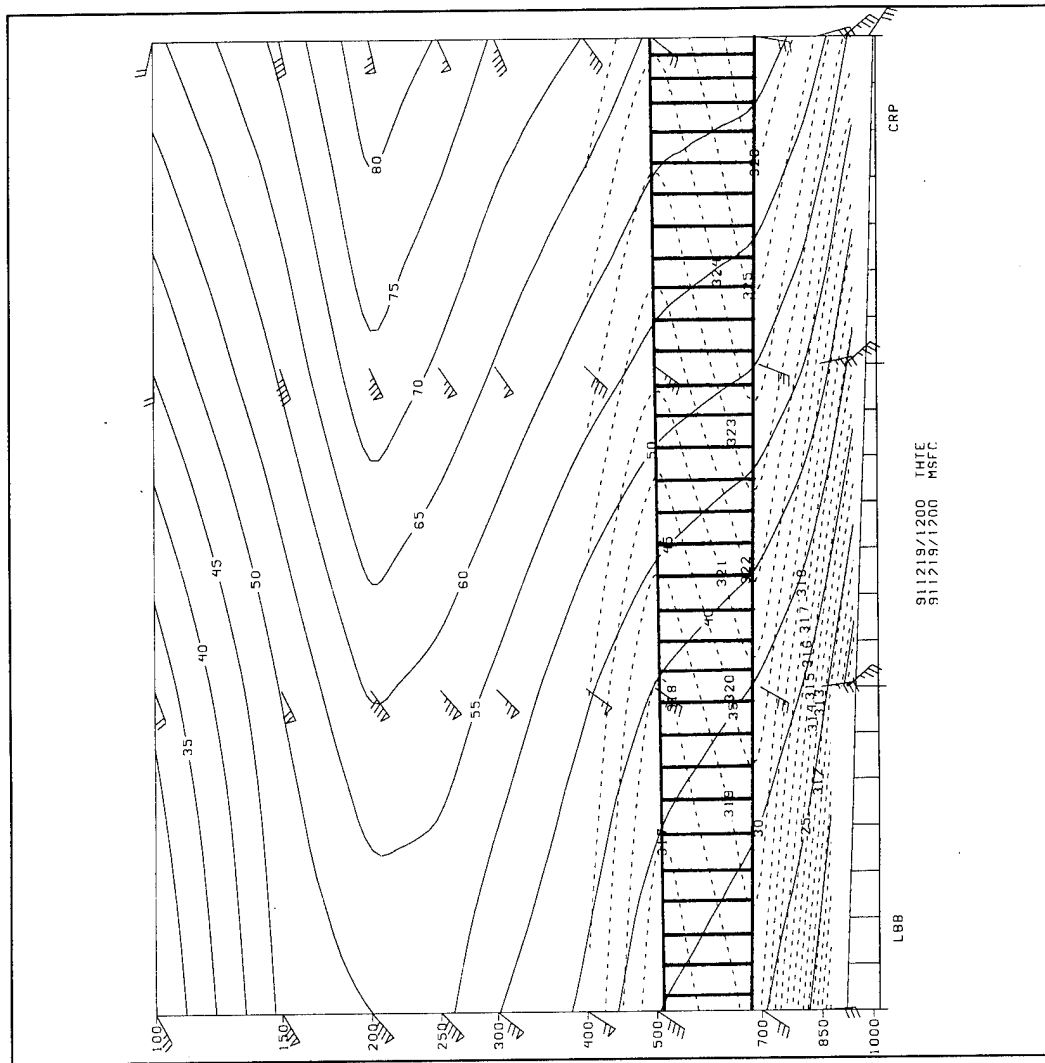


Figure 38. 19 December 1991 12 UTC cross section analyses of equivalent potential temperature surfaces (dashed lines) and psuedo-angular momentum surfaces (solid) from Lubbock (LBB) to Corpus Christi (CRP), Texas. The hatched region depicts a region of potential instability.

many factors created conditions right for flooding in the HLR. A number of these have already been established in the discussion up to this point. These factors were: (1) the presence of deep Gulf moisture, (2) deep PI, (3) upper level diffluence with the approaching trough, (4) a change in the gradients and orientation of the equivalent potential temperature surfaces and pseudo-angular momentum surfaces in response to the return-flow and the approaching low, (5) surface boundary overrunning, and (6) complex terrain inducing orographic lifting. Additional processes such as CSI and winds conducive for elevated convection, will also be established. The combination of these processes provided the catalyst for a flooding event.

00 UTC 20 December 1991

Figure 39 is the 300 mb analysis. The long wave trough continues moving eastward, with the northern portion moving faster than the southern end. The northern region of the trough extends from north central Saskatchewan, through the central Rockies and into a newly developed 9030 meter low located in central Arizona. A 110 knot wind speed maximum now extends around the base of the trough and into far west Texas. Weak anticyclonic curvature remains over the HLR.

Figure 40 shows a 5480 meter closed low at 500 mb that has formed over the far northern Gulf of California. At this time, the long wave trough is located on a nearly north - south axis from Alberta southward across the

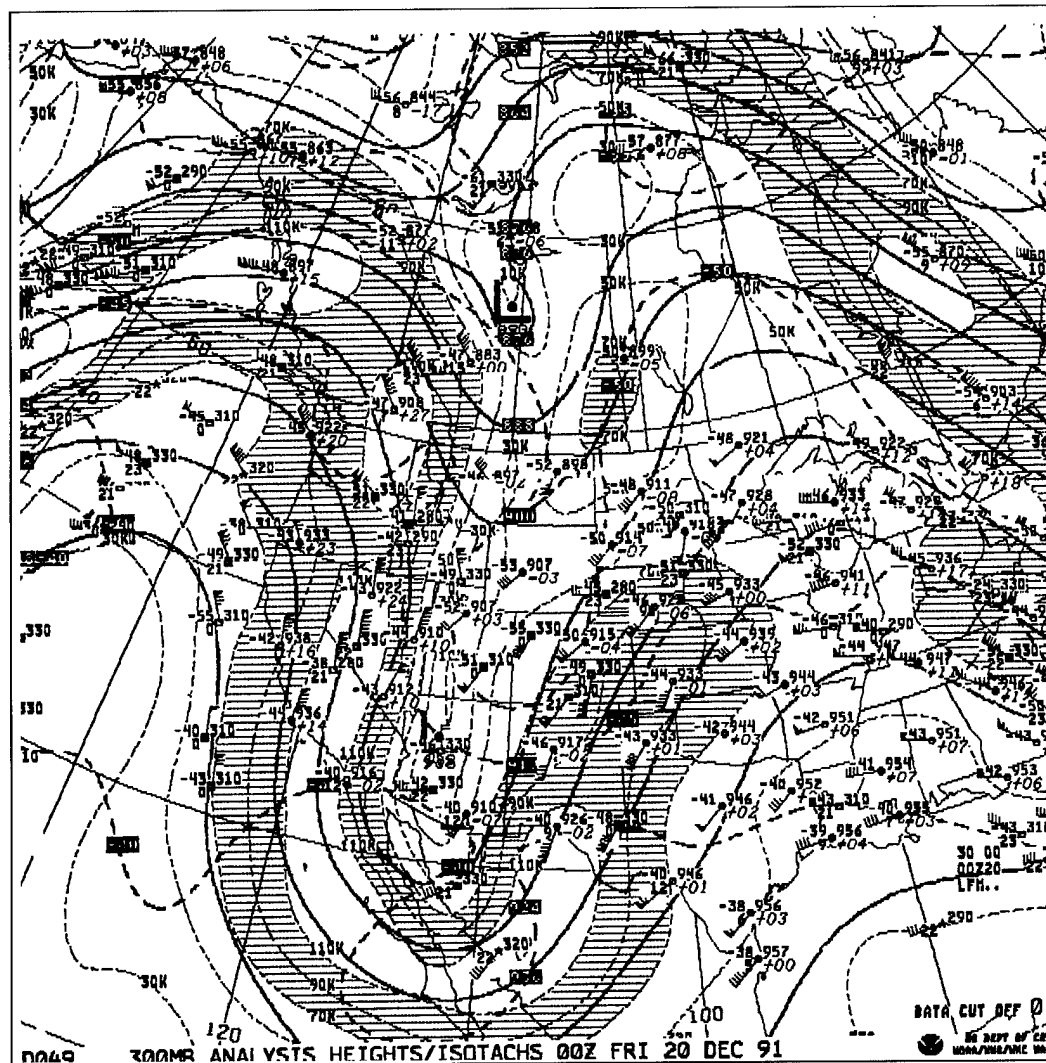


Figure 39. 20 December 1991 00 UTC LFM 300 mb analysis.

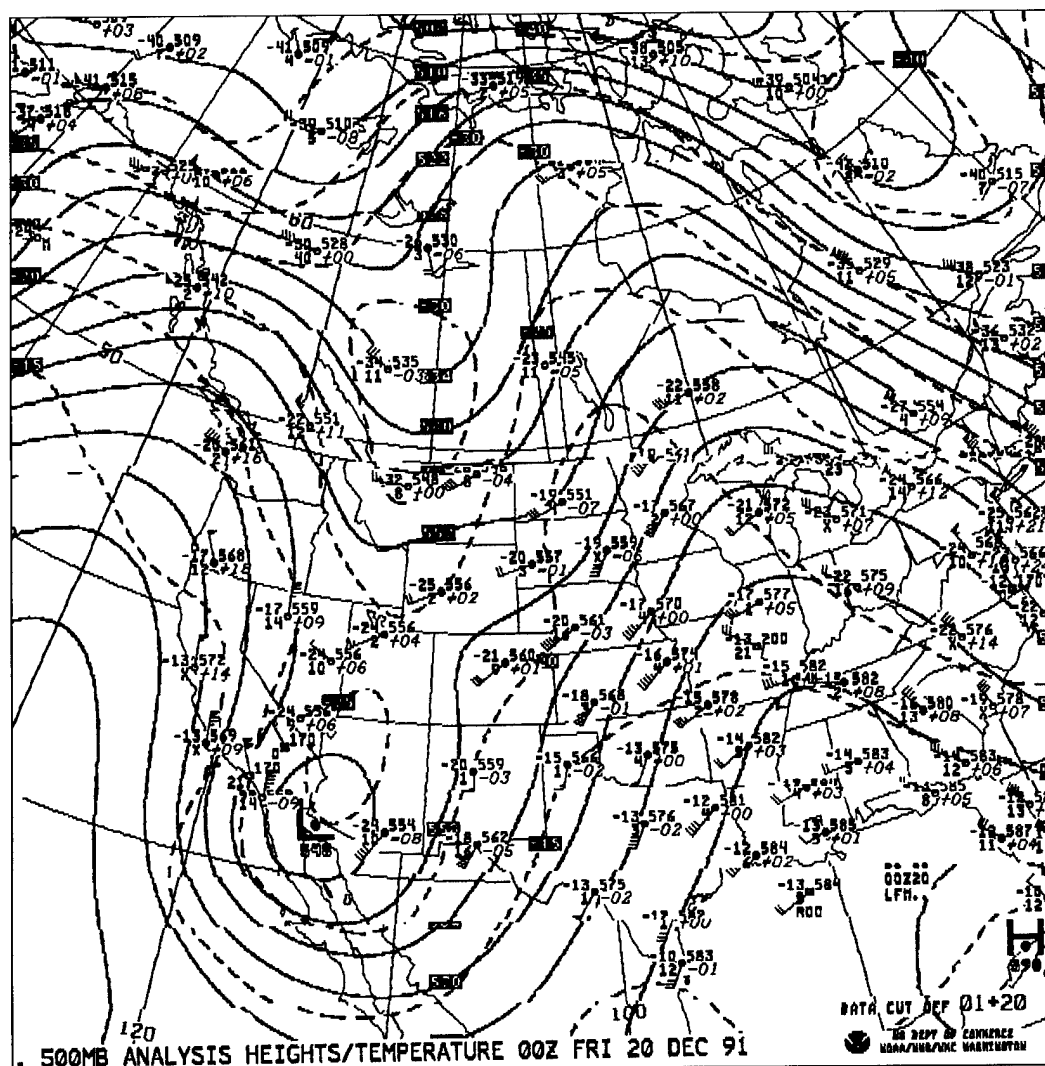


Figure 40. 20 December 1991 00 UTC LFM 500 mb analysis.

western U.S. and along the Pacific coast of northern Mexico. A 50 knot wind speed maximum is evident at DRT and will be moving into the HLR over the next twelve hours. Anticyclonic curvature remains apparent over the HLR and the winds have increased to 40 - 45 knots.

Figure 41 is the 700 mb vertical motion field. Upward vertical motion continues to persist from Mexico into northern Texas and from the Gulf into the HLR. There appears to be a slight increase in the magnitude of the upward motion over the HLR. This vertical motion field acting on an already saturated environment is conducive to heavier precipitation.

Figure 42 is the 850 mb analysis. The strong ridging over the Ohio Valley coupled with the low in the southwest, has dramatically increased the warm air and moisture advection over southern and central Texas, as evidenced by the 70 knot wind maximum at SEP. The approach of the low continues to maintain the cyclonic curvature over the HLR. Evidence of Gulf moisture is now evident as far north as northern Minnesota.

Figure 43 shows a vertical cross section with the PI near the surface at CRP (hatched shading) associated with the influx of Gulf air. Overrunning has created a change in the equivalent potential temperature surfaces and now there is both CSI (cross hatched shading) and PI (hatched shading) present between 700 - 500 mb. The frontal gradient is still evident, but not to the

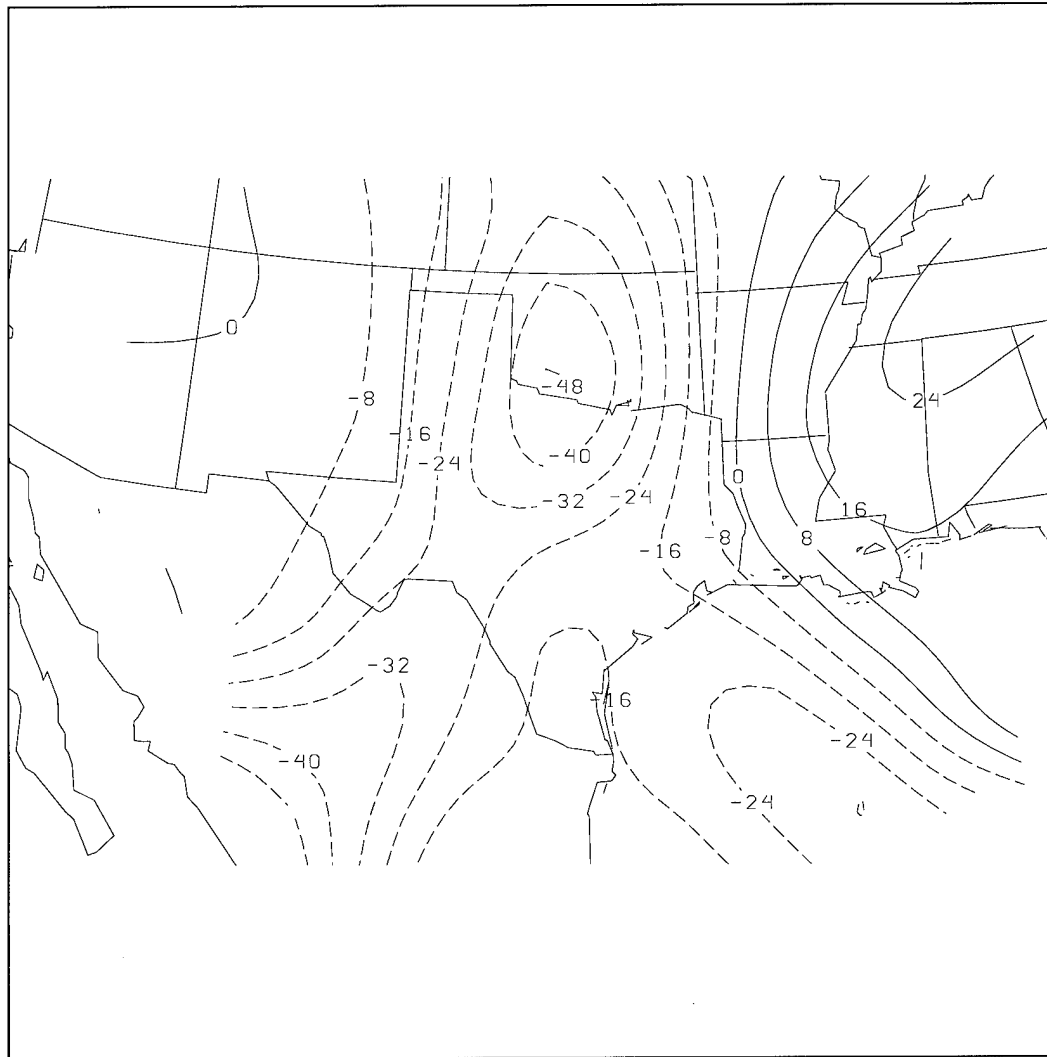


Figure 41. 20 December 1991 00 UTC 700 mb vertical motion field. Negative values (dashed lines) indicate upward motion and positive values (solid lines) indicate downward motion.

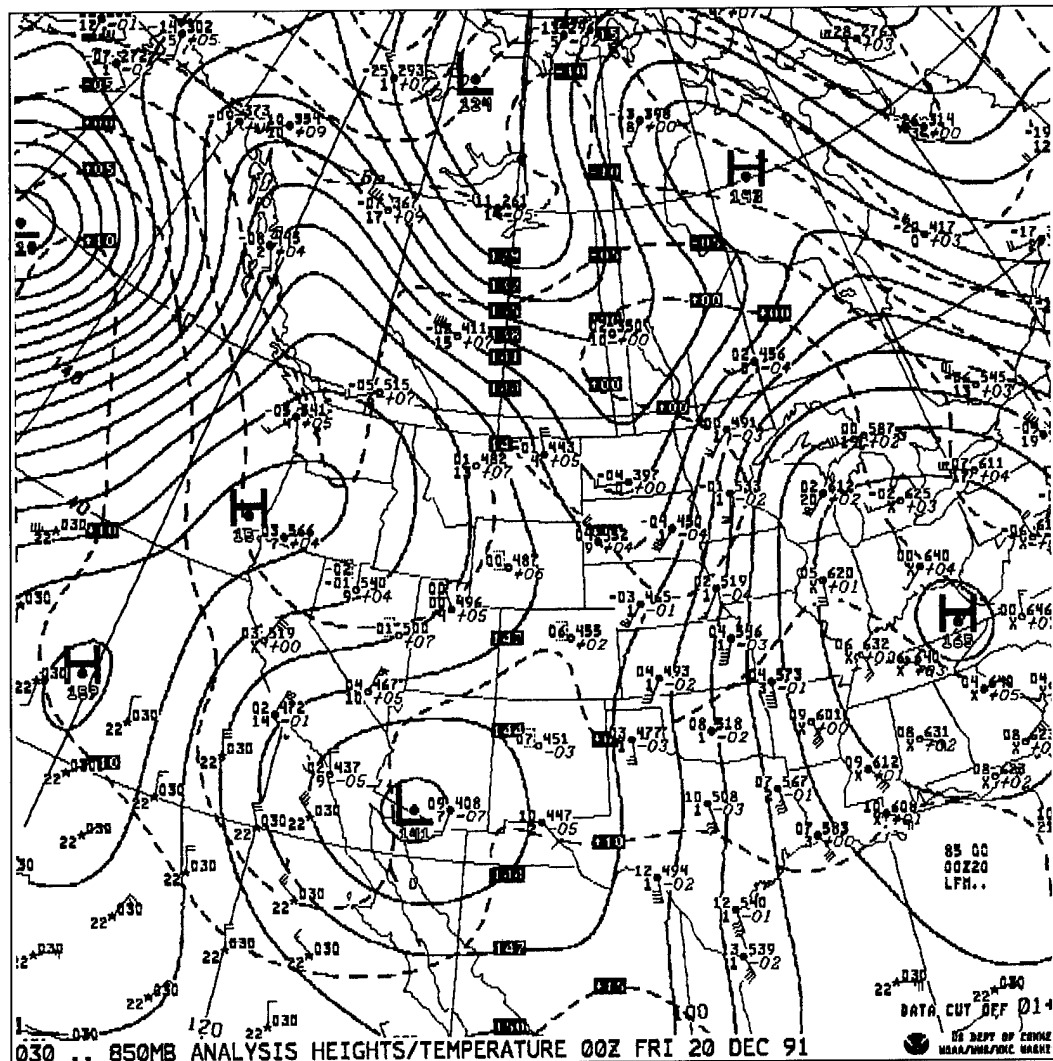


Figure 42. 20 December 1991 00 UTC LFM 850 mb analysis.

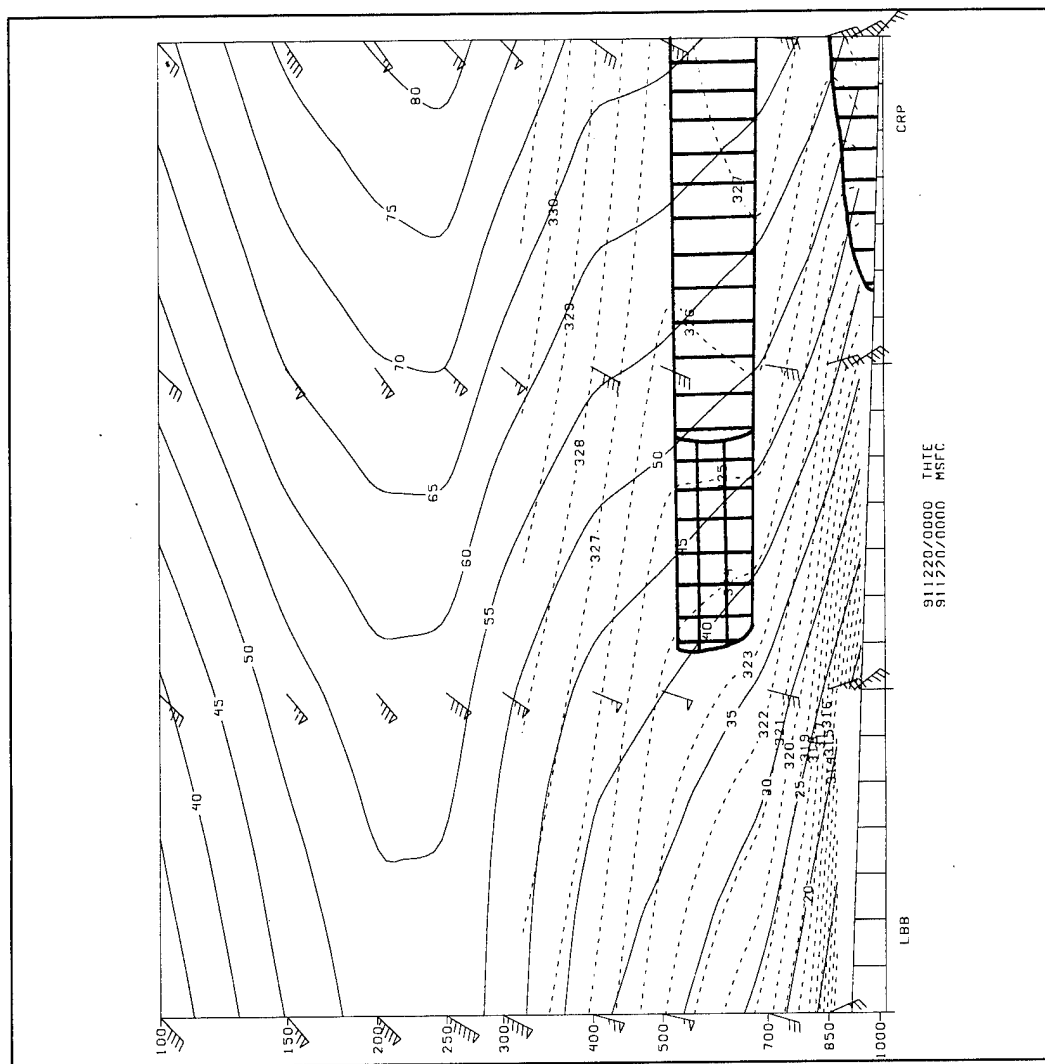


Figure 43. 20 December 1991 00 UTC cross section analyses of equivalent potential temperature surfaces (dashed lines) and psuedo-angular momentum surfaces (solid) from Lubbock (LBB) to Corpus Christi (CRP), Texas. The hatched region depicts a region of potential instability and the cross hatched region depicts CSI.

depth of previous cross sections. The strong stability in the frontal zone is starting to weaken as overrunning becomes more dominant.

Given that there is evidence of a strong 500 mb jet maximum and anticyclonic curvature, strong 850 mb winds in cyclonic curvature, and the presence of CSI over the HLR, one should consider the possibility for elevated thunderstorms. This configuration provides a mechanism for the winds to veer with height, indicating warm air advection and an environment conducive to elevated thunderstorms.

12 UTC 20 December 1991

Figure 44 shows the 300 mb analysis. A wind speed maximum is entering the base of the long wave trough. The low has moved to northwestern Mexico and is closed with a 9050 height center. Another wind speed maximum is entering the base of the trough which is oriented southwest - northeast over northern Mexico.

Figure 45 shows the 500 mb analysis. The closed low has moved south approximately two degrees latitude, but remained in the north central Gulf of California. The northern portion of the long wave trough is located from central Manitoba and extends into North Dakota, with the southern end extending into the closed low in the northern Gulf of California. Because the data at SEP is missing, it is difficult to assess the curvature and wind speeds in the HLR. Although wind speeds are not shown over the HLR, one can see the

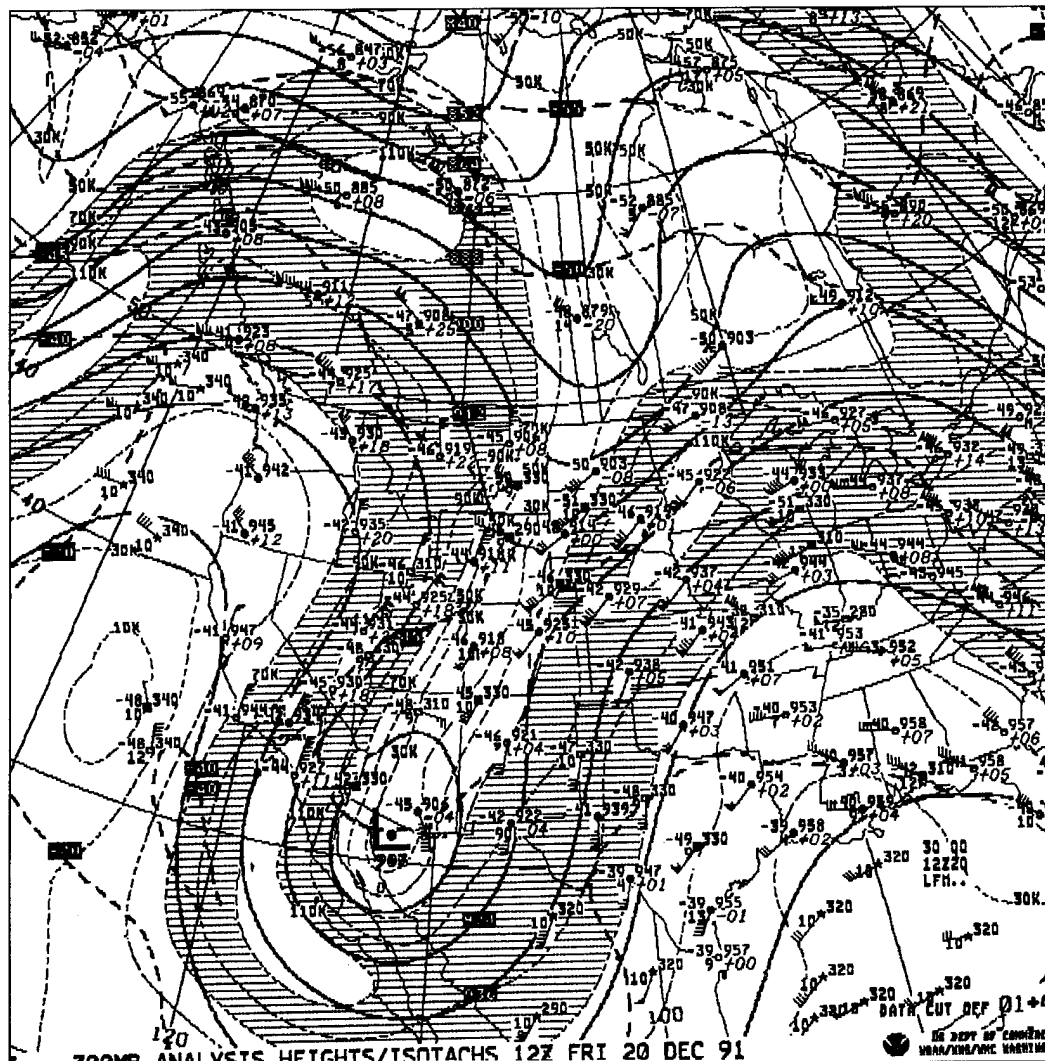


Figure 44. 20 December 1991 12 UTC LFM 300 mb analysis.

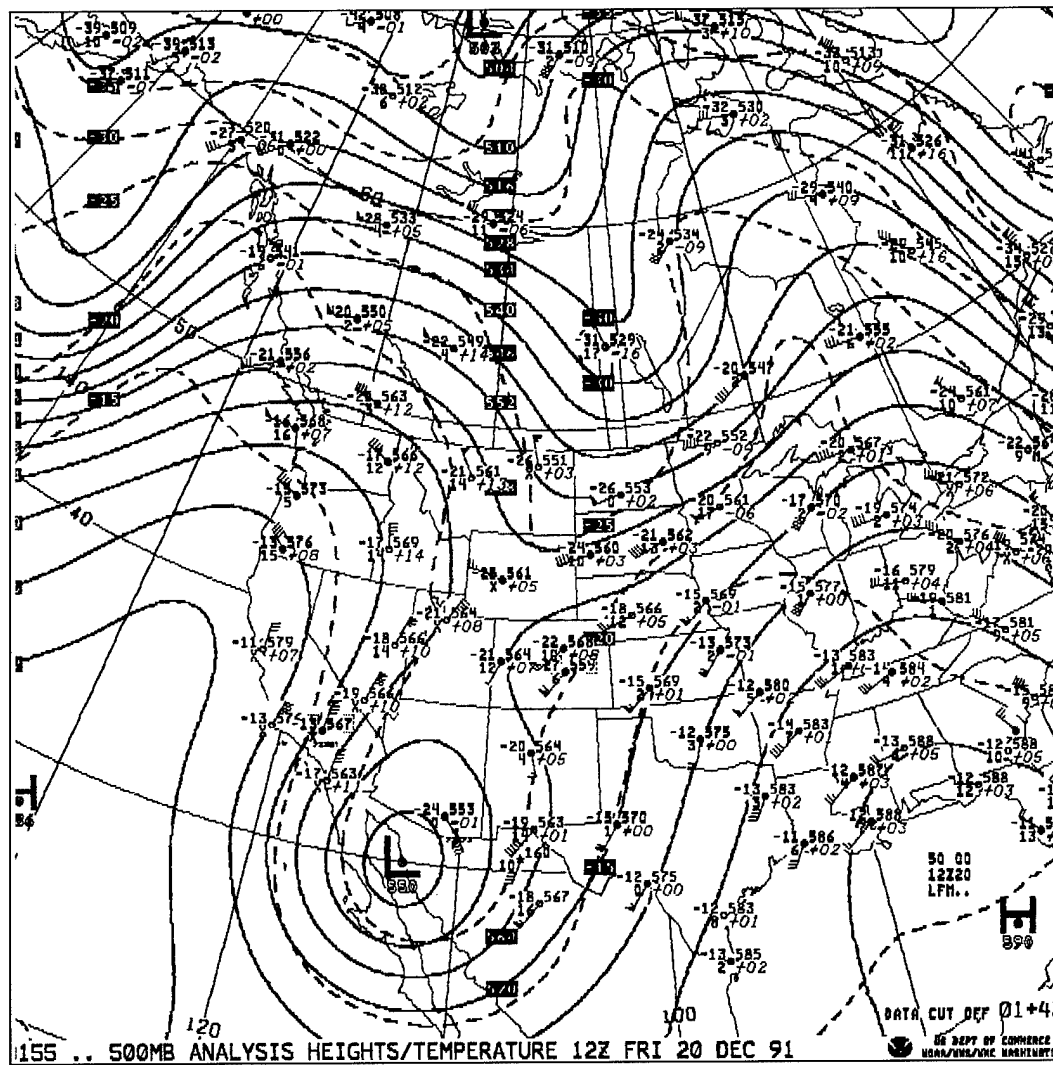


Figure 45. 20 December 1991 12 UTC LFM 500 mb analysis.

height gradient become stronger, which would result in stronger winds. The incorporation of at least one, if not more reporting stations (radiosonde) in central Texas and Mexico, could have prevented one from inferring wind speeds and curvature. The additional data could have filled the data void area over this region, and allowed one to provide a more accurate assessment of the impending flood event.

Figure 46 shows the 700 mb vertical motion field. There continues to be upward motion over the southwest and southeast regions of Texas which continues to enhance precipitation over the region.

Figure 47 shows the 850 mb analysis. The closed low is nearly vertically stacked between 850 mb and 500 mb. Advection of Pacific and Gulf moisture is evident throughout northern Mexico and southern Texas. Dewpoint depressions shown in these regions are consistently less than five degrees Celsius. One can see indications of cyclonic curvature over the HLR. The maximum wind speed in that region can be interpolated to be near 40 - 45 knots.

Figure 48 shows a re-analysis of the daily surface weather map. This re-analysis was done to accommodate for the mM air mass which was not analyzed on the daily surface weather map. There are three distinct air masses present, mT over the Rio Grande Valley, mM over southeast Texas, and cM over most of north Texas. A surface low is located southeast of El

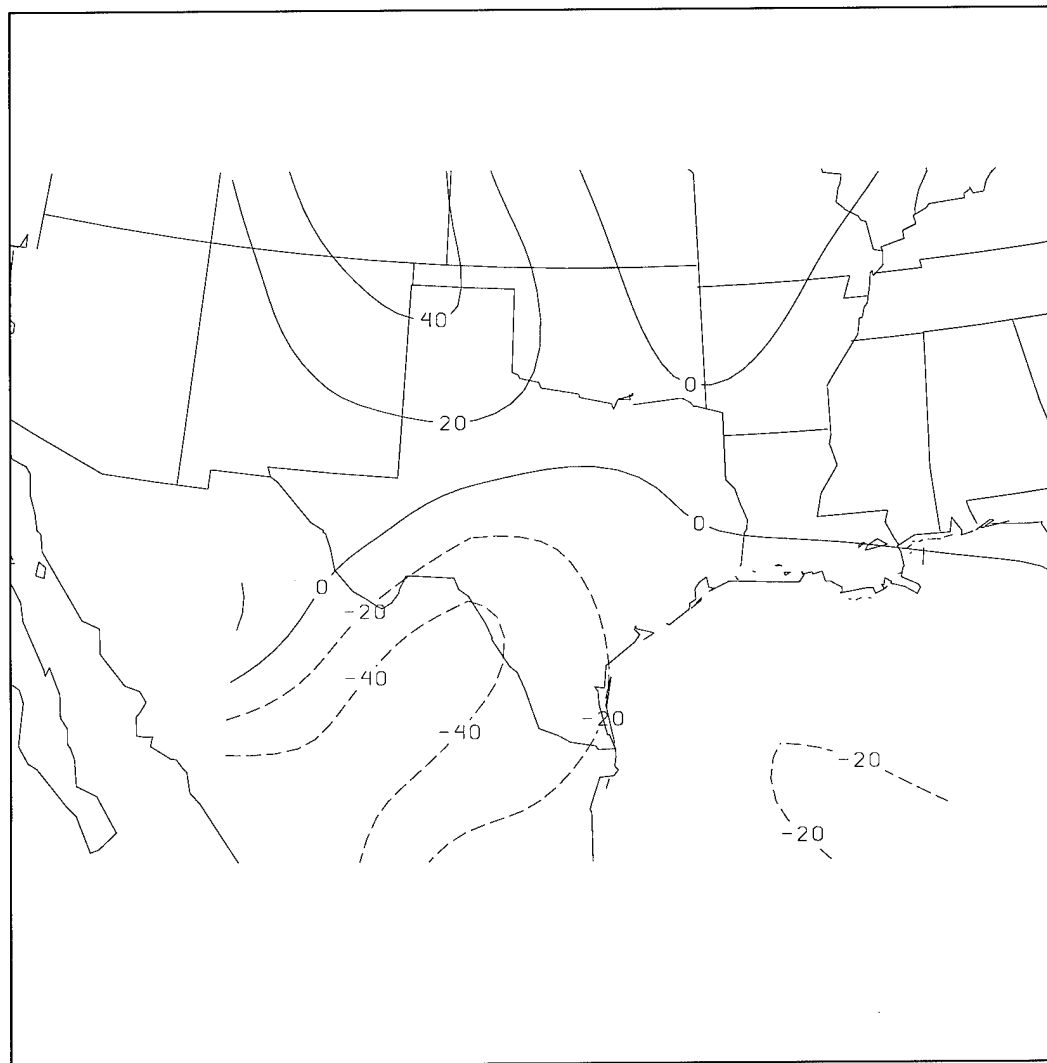


Figure 46. 20 December 1991 12 UTC 700 mb vertical motion field. Negative values (dashed lines) indicate upward motion and positive values (solid lines) indicate downward motion.

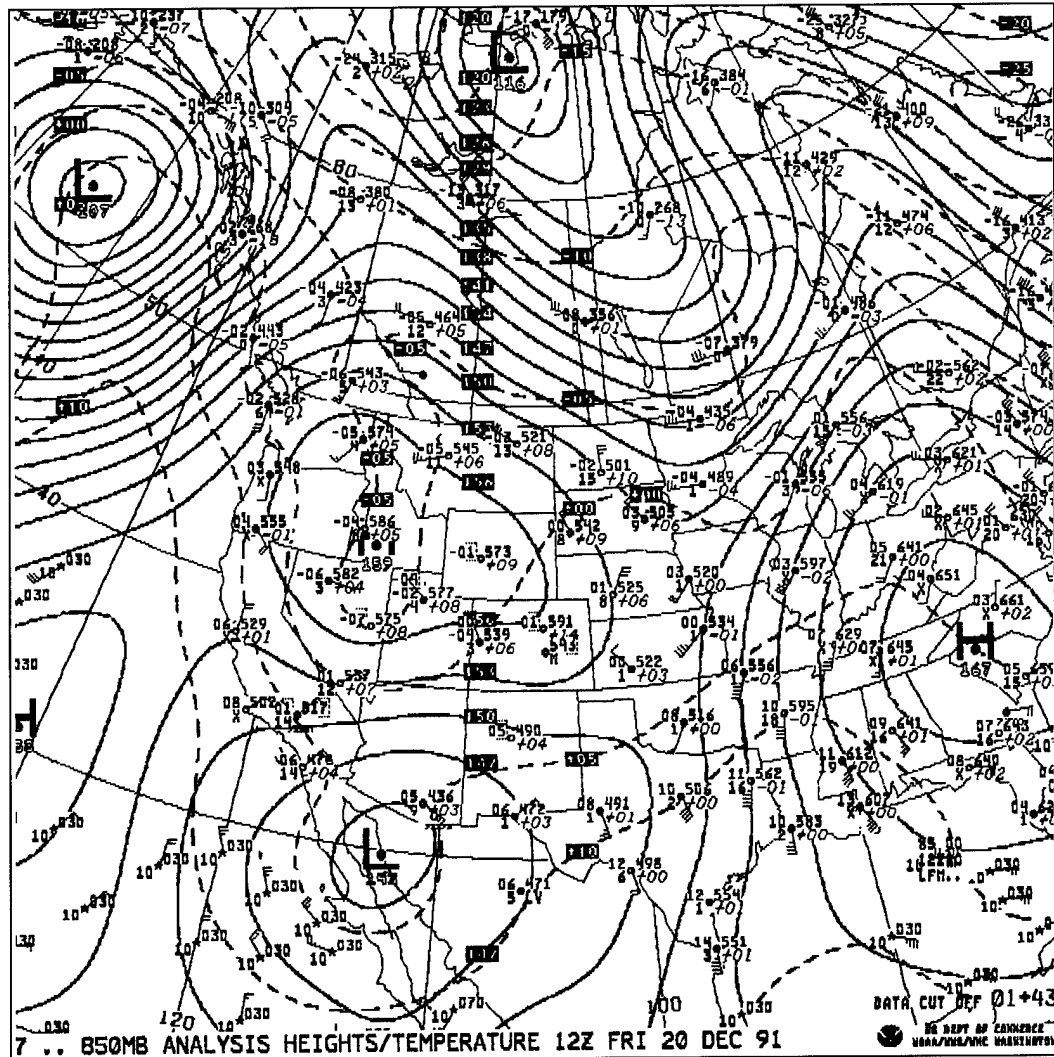


Figure 47. 20 December 1991 12 UTC LFM 850 mb analysis.

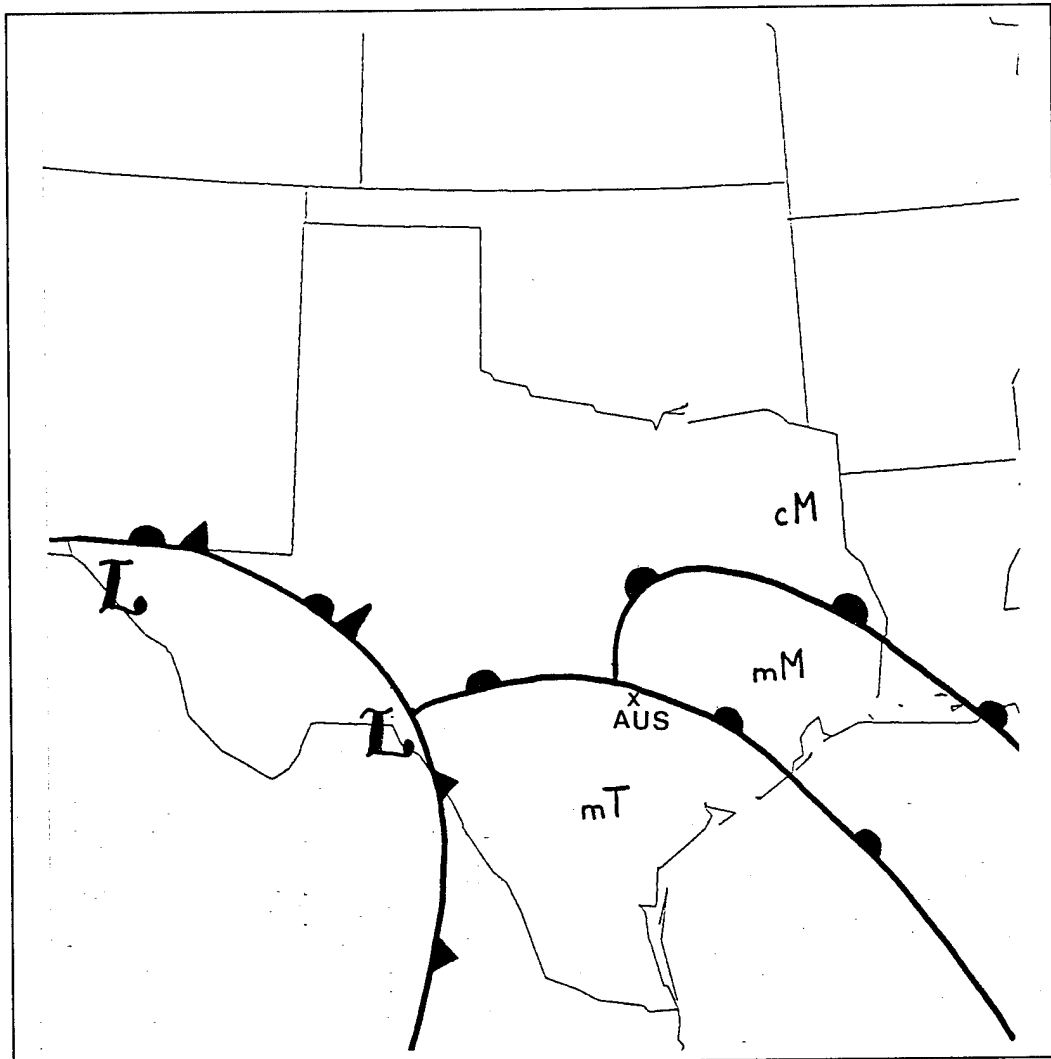


Figure 48. 20 December 1991 12 UTC re-analysis of daily surface weather map.

Paso. It is difficult to pinpoint the exact location of the center as the northern Mexico surface data were missing. There is an occluded frontal system associated with this low and the triple point is located north of Del Rio, Texas. There is a warm front that extends across the HLR. Southeasterly winds in the HLR continue to exist at this time, increasing the low level moisture content, and enhancing the orographic lifting.

Figure 49 shows a vertical cross section analysis with CSI (cross hatched shading) and PI (hatched shading). The depth of this region has decreased from the previous twelve hours. The fact that the synoptic conditions have not changed appreciably over the last twelve hours indicates the possible release of CSI in the form of convective mixing. It is at this time that convection becomes evident in the visible satellite imagery shown in Figures 50 a - d. The deep convection noted on the satellite images (Figures 50 a - d) appear to be forming both north and south of the warm frontal boundary and at the intersection of the three air masses. The convection north of the boundary is likely "elevated" due to its location north of the surface front. In addition, the wind shear at 500 and 850 mb favorable for elevated convection, is evident over the HLR (Figure 49). The wind shear coupled with CSI, orographic lifting over the Balcones Escarpment, strong overrunning in the warm frontal zone, and tremendous amounts of warm moist air parcels above the frontal surface created the conditions for the heavy precipitation.

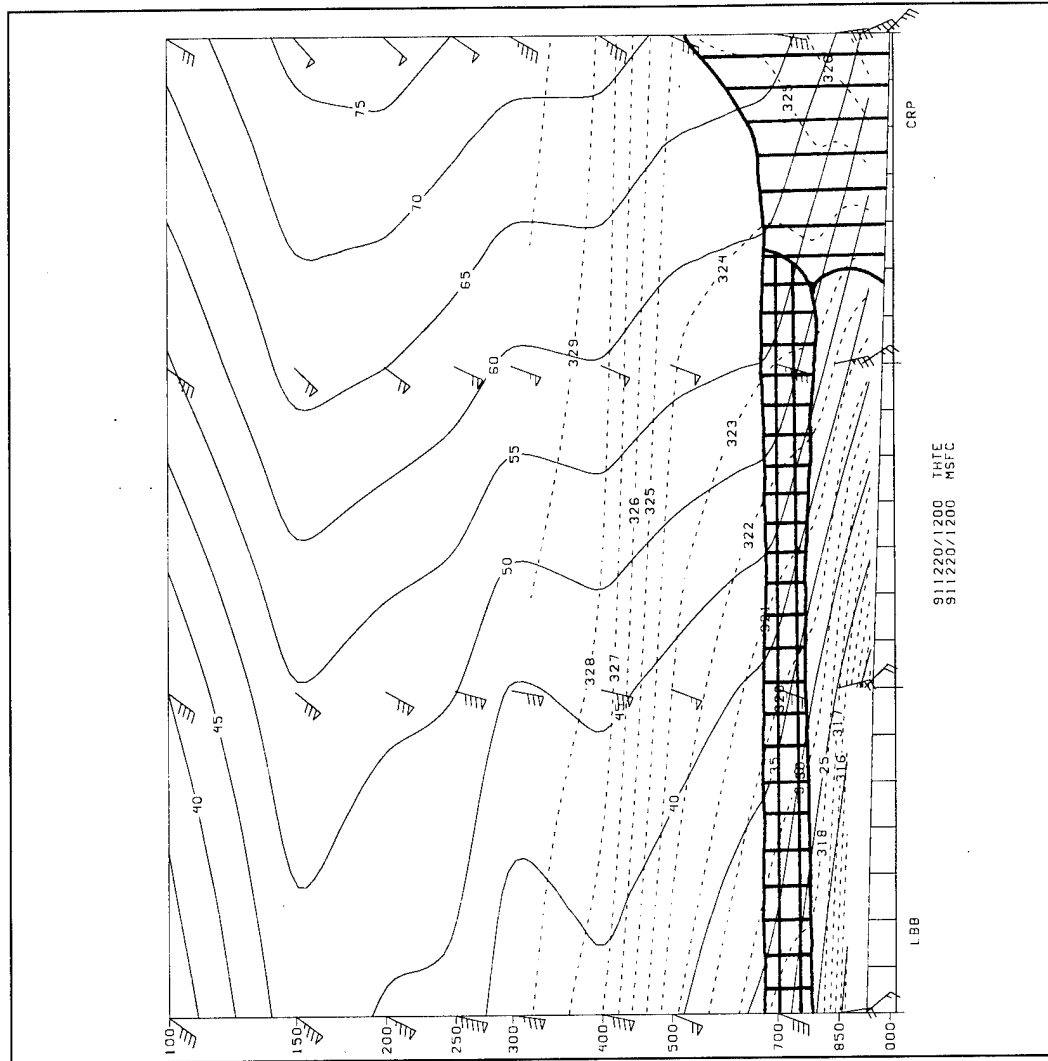


Figure 49. 20 December 1991 12 UTC cross section analyses of equivalent potential temperature surfaces (dashed lines) and psuedo-angular momentum surfaces (solid) from Lubbock (LBB) to Corpus Christi (CRP), Texas. The hatched region depicts a region of potential instability and the cross hatched region depicts CSI.

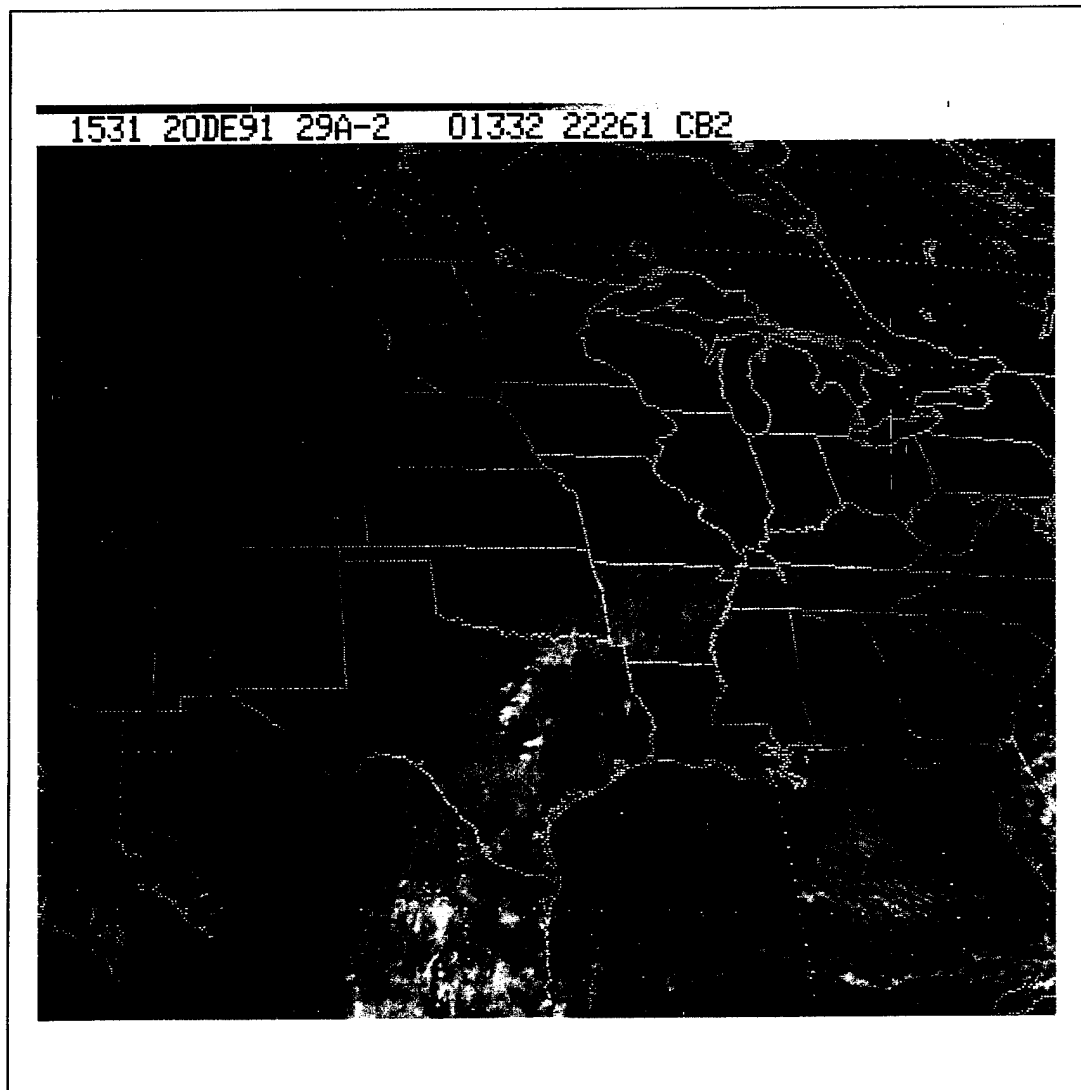


Figure 50a. 20 December 1991 1531 UTC visible satellite image.

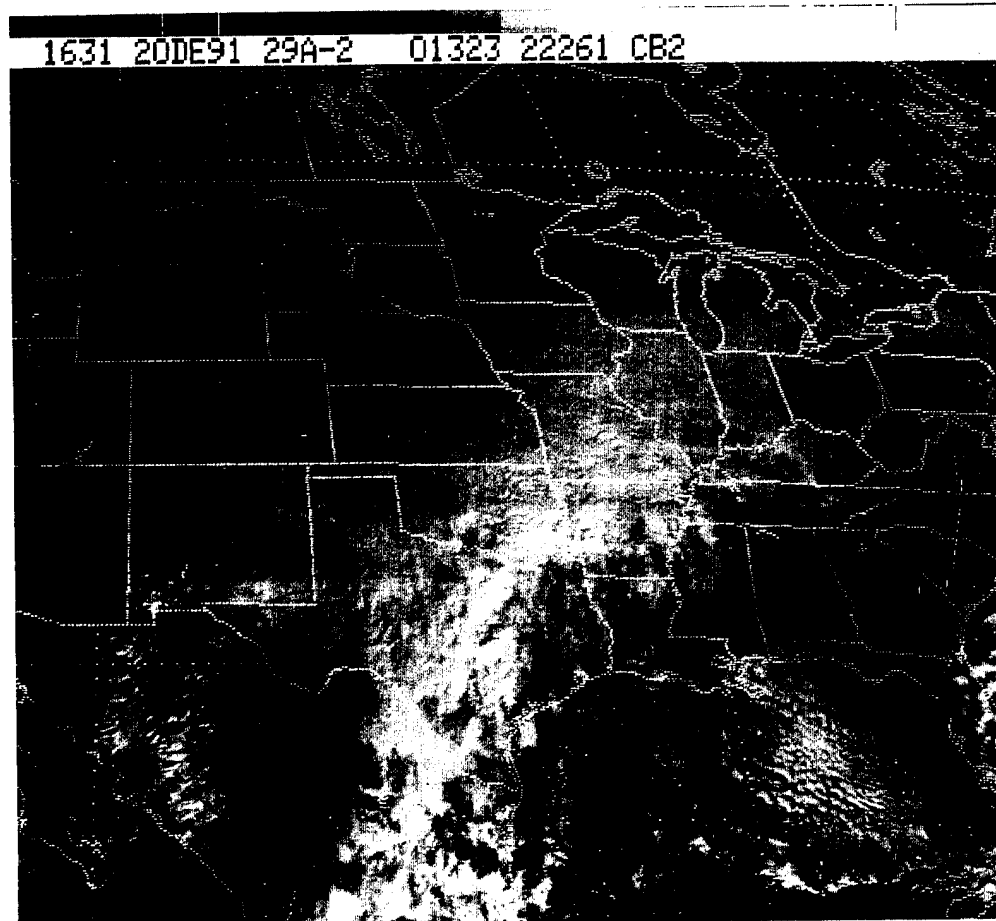


Figure 50b. 20 December 1991 1631 UTC visible satellite image.

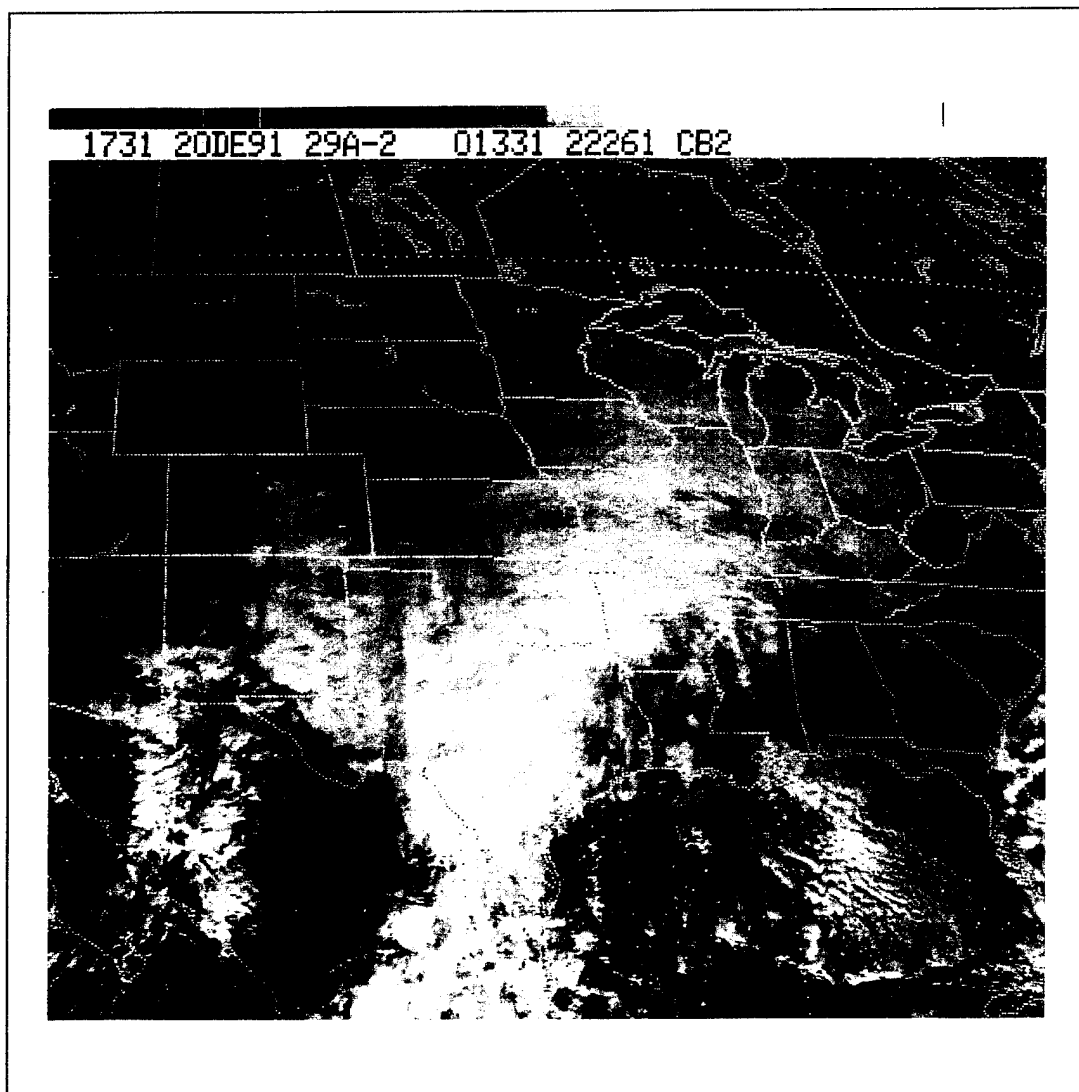


Figure 50c. 20 December 1991 1731 UTC visible satellite image.

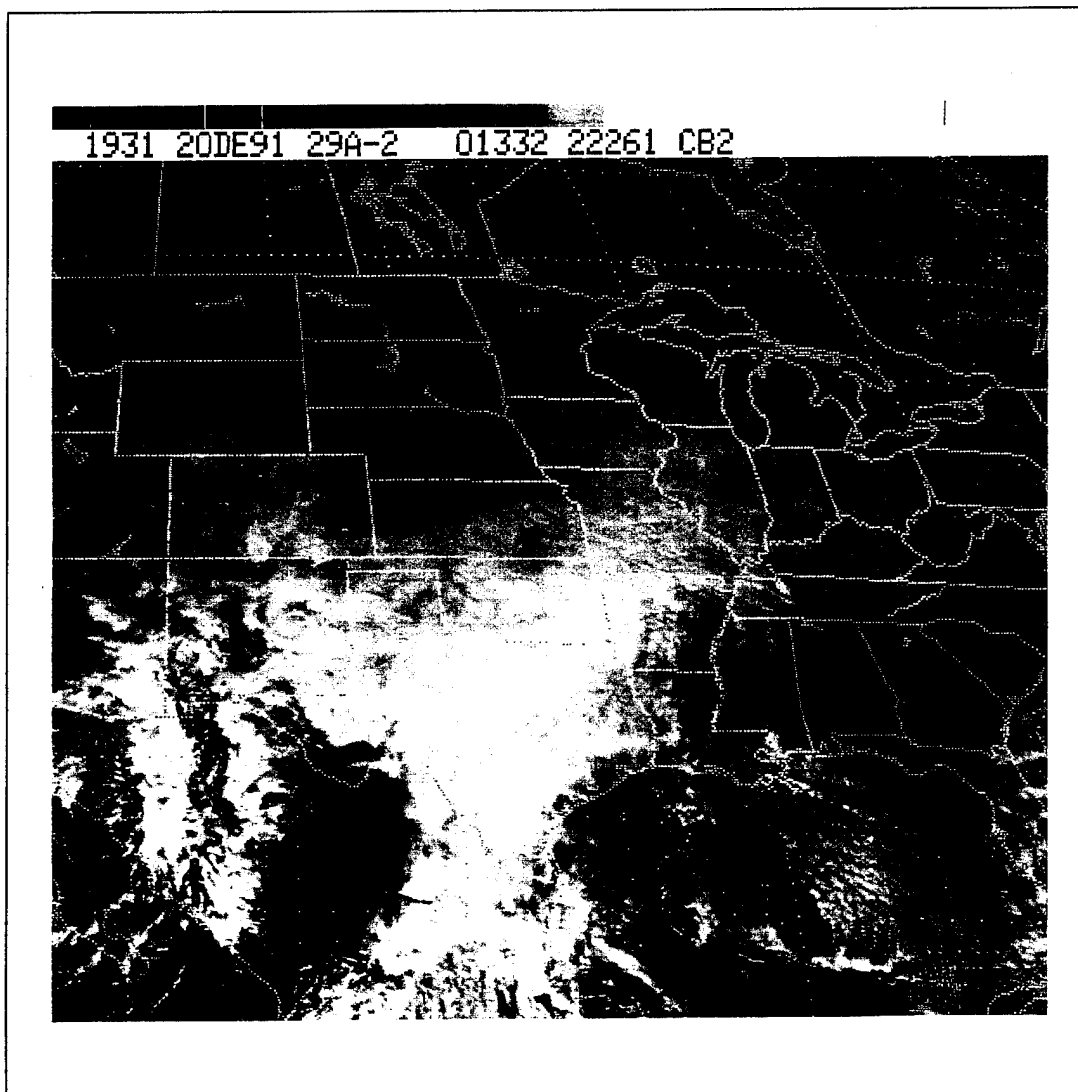
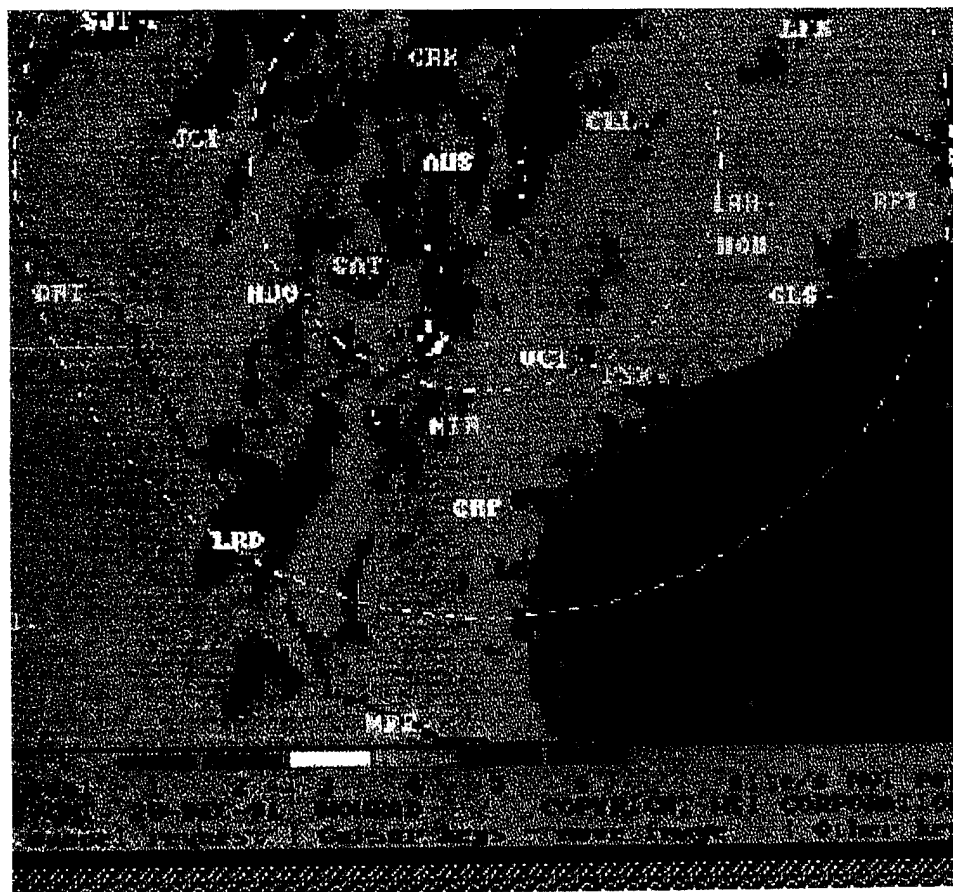


Figure 50d. 20 December 1991 1931 UTC visible satellite image.

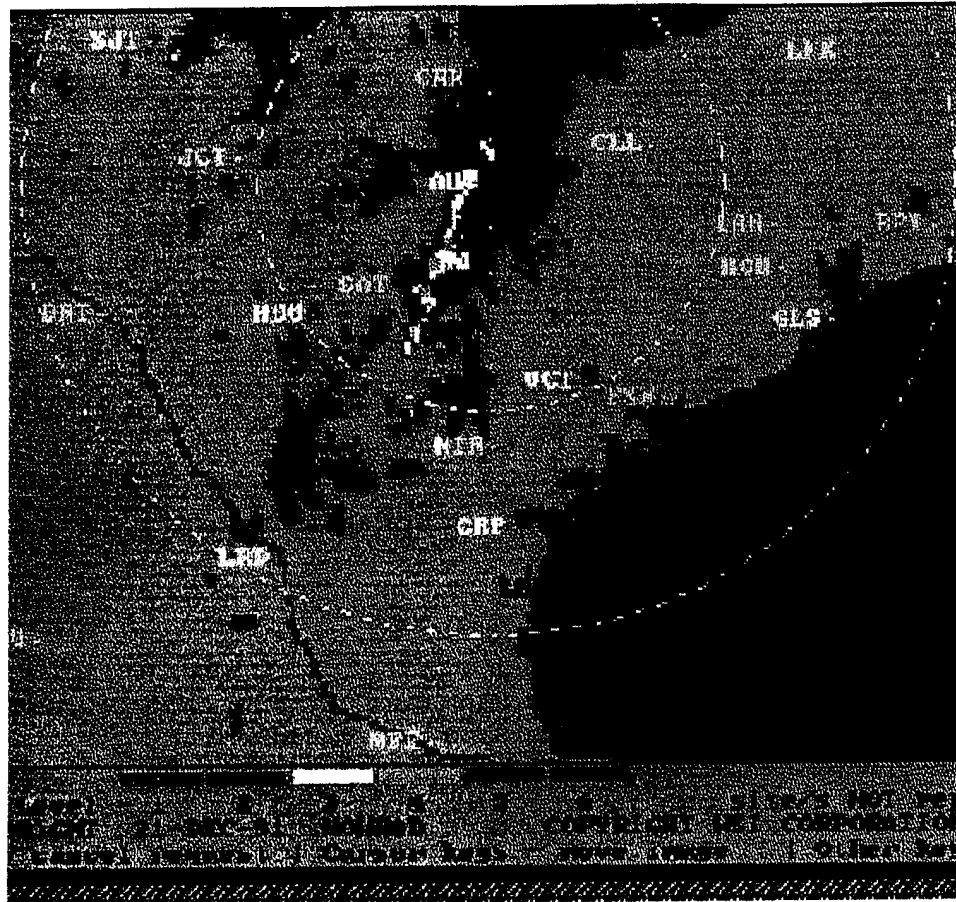
Figure 50a shows two protruding convective cells over the HLR, and two poorly defined cells due north of that location. Figure 50b shows the merging of the two HLR convective cells. The cirrus anvils to the north are also becoming merged with one another. Figure 50c and 50d continue to show merging of cirrus anvils. The spreading anvil cloudiness makes it difficult to discern the banded structure typically associated with the release of CSI. Therefore, WSR57 radar imagery from the Austin, Texas NWS was used to identify the banded structure of the precipitation.

Figures 51a-e are hourly radar imagery from the NWS Office in Austin for 22 UTC on December 20th to 02 UTC on December 21st showing the convection oriented southwest to northeast along the Balcones Escarpment. The first image (Figure 51a), depicts an abundant amount VIP level 1's and 2's (Table 4), (Chapter 2). A small area of VIP level 3's appear in the warm sector well to the south of Austin (AUS). Figures 51b-d show the increasing areal coverage of VIP levels 3 and some VIP levels 4 and 5, indicative of very heavy to intense rainfall. This band of heavy precipitation persisted throughout the evening of the 20th and maintained its orientation along the Balcones Escarpment. By the night of the 20th, the convection had subsided (Figure 51e) and the VIP level 3, 4, and 5 regions decreased considerably. However, very intense cells were still located along the Balcones Escarpment where southeasterly surface flow continued to feed warm moist air into the HLR.



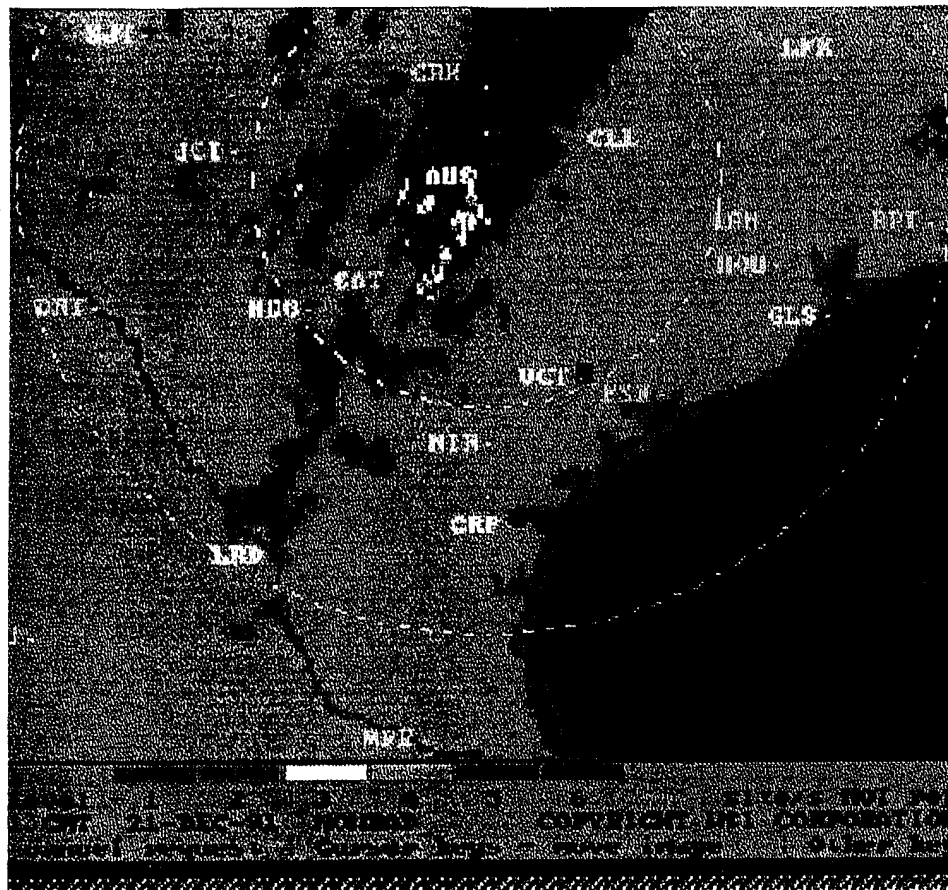
Dec 20, 1991 @ 4:00pm CST

Figure 51a. 20 December 1991 22 UTC WSR57 weather radar image.



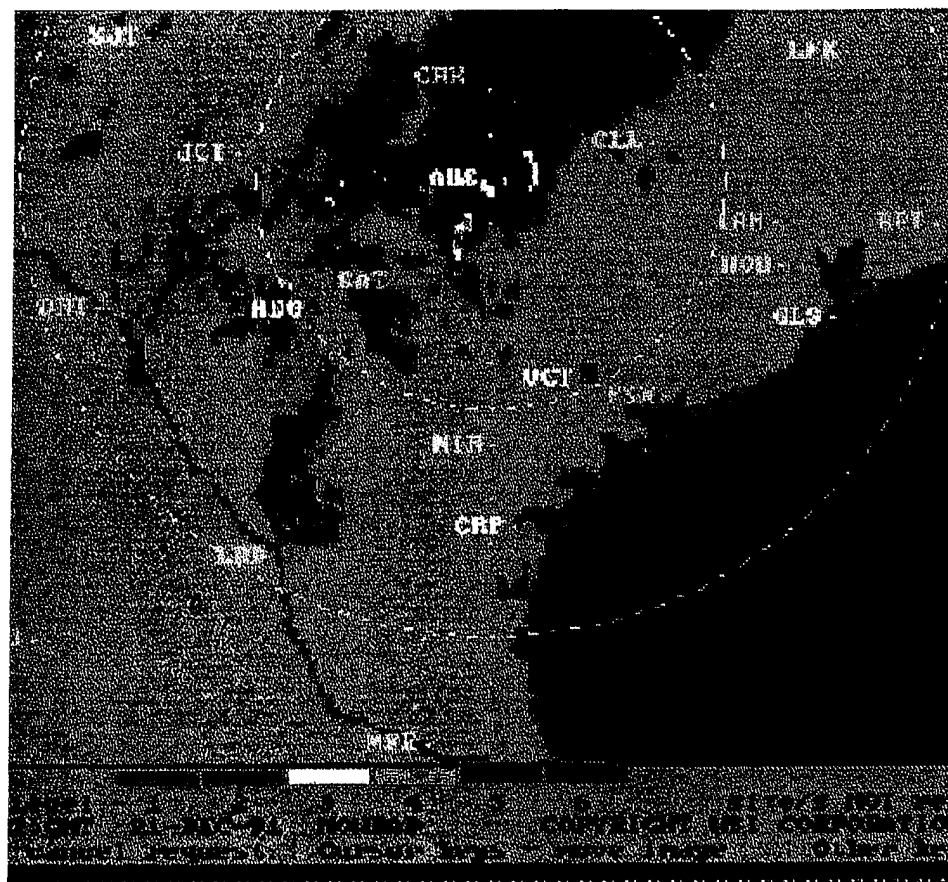
Dec 20, 1991 @ 6:00pm CST

Figure 51c. 21 December 1991 00 UTC WSR57 weather radar image.



Dec 20, 1991 @ 7:00pm CST

Figure 51d. 21 December 1991 01 UTC WSR57 weather radar image.



Dec 20, 1991 @ 8:00pm CST

Figure 51e. 21 December 1991 02 UTC WSR57 weather radar image.

Figure 52 shows a contour plot of rainfall totals on this day. Three distinct precipitation bands oriented southwest to northeast are depicted. The northernmost band is located in the Texas Hill Country, the central band located west of the Balcones Escarpment, and the southern most band is located just east of the Balcones Escarpment. Notice that none of the bands are oriented along the more west to east surface frontal features, but along the terrain features and parallel to the mean wind in the lower troposphere. This finding is evidence that surface terrain and CSI played significant roles in focusing the precipitation in the HLR. The fact that the CSI bands were oriented nearly parallel to the Balcones Escarpment enhanced the precipitation in this region. Notice that the heaviest precipitation (in excess of five inches), fell in the central band where the terrain forcing probably was most important. Figure 53 is a composite map showing the location of surface frontal features, precipitation bands, and the location of the Balcones Escarpment. Rain fall averages for this day were just over three inches. There were five rain gauge stations recording over five inches this day. The maximum amount of precipitation was recorded at Red Bluff (B00) with 5.74 inches.

00 UTC 21 December 1991

Figure 54 shows the 300 mb analysis. The closed low located in northwestern Mexico has remained stationary. The wind speed maximum that was in the

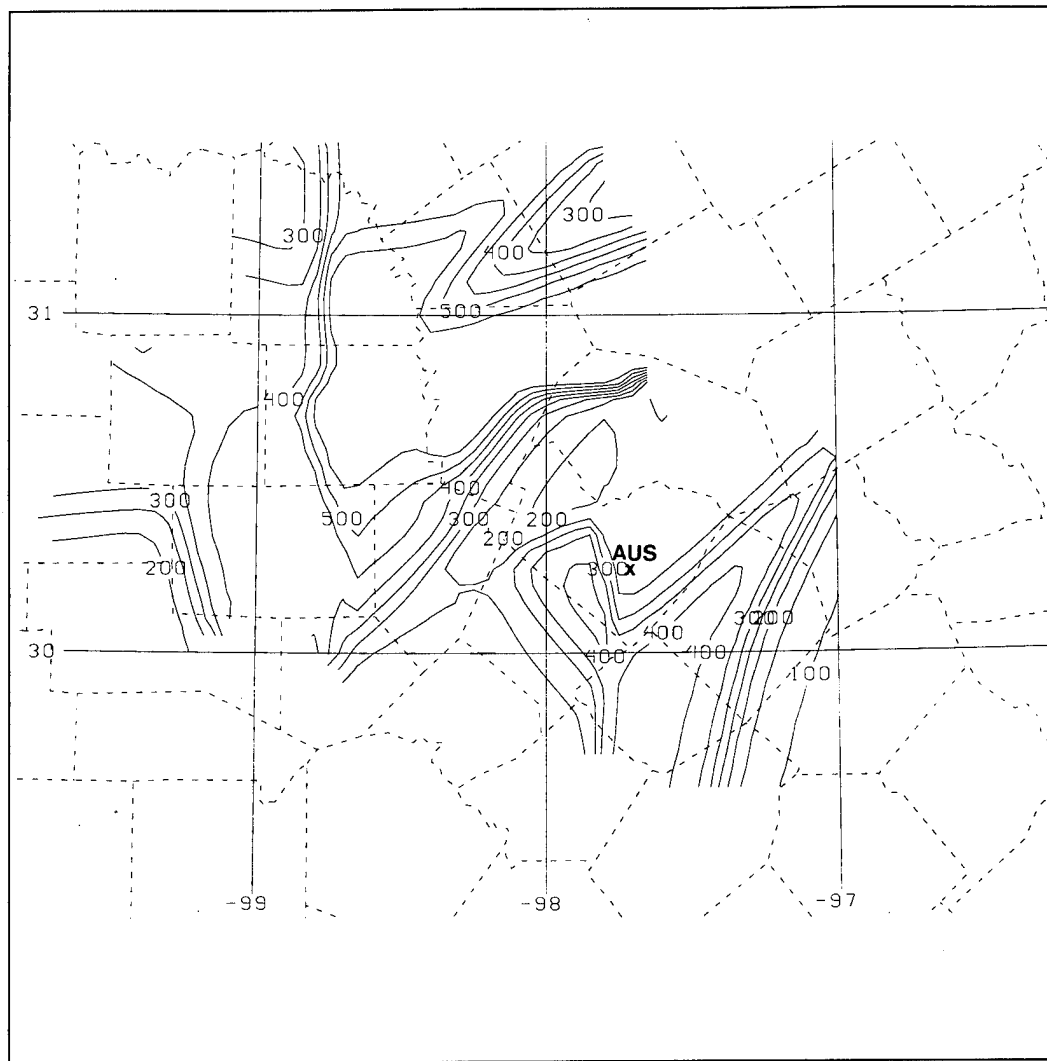


Figure 52. Isopleths of daily rainfall amounts at each LCRA rain gauge location on 20 December 1991. Rainfall amounts are shown in inches $\times 10^2$.

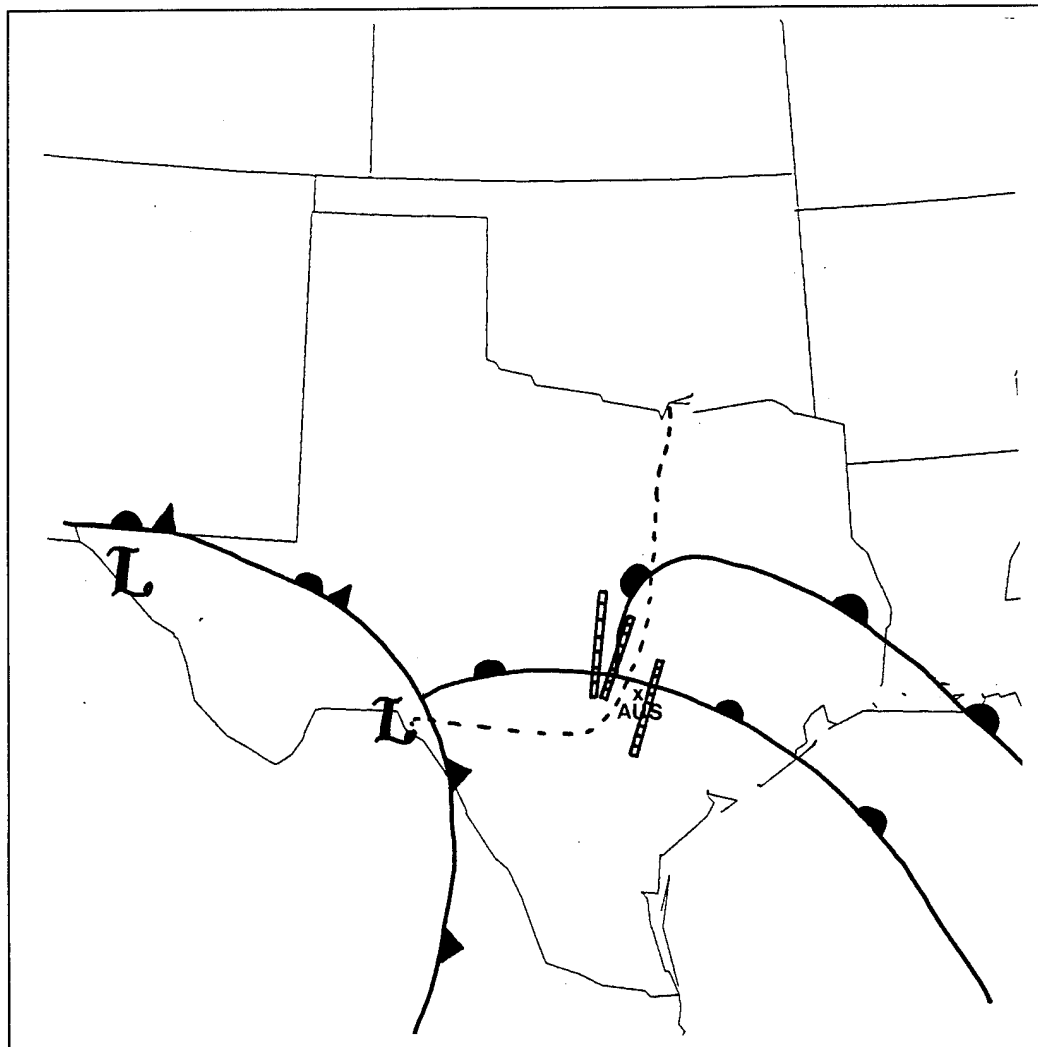


Figure 53. 20 December 1991 composite map showing location of surface frontal features (solid lines), precipitation bands (hatched region), and location of Balcones Escarpment (dashed lines).

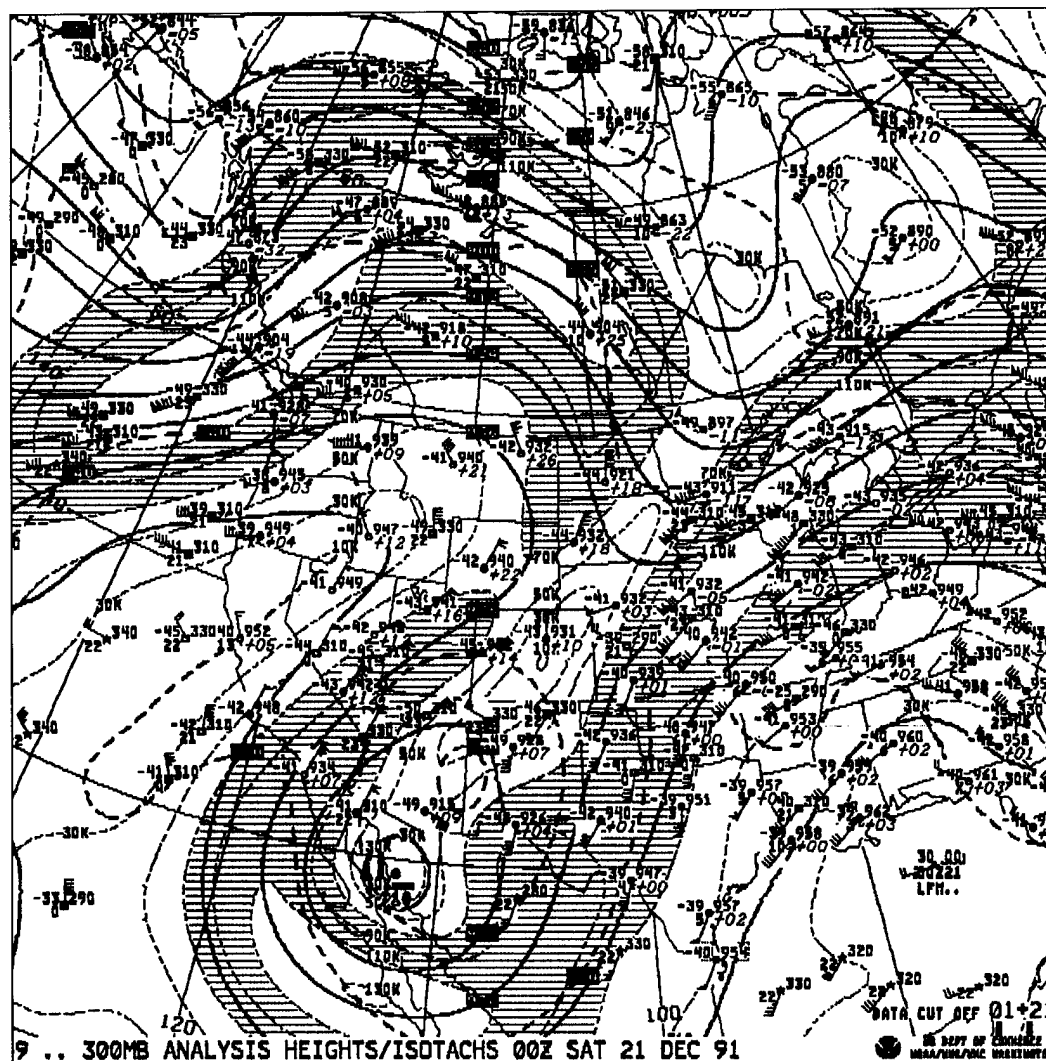


Figure 54. 21 December 1991 00 UTC 300 mb analysis.

Gulf of Alaska has moved into western British Columbia and is oriented west southwest to east northeast along the ridgeline and appears to be cutting the system off to the south. It is at this time that the flow becomes more zonal than meridional. An anticyclonically curved jet streak continues to be situated south-southwest to north-northeast across Texas with the favorable right-entrance region centered across Texas. It has been shown that the right-rear quadrant of an anticyclonically curved jet is the favored region for enhanced upward motion. It, no doubt, played a significant role in the heavy rainfall during December 20-21. The analysis also indicates that another significant jet streak would soon translate out of Mexico, although the lack of supportive upper air data out of Mexico casts some uncertainty into the strength and timing of the jet. The left-exit region of this jet along with the right-entrance region of the upper jet over the middle Mississippi Valley combined to produce the strong, large-scale, vertical-motion field observed over Texas (Mahler 1995).

Figure 55 shows the 500 mb analysis. The ridging continues to persist in the Pacific Northwest. The low, located in northwestern Mexico, is still apparent. Diffluence is still evident over the HLR which continues to enhance upward motions, although the strongest diffluence has shifted to the northeast of the HLR (between SEP and GGG).

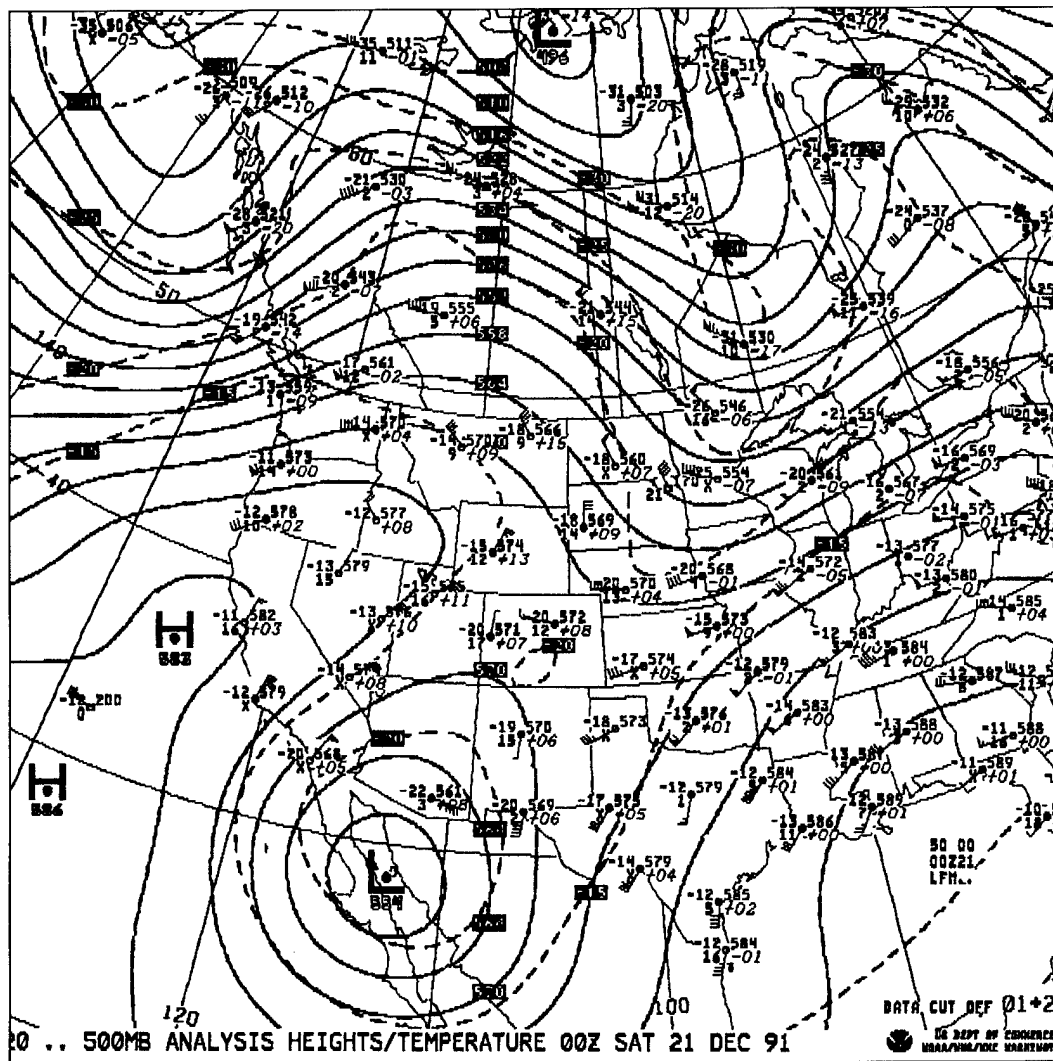


Figure 55. 21 December 1991 00 UTC LFM 500 mb analysis.

Figure 56 shows the 700 mb vertical motion field. There is an upward motion axis located from Mexico into northeastern Texas. This aligns well with the jet streaks and the surface cold front moving through the region which continues to enhance the precipitation.

Figure 57 shows the 850 mb analysis. The Gulf flow is still evident, however, the axis of warm, moist advection has moved eastward into eastern Texas. Ridging is influencing northern Texas and the winds have shifted to a more northerly component. Drier air is being advected into the region from the north. Temperature and dewpoints have dropped at AMA indicating the presence of the cooler, drier air mass. This is the first indication that the Gulf moisture, which was so important in setting the stage for the flooding event is moving out of the HLR.

12 UTC 21 December 1991

Figure 58 shows the 300 mb analysis. The Pacific ridge axis extends zonally into Iowa. This orientation has forced the jet axis to become zonal across the northern United States and cutting off energy to the low in northwestern Mexico. It is at this point, that this low begins to weaken. One last jet streak is moving from the base of the trough over central Baja into western Texas.

Figure 59 is the 500 mb analysis. The low over central Baja has been cut-off and, like the 300 mb low, will dissipate over the next twenty-four hours.

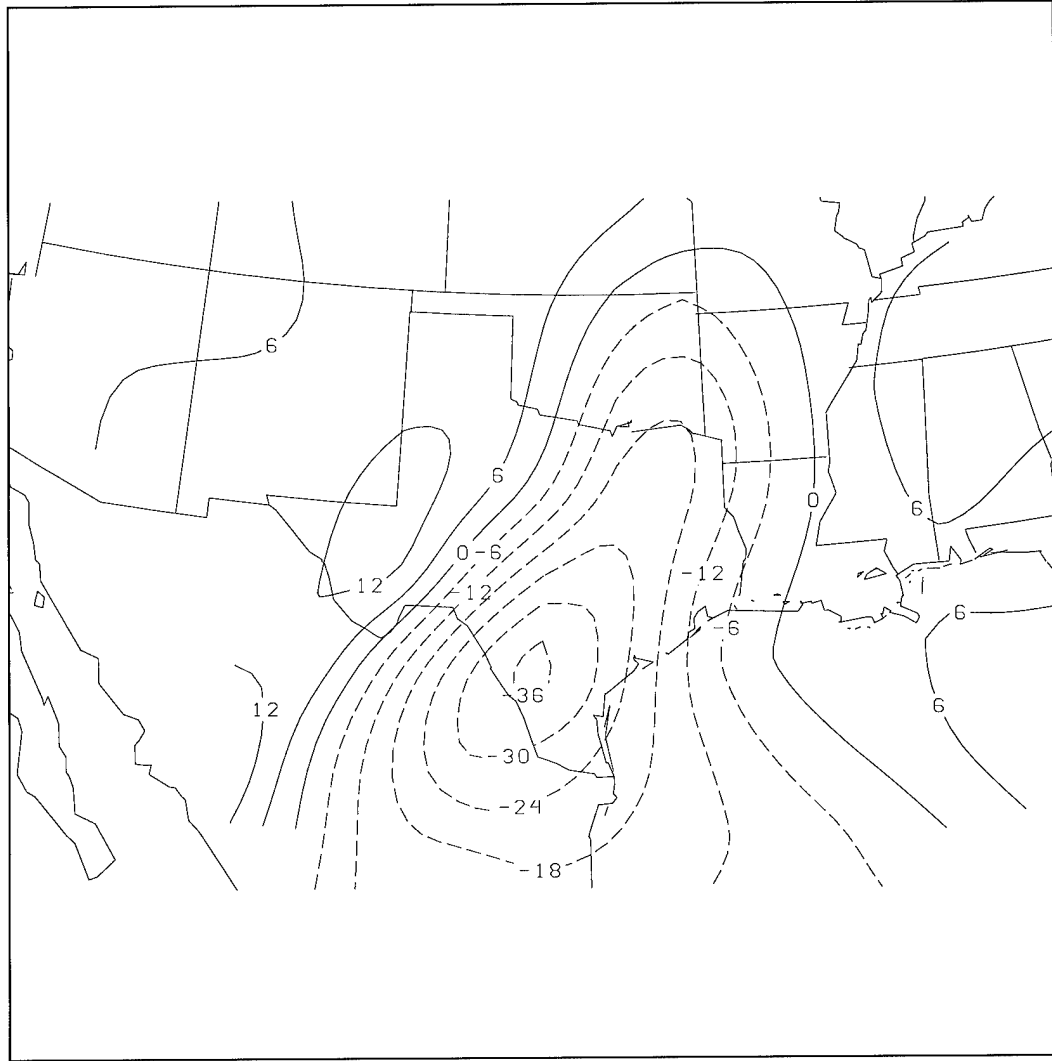


Figure 56. 21 December 1991 00 UTC 700 mb vertical motion field. Negative values (dashed lines) indicate upward motion and positive values (solid lines) indicate downward motion.

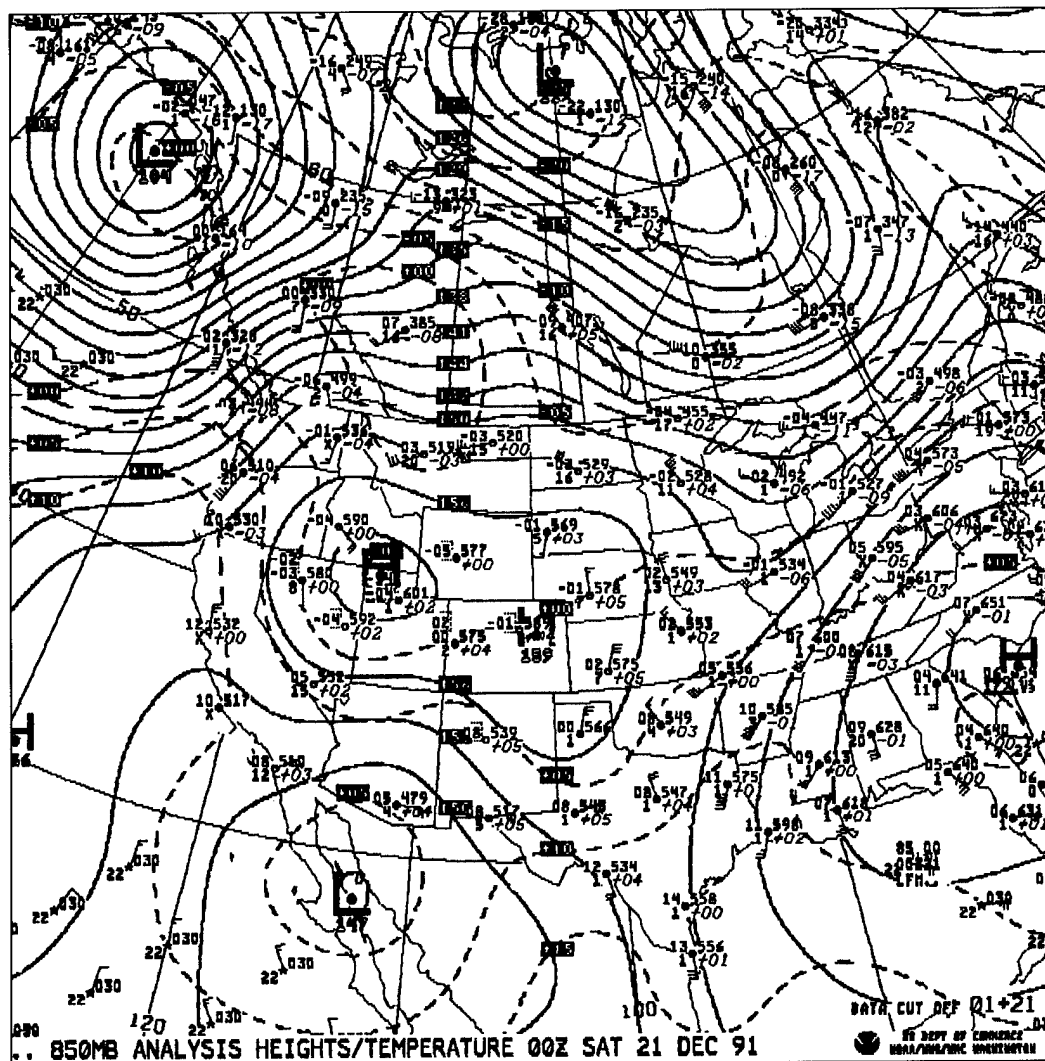


Figure 57. 21 December 1991 00 UTC LFM 850 mb analysis.

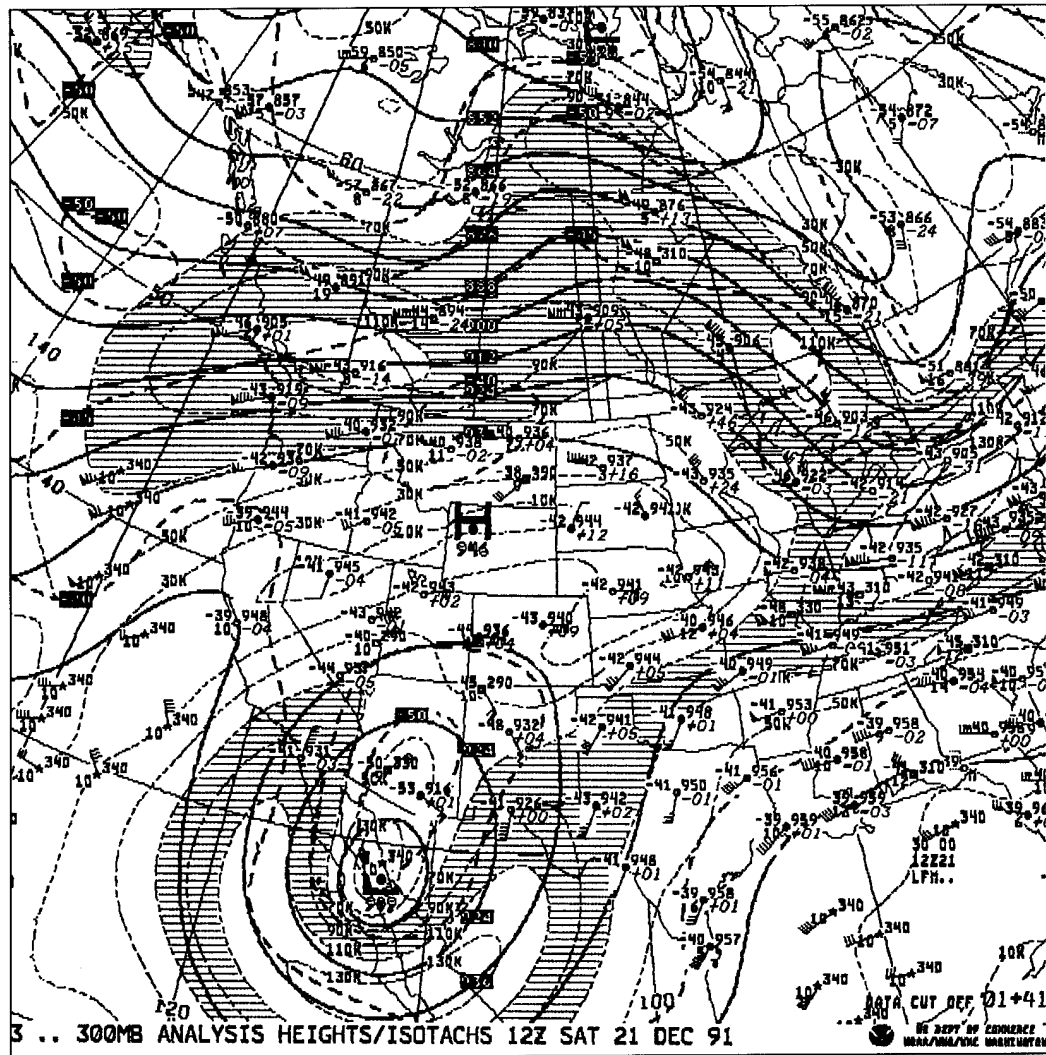


Figure 58. 21 December 1991 12 UTC LFM 300 mb analysis.

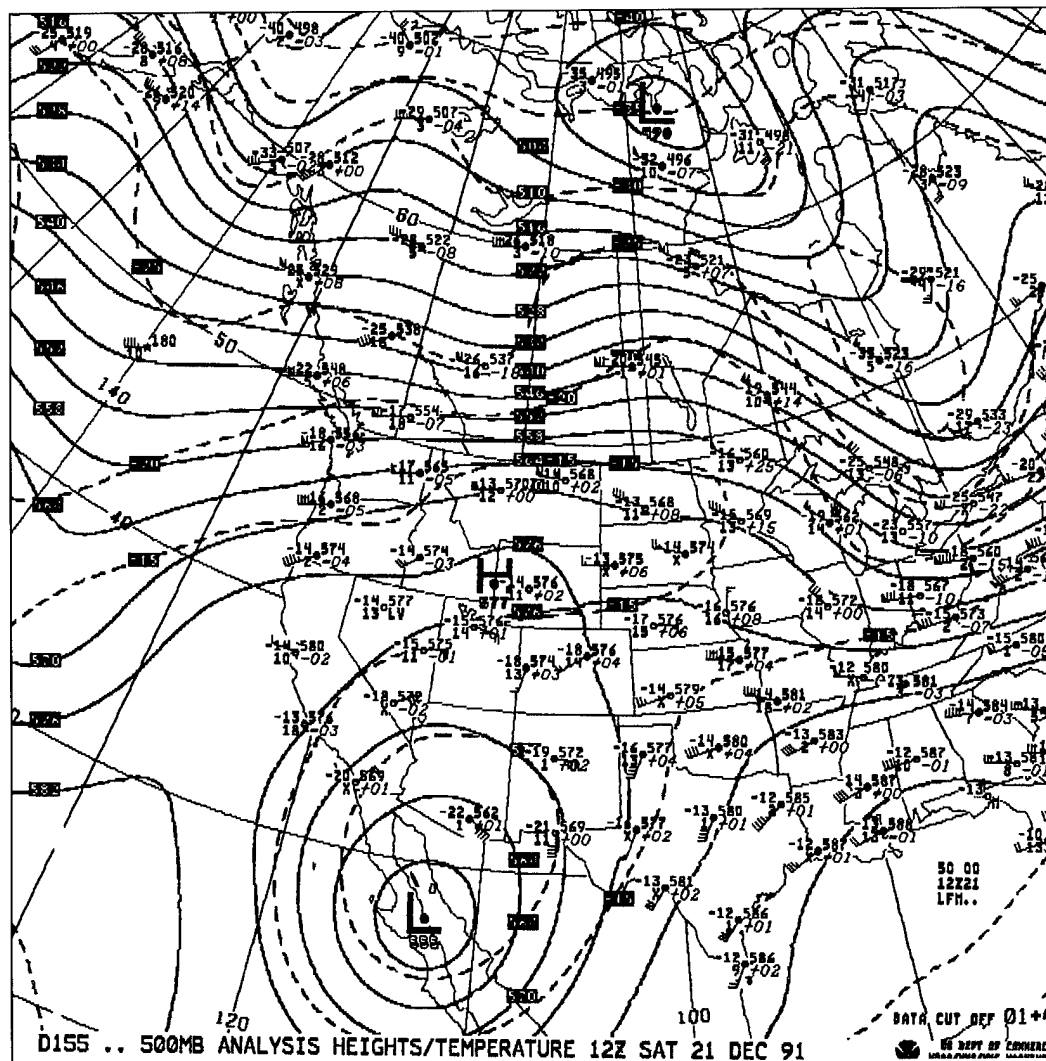


Figure 59. 21 December 1991 12 UTC LFM 500 mb analysis.

Weak diffluence exists over southeast Texas continuing to give support for upward motions with the departing system.

Figure 60 shows the 700 mb vertical motion field. Upward motion continues to persist on an axis through southern and eastern Texas and mirrors the surface cold front. The upward motion is probably enhanced by the jet streak moving into western Texas.

Figure 61 is the 850 mb analysis. Ridging continues to make its way southward over northern Texas. The Gulf flow is still evident along the Gulf coast and in eastern Texas. Just north of the HLR there is a diffluent zone indicating downward motion and stability.

Figure 62 is the surface analysis. The cold front is slowly moving eastward. Cooler air is evident in the HLR with temperatures in the upper 30's to middle 40's ($^{\circ}\text{F}$). There are still reports of light rain and drizzle behind the cold front. Rain and thunderstorms persist from the Balcones Escarpment southeastward across south and southeast Texas.

Figure 63a and 63b show water vapor satellite images. The cut-off low shows up well over northwestern Mexico. Notice the sharp western edge of the moisture boundary in west central Texas. One can still see convection occurring over central and eastern Texas, along and ahead of the advancing cold front, as cold dry air is displacing a region of warm moist air.

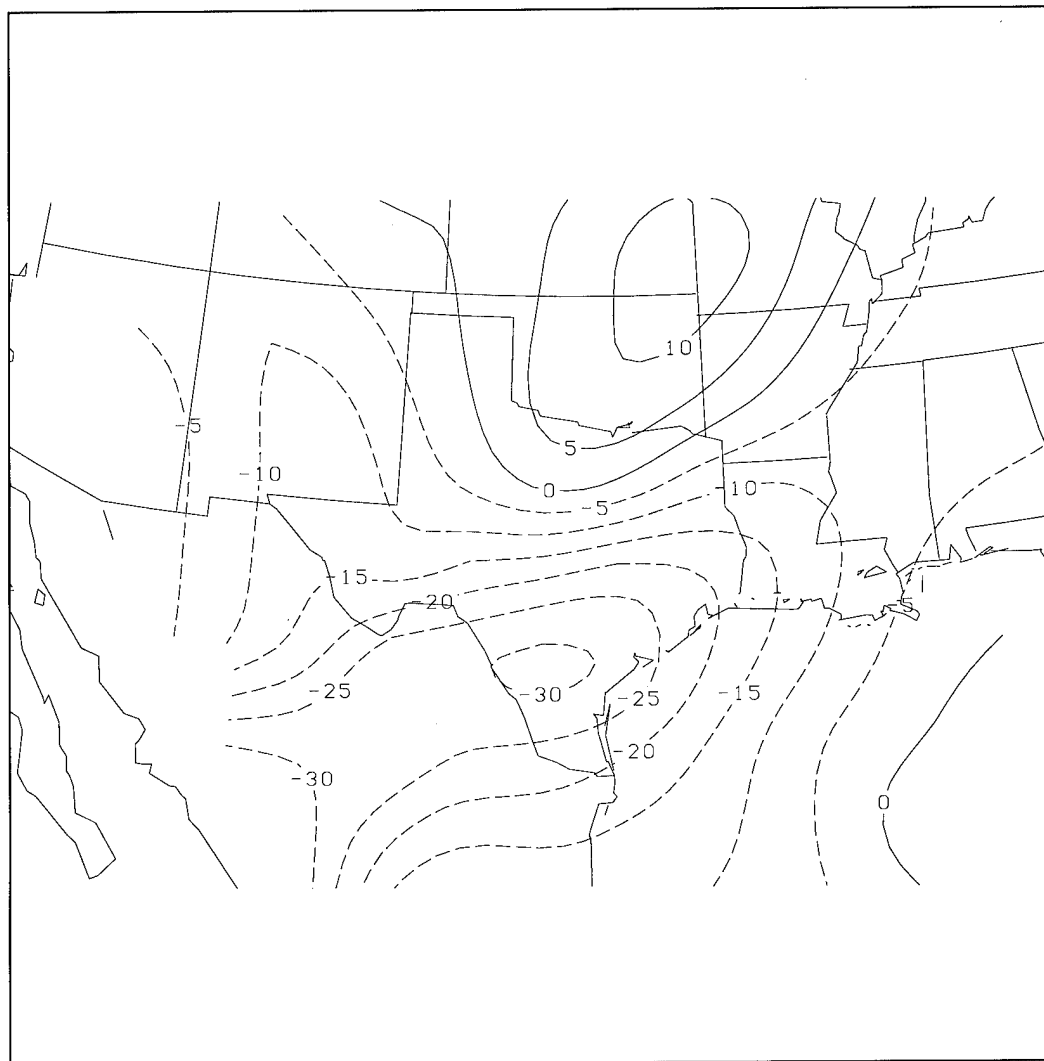


Figure 60. 21 December 1991 12 UTC 700 mb vertical motion field. Negative values (dashed lines) indicate upward motion and positive values (solid lines) indicate downward motion.

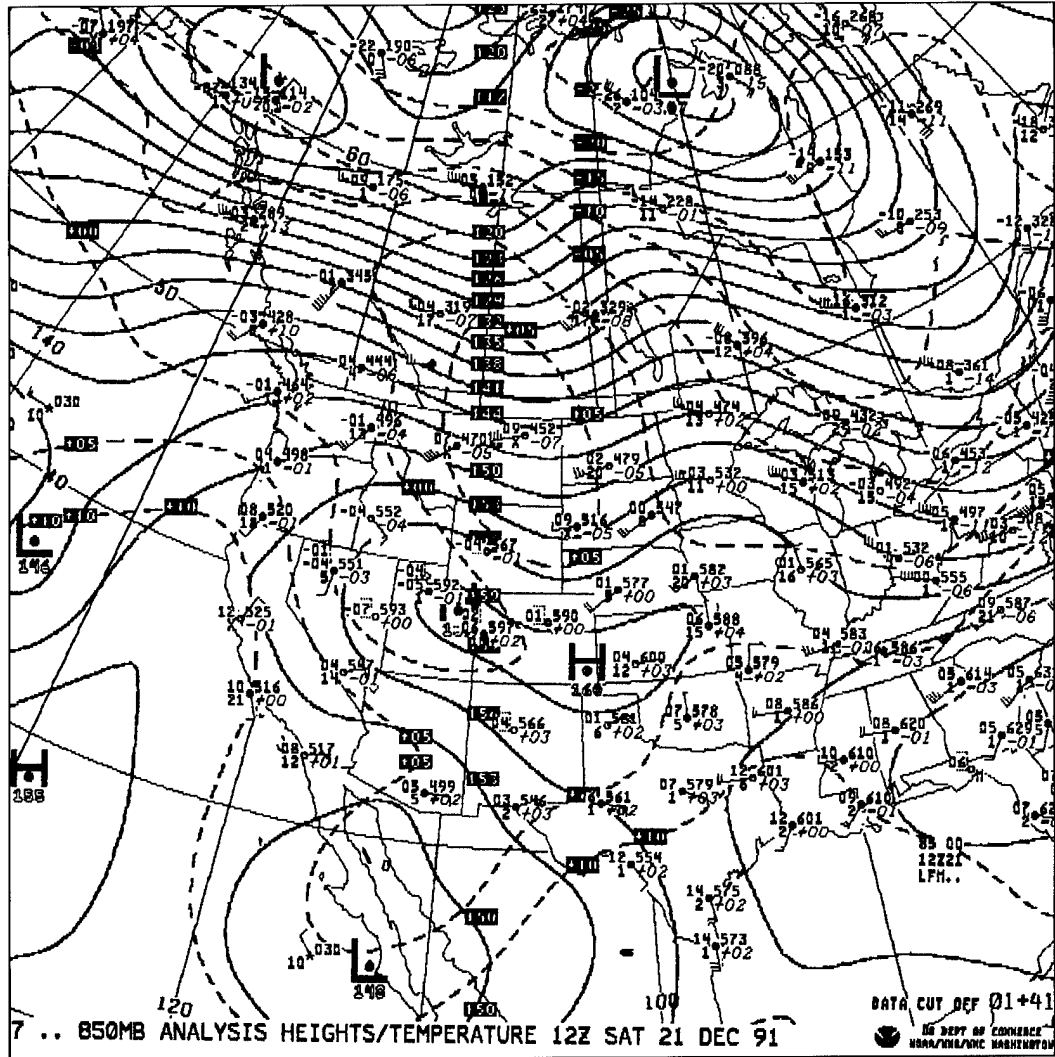


Figure 61. 21 December 1991 12 UTC LFM 850 mb analysis.

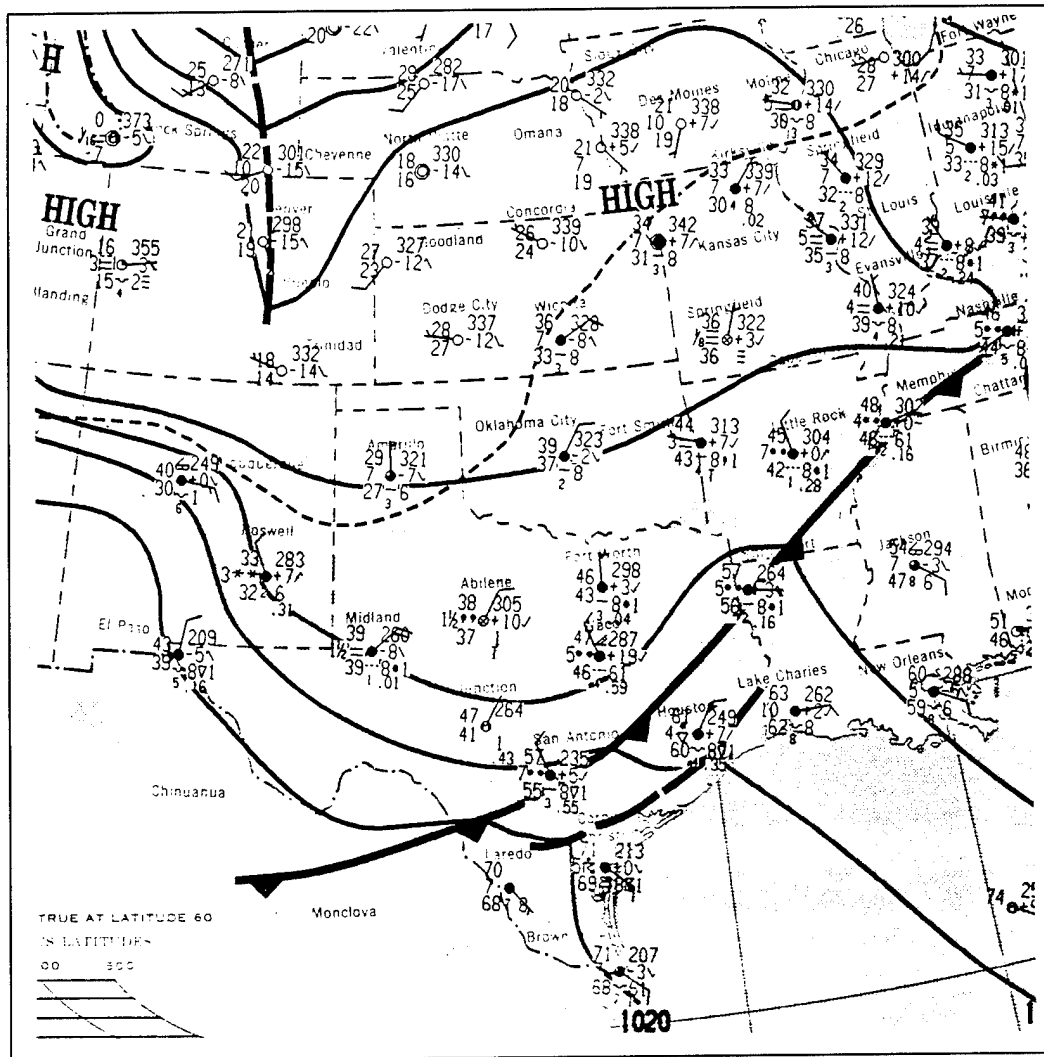


Figure 62. 21 December 1991 12 UTC daily surface weather map.

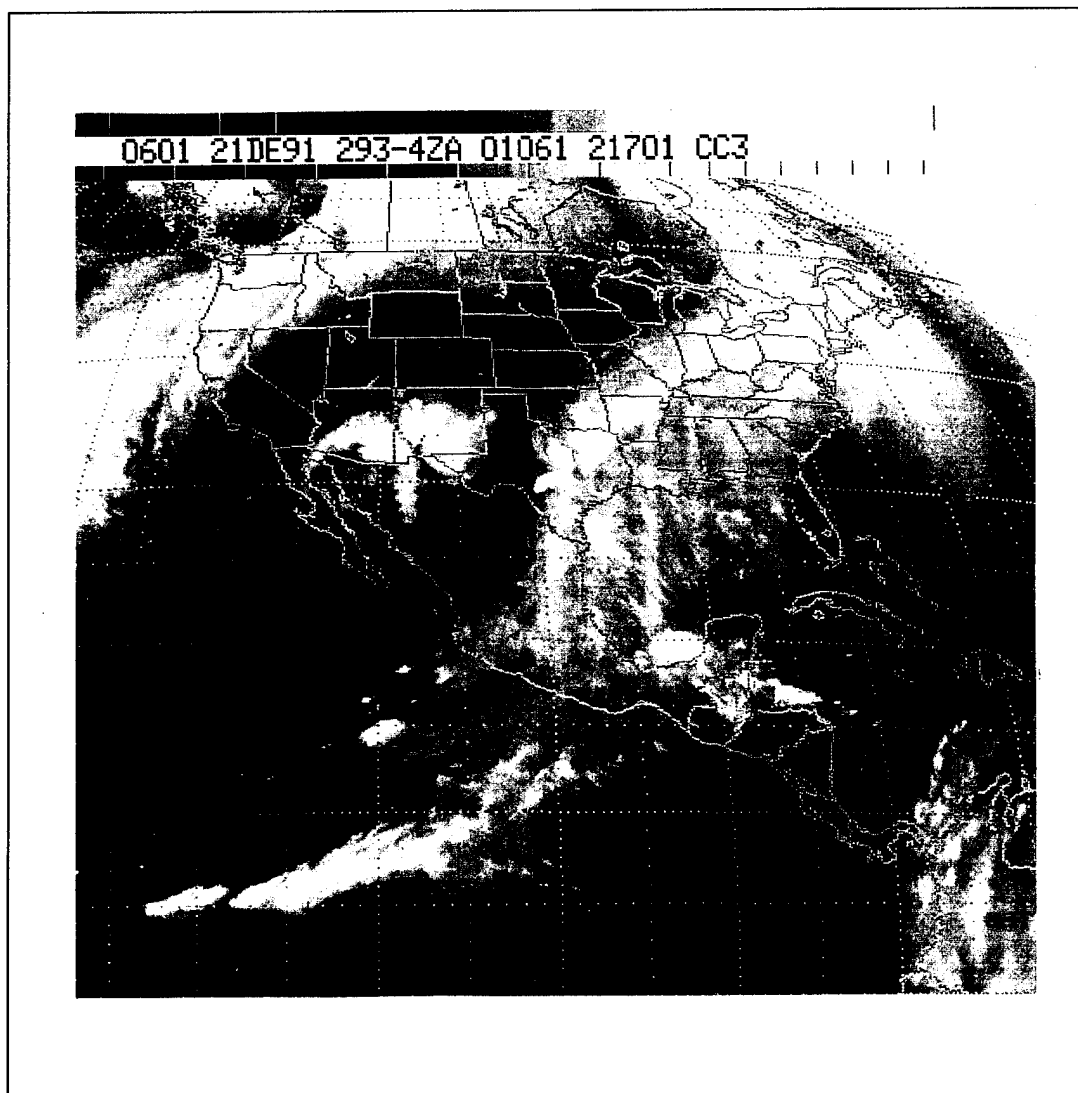


Figure 63a. 21 December 1991 0601 UTC water vapor satellite image.

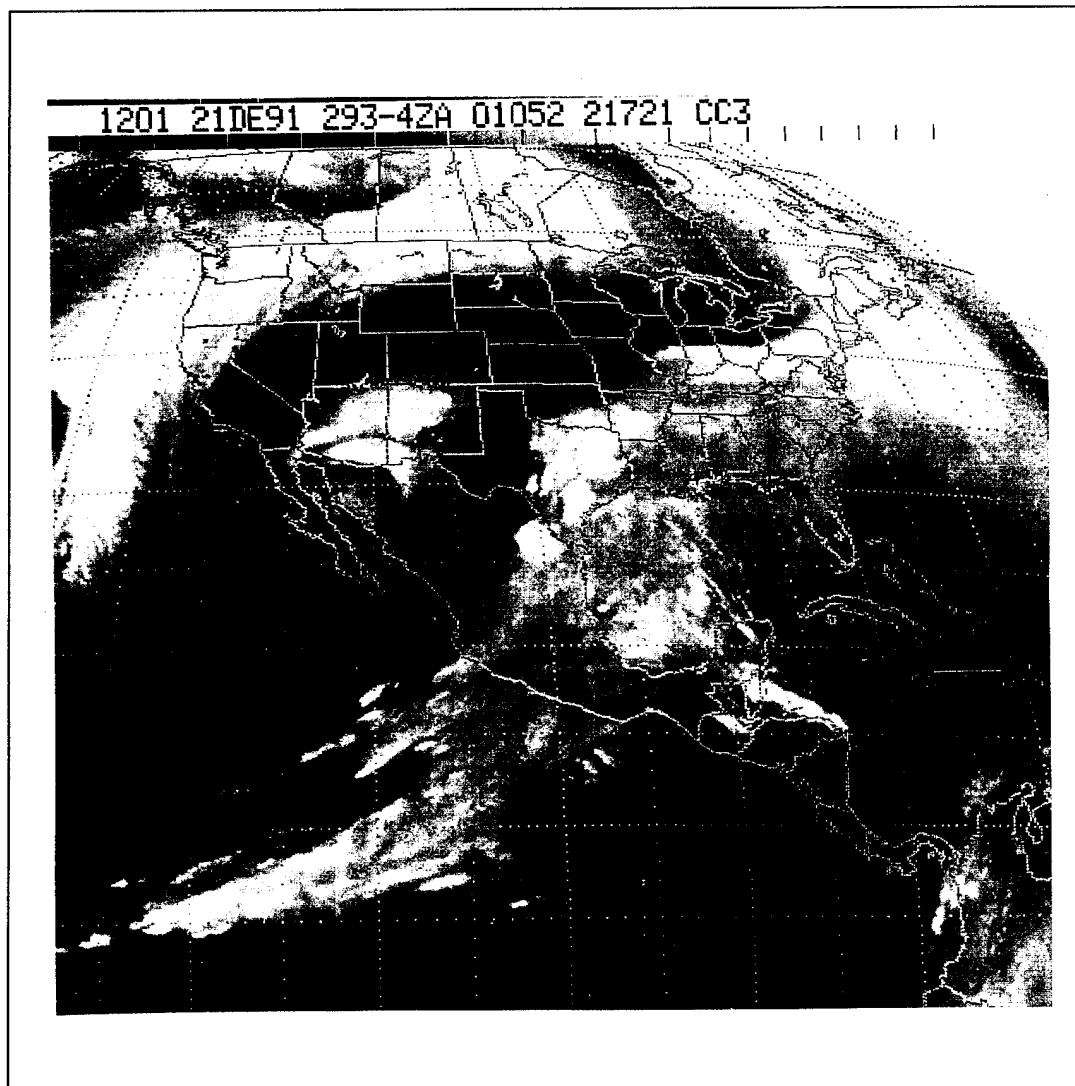


Figure 63b. 21 December 1991 1201 UTC water vapor satellite image.

The precipitation totals for this day have decreased to below two inches on average. It is evident at this time, that the primary dynamics and thermodynamics responsible for the flooding continue to slowly move eastward. Rapidly improving conditions were evident over the HLR as the cold front continued a slow progression eastward, and precipitation ceased by 23 December 1991.

Summary

Figure 64 shows the weekly rainfall totals map over the HLR for this event. Although this is a compilation of days, one can still see regions where southwest to northeast banded precipitation was evident. For the week, the heaviest precipitation appears to the west and southwest of Austin (north northwest of San Antonio (SAT)) where ≥ 14 inches of rain fell. This region is just north and west of the Balcones Escarpment.

Figure 65 shows the Colorado River and the location of the six HLR dams. Figures 66 a - f show December 1991 daily water levels at these dams. In addition to daily water level traces, also included are normal, 10, 50, and 100 year pool levels. Note, each graph is scaled independently from the others. The demands of the rice growers and the abnormally wet year forced the LCRA to maintain the high lake levels observed before the onset of precipitation. The heavy rain event during the week of 17 - 23 December produced more run-off than could be handled by the lake, thus rapidly

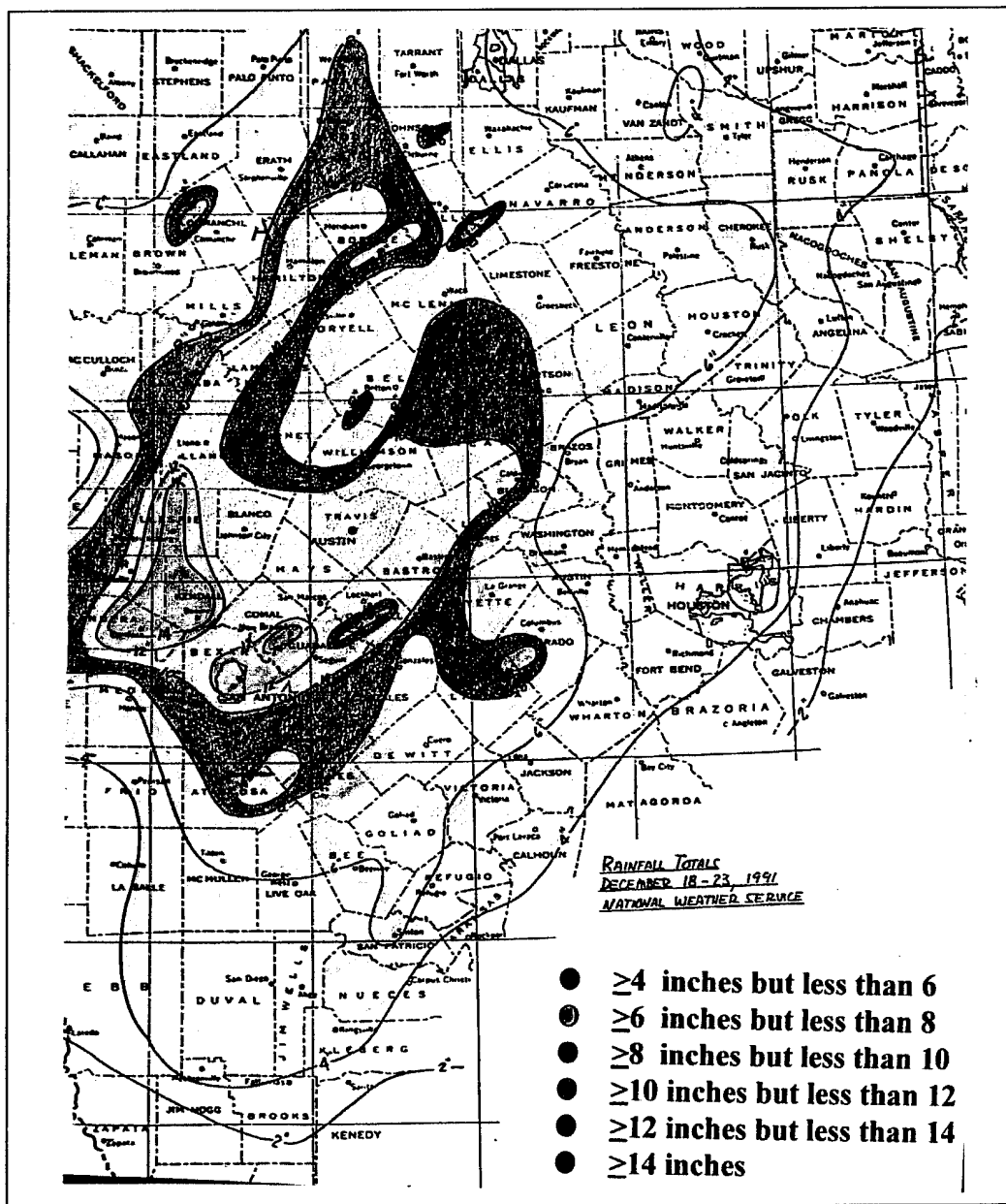


Figure 64. Rainfall totals reported by the National Weather Service for the week 18 - 23 December 1991.

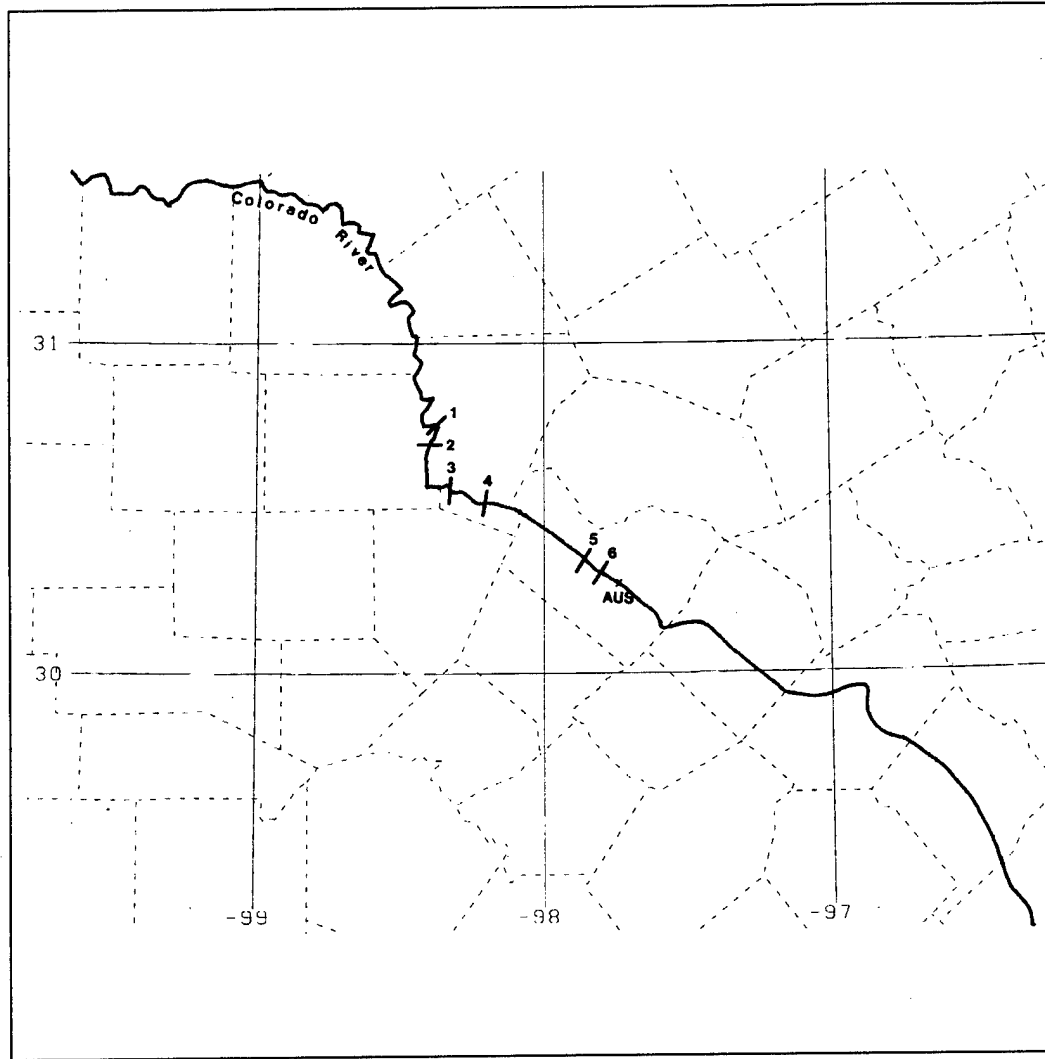


Figure 65. Location of the six HLR dams where (1) is the Buchanan Dam, (2) Inks Dam, (3) Wirtz Dam, (4) Max Starcke Dam, (5) Marshall Ford Dam, and (6) Tom Miller Dam.

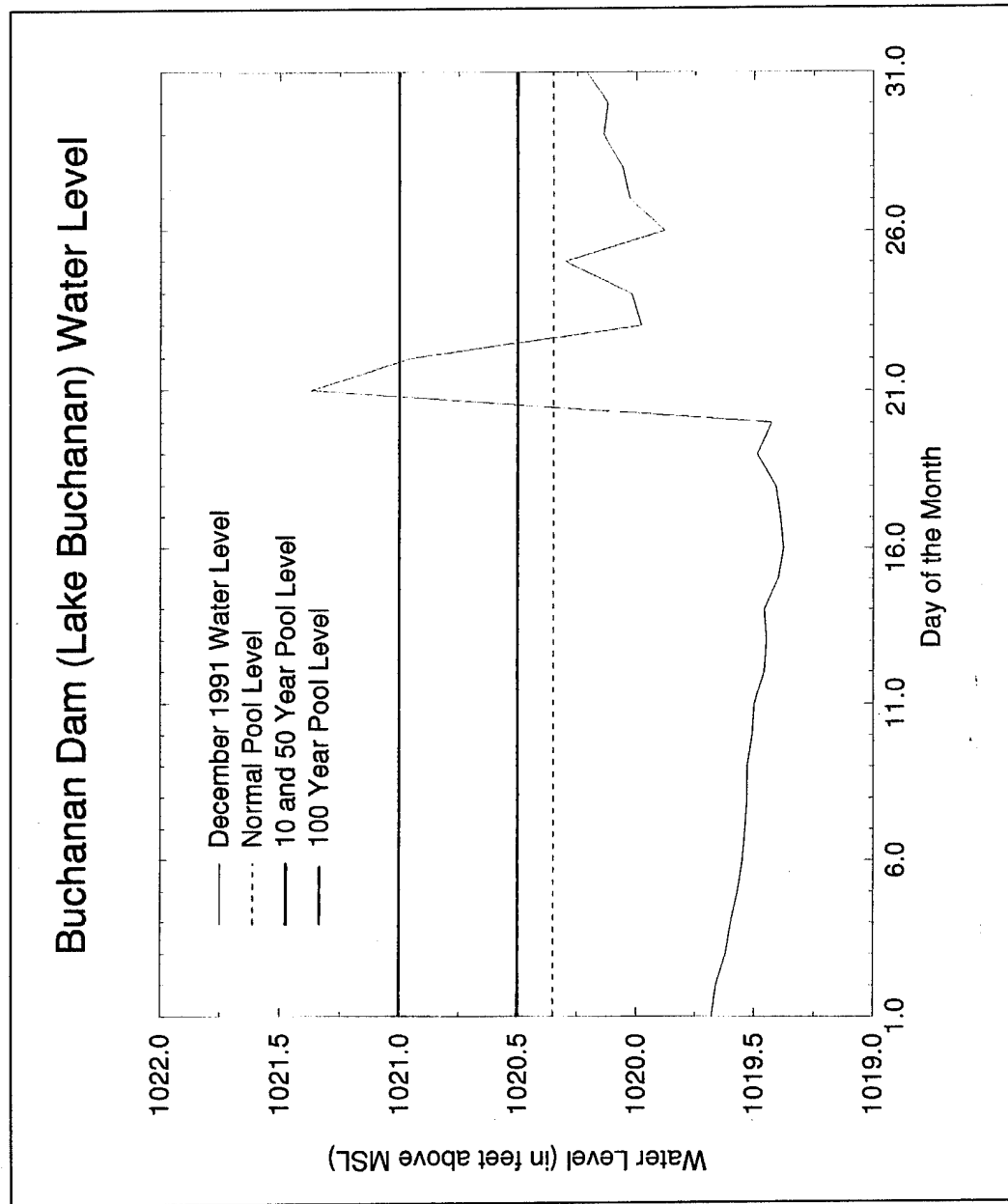


Figure 66a. December 1991 Buchanan Dam water level information.

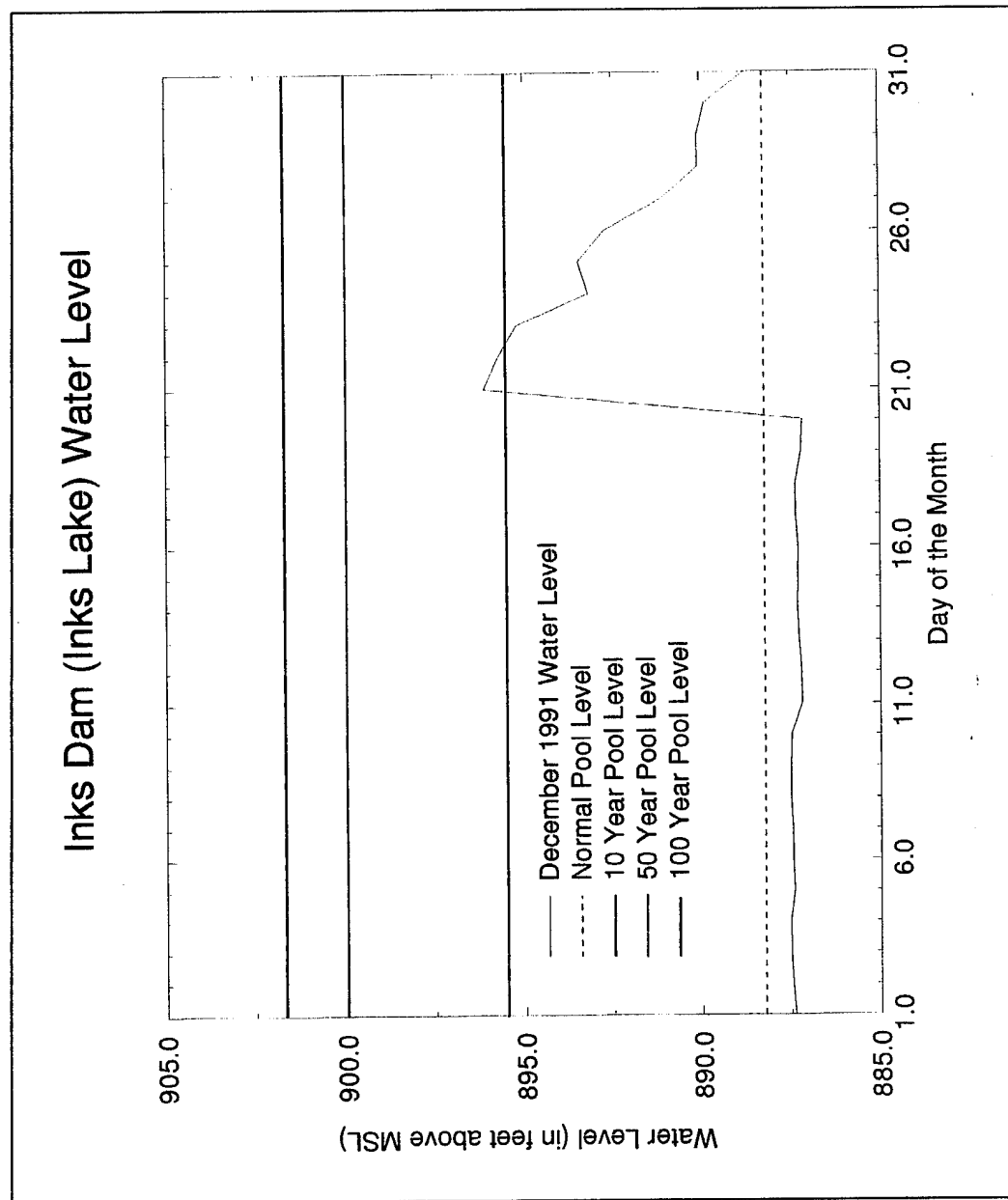


Figure 66b. December 1991 Inks Dam water level information.

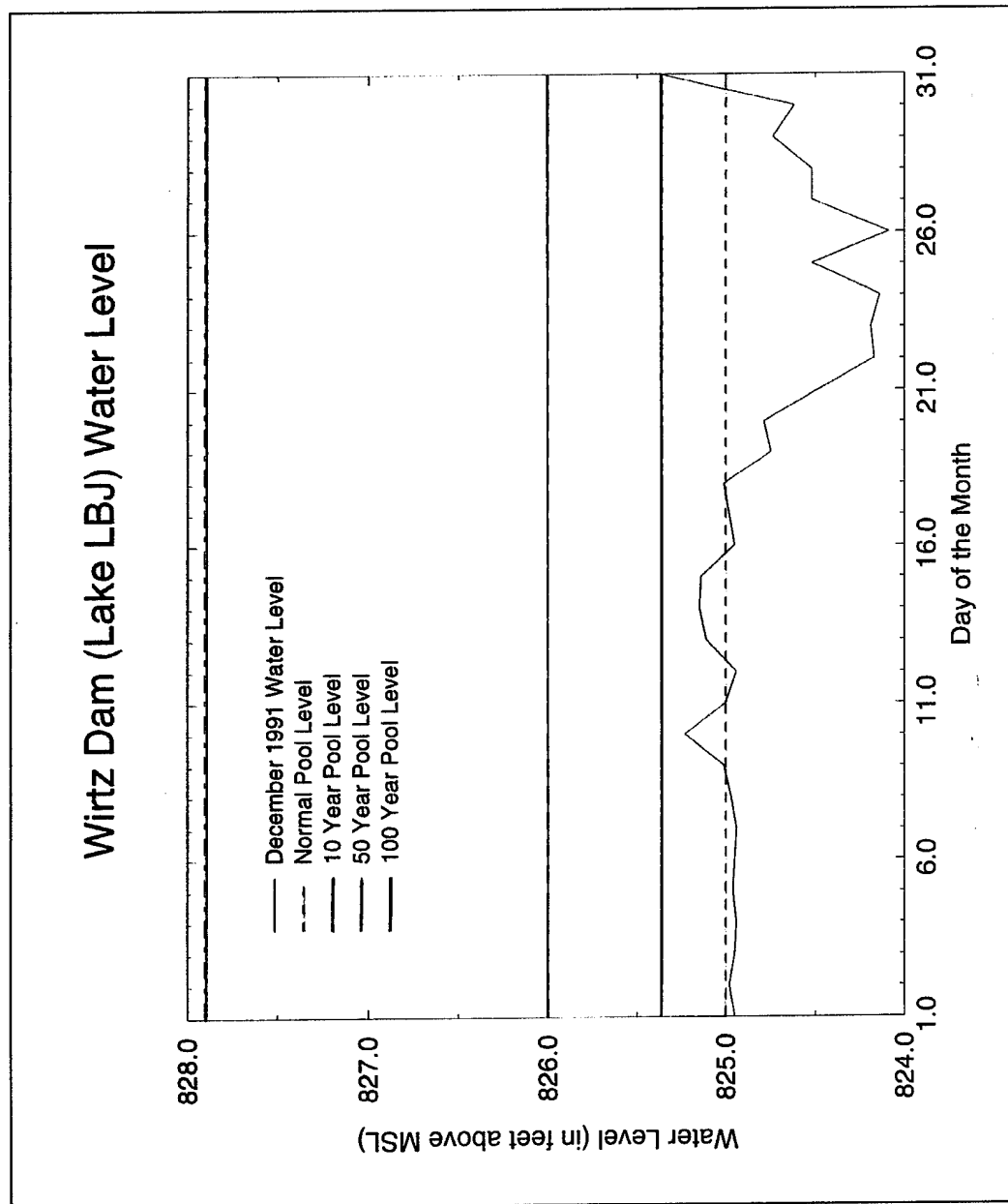


Figure 66c. December 1991 Wirtz Dam water level information.

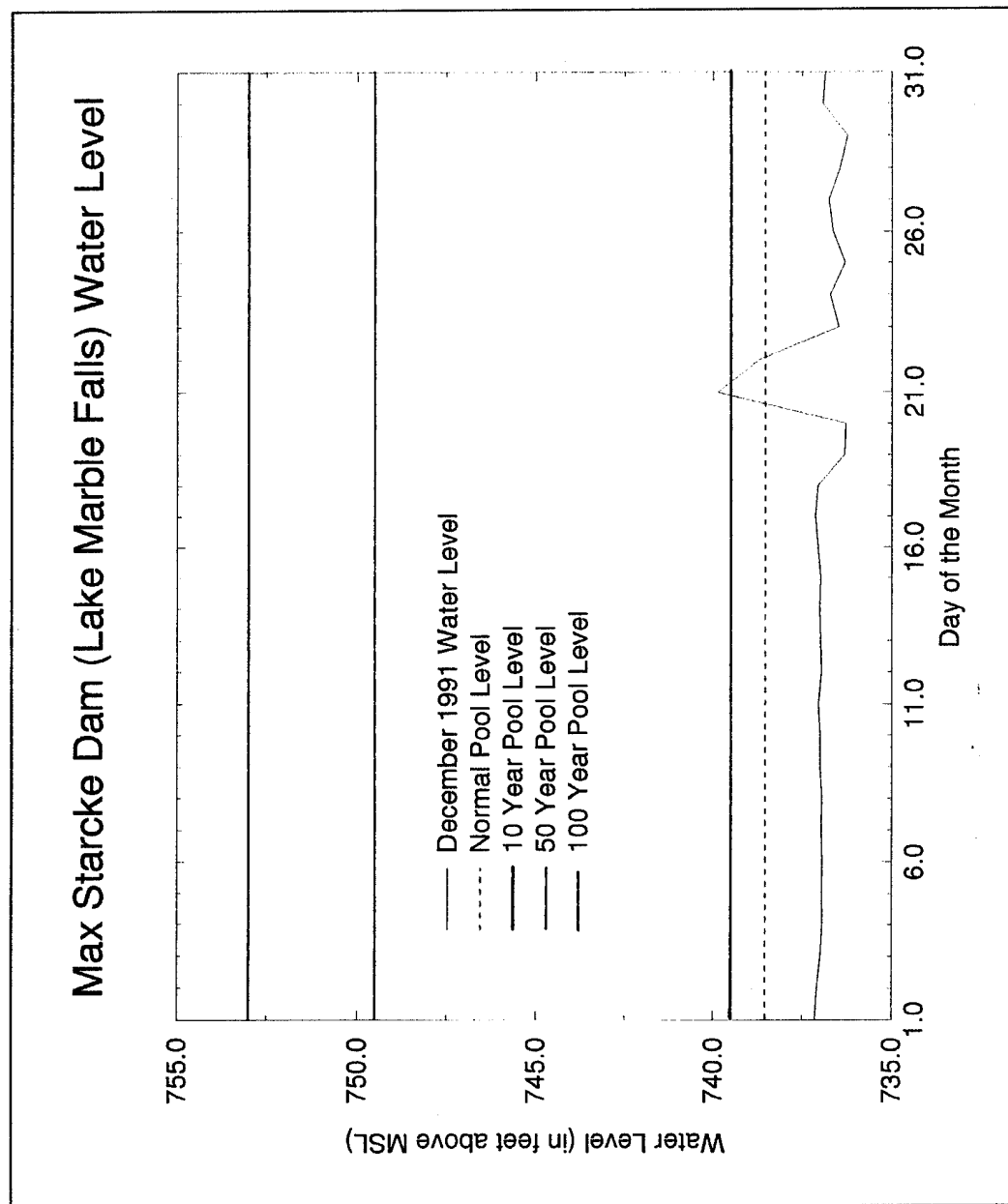


Figure 66d. December 1991 Max Starcke Dam water level information.

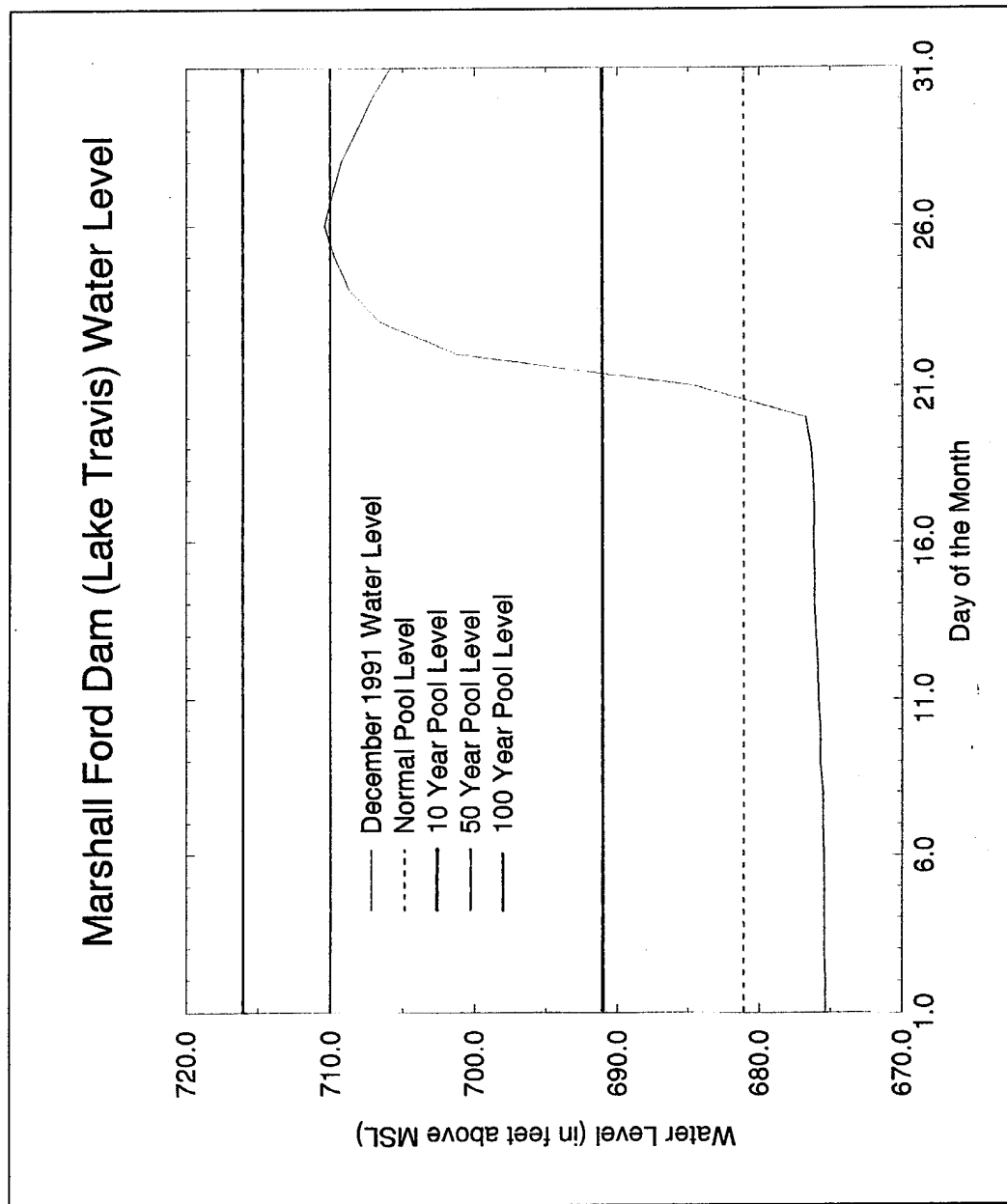


Figure 66e. December 1991 Marshall Ford Dam water level information.

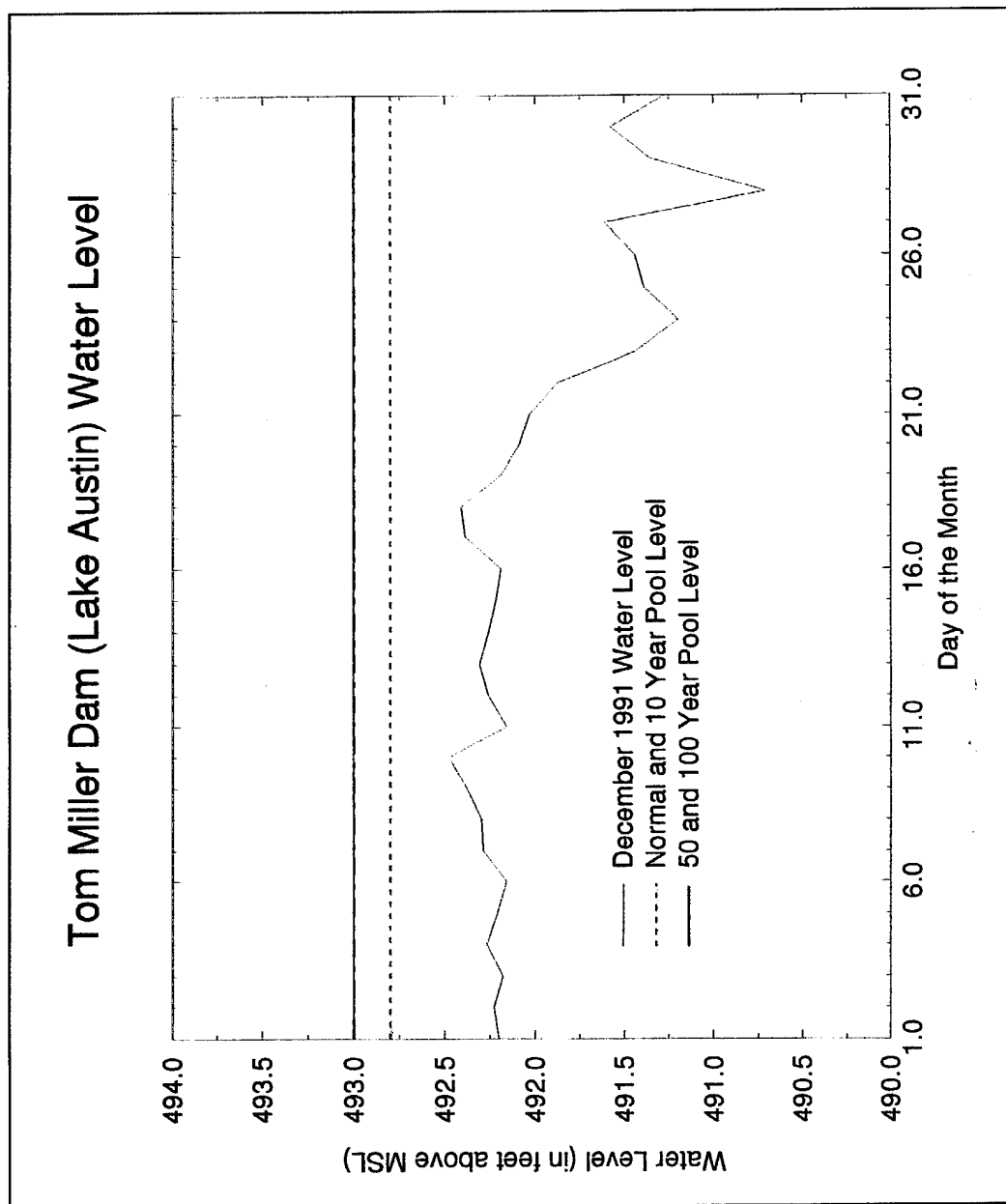


Figure 66f. December 1991 Tom Miller Dam water level information.

increasing lake levels. In fact, record lake levels were observed at Lakes Buchanan and Travis on the 21st during the most severe flooding in the HLR.

From these figures, one can see that it is important to assess conditions for elevated convection in complex terrain regions that are already saturated, because the massive runoff from the convection dramatically raised lake levels. It is the unexpected sudden rise in lake levels that lead to devastating flood events.

CHAPTER 5

CONCLUSIONS

Since winter time flood events constitute a minority of annual flooding events, limited information is available on why they occur. Most of the research on flooding concentrates on the spring through fall seasons. The HLR flood was studied to get a better understanding of what meteorological factors are responsible in a winter time flood event.

In order to study winter season flood events, one must not look at typical upright convective processes. Classical thermodynamic processes are not as dominant during the winter, therefore other processes must be addressed to explain winter flood events. Meteorological processes such as orographic lifting, overrunning, PI, CSI, and elevated thunderstorms should be considered when looking for winter flood causes.

During the winter season, a return-flow event can provide abundant amounts of Gulf moisture. The onset of this event can be detected by using surface charts, satellite images, upper air data, and isentropic analyses. Along with return-flow, meteorological processes like overrunning, orographic

lifting, PI, and CSI should be evaluated; all of which were contributors to the HLR flooding. Return-flow can be easily detected, but processes like PI, CSI, and parameters like MSF and moisture convergence are often difficult to detect from conventional surface charts, upper air data, and satellite imagery. To detect these processes, specific products need to be produced which address these parameters quickly.

Computer programs such as GEMPAK can be used to create products that allow one to detect regions of PI, CSI, and MSF. Gridded data sets can be incorporated allowing one to do conventional isobaric analyses. GEMPAK also offers flexibility, in that one can create isentropic gridded data sets and evaluate isentropic fields.

For this study, construction of pseudo-angular momentum and equivalent potential temperature diagrams allowed one to detect regions of PI, CSI, and the vertical structure of frontal systems. Diagrams such as these could be used operationally to help diagnose the onset and persistence of these instabilities. The importance of diagnosing elevated convection allows one to warn for heavy precipitation and once the convection started one could warn the local population where the threat of flooding would occur.

The incorporation of the LCRA rain gauge network was important in this study. It provided a good source of rainfall information and covered a large

spatial area as shown earlier. These data enabled one to see the spatial variation of the heaviest rain bands lending support to the CSI argument.

Suggested areas for future research would be the implementation of other meteorological upper air data collection sites in central Texas and northern Mexico to verify return-flow events more quickly. Incorporation of new data gathering platforms would provide a more dense network to address the parameters listed above. It would also allow one to assess the strength and location of jets at all levels, as well as locating areas of abundant Pacific and Gulf moisture. The acquisition of this data would provide more useful information with which to analyze dangerous situations, especially in areas of complex terrain. The role of CSI over complex terrain coupled with elevated convection in almost all winter flood cases where abundant Gulf moisture, surface boundaries, and upper level conditions exist should also be addressed.

REFERENCES

- Andrews, J., 1993: *Flooding: Canada Water Book*. Canada Communication Group, 171 pp.
- Banks, J. H., and J. E. Babcock, 1988: *Corralling the Colorado*. Eakin Press, 278 pp.
- Bluestein, H. B., 1992a: *Synoptic-Dynamic Meteorology in Midlatitudes, Volume 1, Principles of Kinematics and Dynamics*. Oxford University Press, 431 pp.
- Bluestein, H. B., 1992b: *Synoptic-Dynamic Meteorology in Midlatitudes, Volume 2, Observations and Theory of Weather Systems*. Oxford University Press, 594 pp.
- Carlson, T. N., 1991: *Mid-Latitude Weather Systems*. Harper Collins Academic, 507 pp.
- Colman, B. R., 1990: Thunderstorms above frontal surfaces in environments without positive CAPE. Part I: A climatology. *Monthly Weather Review*, **118**, 1103-1121.
- Crisp, C. A., and J. M. Lewis, 1992: Return flow in the Gulf of Mexico. Part I: A classificatory approach with a global historical perspective. *Journal of Applied Met.*, **31**, 868-881.
- desJardins, M. L., K. F. Brill, and S. S. Schotz, 1991: *NASA Technical Memorandum 4260- GEMPAK5 User's Guide, Version 5.0*. National Aeronautics and Space Administration, 221 pp.
- Dittman, R. H., 1994: *NOAA Technical Memorandum NWS SR-153 - Annual Flood Death Statistics Per State Per Capita for the United States and Puerto Rico During the Period 1959 - 1991*. National Oceanic and Atmospheric Administration, 11 pp.
- Djuric, D., 1994: *Weather Analysis*. Prentice Hall, 304 pp.

- Emanuel, K. A., 1983: On assessing local conditional symmetric instability from atmospheric soundings. *Monthly Weather Review*, **111**, 2016-2033.
- Emanuel, K. A., 1984: Conditional symmetric instability. In *Dynamics of Mesoscale Weather Systems, NCAR Summer Colloquium Lecture Notes, 11 June - 6 July 1984*, Boulder, Colorado, 159-183.
- Goodge, G. W., 1991: Outstanding storms of the month. *Storm Data*, **33**, Number 12, 8-58.
- Huschke, R. E., 1959: *Glossary of Meteorology*. Amer. Meteor. Soc., 638 pp.
- Liu, Q., J. M. Lewis, and J. M. Schneider, 1992: A study of cold-air modification over the Gulf of Mexico using in situ data and mixed-layer modeling. *Journal of Applied Met.*, **31**, 909-924.
- Ludlum, D. M., 1991: *The Audubon Society Field Guide to North American Weather*. Alfred A. Knopf, Inc., 656 pp.
- Maddox, R. A., and C. F. Chappell, 1978: Meteorological aspects of twenty significant flash flood events. *Preprints, Conference on Flash Floods: Hydrometeorological Aspects and Human Aspects* (Los Angeles), Amer. Meteor. Soc., 1-9.
- Maddox, R. A., C. F. Chappell, and L. R. Hoxit, 1979: Synoptic and meso - α scale aspects of flash flood events. *Bull. Amer. Met. Soc.*, **60**, 115-123.
- Mahler, R., 1995: *Natural Disaster Survey Report, Disastrous Floods on the Trinity, Brazos, Colorado, and Guadalupe Rivers in Texas December 1991 - January 1992*. National Oceanic and Atmospheric Administration, 148 pp.
- Merrill, R. T., 1992: Synoptic analysis of the GUFMEX return-flow event of 10-12 March 1988. *Journal of Applied Met.*, **31**, 849-867.
- Moore, J. T., 1993: *Isentropic Analysis and Interpretation, Operational Applications To Synoptic and Mesoscale Forecast Problems*. National Weather Service Training Center, 99 pp.
- Moore, J. T., and T. E. Lambert, 1993: The use of equivalent potential vorticity to diagnose regions of conditional symmetric instability. *Weather and Forecasting*, **8**, Number 3, 301-308.

Moran, J. P., and L. W. Morgan, 1991: *Meteorology, The Atmosphere and Science of Weather*. MacMillan Publishing, 586 pp.

Reinking, R. F., and J. F. Boatman, 1986: Upslope precipitation events. *Mesoscale Meteorology and Forecasting*, P. S. Ray, Ed., Amer. Meteor. Soc. 793 pp.

Wolfsberg, D. G., K. A. Emanuel, and R. E. Passarelli, 1986: Band formation in a New England winter storm. *Monthly Weather Review*, **114**, 1552-1569.

BIOGRAPHICAL SKETCH

Captain Rodney L. Clements was born on August 9, 1960, in Misawa AB Japan. He graduated from Clay High School, South Bend, Indiana, in 1978 and enlisted in the Air Force where he served for five years at Minot AFB, North Dakota. Upon completion of his enlistment he attended Arizona State University and received a Bachelor of Science degree in Geography in 1988. After graduation he was commissioned in the United States Air Force as a second lieutenant and went to Offutt AFB, Omaha, Nebraska. While at Offutt he held jobs in the Strategic Air Commands Weather Support Unit, Global Reconnaissance Center, and flew part time on the Looking Glass. From Offutt, he was transferred to Osan AB, Korea for one year where he was an Assistant Staff Weather Officer and the summer of 1993 he was transferred to FSU to begin work on his graduate degree.